Self-Sorting and Directed Molecular Self-Assembly towards New Soft Materials

Wang, Yiming

DOI
10.4233/uuid:c71f55e1-9049-47ae-85ba-cda251757064

Publication date
2019

Document Version
Final published version

Citation (APA)
Wang, Y. (2019). *Self-Sorting and Directed Molecular Self-Assembly towards New Soft Materials*. [Dissertation (TU Delft), Delft University of Technology]. https://doi.org/10.4233/uuid:c71f55e1-9049-47ae-85ba-cda251757064

Self-Sorting and Directed Molecular Self-Assembly towards New Soft Materials

Yiming WANG

Self-Sorting and Directed Molecular Self-Assembly towards New Soft Materials

Dissertation

for the purpose of obtaining the degree of doctor

at Delft University of Technology

by the authority of the Reactor Magnificus, prof. dr. ir. T. H. J. J. van der Hagen,

chair of the Board for Doctorates

to be defended publicly on

Tuesday 2 April 2019 at 15:00 o'clock

by

Yiming WANG

PhD of Science in Chemical Engineering and Technology,

East China University of Science and Technology, China

born in Anhui, China

This dissertation has been approved by the promoters.

Composition of the doctoral committee:

Rector Magnificus	chairperson
Prof. dr. J. H. van Esch	Delft University of Technology, promoter
Dr. R. Eelkema	Delft University of Technology, promoter

Independent members:

Prof. dr. J. Boekhoven	Technical University of Munich
Prof. dr. N. A. J. M. Sommerdijk	Eindhoven University of Technology
Dr. H. B. Eral	Delft University of Technology
Prof. dr. S. J. Picken	Delft University of Technology
Prof. dr. E. J. R. Sudhölter	Delft University of Technology, reserve member

Other members:

Prof. dr. X. Guo	East China University of Science and Technology

The work described in this thesis was carried out in the Advanced Soft Matter group at Delft University of Technology, Faculty of Applied Sciences, Department of Chemical Engineering. This research was financially supported by China Scholarship Council (CSC) and the Netherlands Organization for Scientific Research (NWO).

Cover design by Yiming Wang

Printed by: Gildeprint - Enschede

Propositions

Belonging to the thesis:

Self-sorting and directed molecular self-assembly towards new soft materials

by Yiming Wang

1. In multicomponent self-assembly systems, the difference in self-assembly rates of the distinct species is an overlooked approach towards self-sorting.
   - *Chem. Commun*. **2015**, *51*, 5170.
   - Chapter 2 of this thesis.
2. One never knows how many kinds of states retained in a local minimum of energy landscape can be obtained in a given supramolecular self-assembly system.
   - *Chem. Soc. Rev*. **2017**, *46*, 5476.
   - Chapter 3, 4 of this thesis.
3. For surface-assisted self-assembly, the template determines how well control of the self-assembly can be achieved.
   - Angew. Chem. Int. Ed. **2018**, *57*, 1448.
   - Chapter 5, 6 of this thesis
4. DNA is a useful building block for the construction of beautiful nanostructures, but one needs to take into account the risks of contamination of DNA nanostructures to the environment before the practical applications.
   - *Nature* **2006**, *440*, 297.
5. The development of artificial intelligence creates a strong competitor to organic chemists in terms of design of molecules.
   - *Chem* **2018**, *4*, 522.
6. For scientific research, raising a creative perspective is more important than telling a beautiful story.
7. Whether a scientific paper can be published in high-impact journals strongly depends on how comfortable a reading experience the writer can provide to the readers.
   - *Day*, R.; & Gastel, B.: *How to write and publish a scientific paper*. Cambridge University Press (**2012**).
8. The experience of organic synthesis is also useful for cooking food.
9. Dreamland is a virtual world of the magnification of the real life.
10. Confidence comes from giving up.

These propositions are considered as apposable and defendable, and as such have been approved by the promotors prof. dr. Jan H. van Esch and dr. Rienk Eelkema.

Contents

Chapter 1

Introduction

Abstract: Molecular self-assembly has been realized as a powerful approach to control the organization of materials from molecular to macroscopic length scale. While for a long time molecular self-assembly has focused on the investigation of systems involving a single component and under thermodynamic equilibrium. In recent years the interests are shifting towards more complex multicomponent and non-equilibrium self-assembly systems, where the richest functions of the resulted supramolecular objects can be harnessed. In this thesis, multicomponent supramolecular self-assembly and directed molecular self-assembly leading to out-of-equilibrium supramolecular systems are investigated, with the aim to construct new soft functional materials.

1.1 General introduction

Molecular self-assembly refers to the spontaneous organization of molecular building blocks through reversible, non-covalent interactions towards ordered higher level structures.[1-3] As such, molecular self-assembly belongs to the field of supramolecular chemistry. The development of supramolecular chemistry can be traced back to the late 19th century,[4] when some of the most fundamental concepts of supramolecular self-assembly were proposed, e.g. coordination chemistry,[5] lock-key model,[6] and cyclodextrin based host-guest inclusion.[7] Currently, supramolecular chemistry and molecular self-assembly continue to be a theme of great interest in science, particularly in material science, as it offers an easy and powerful bottom-up approach to control the organization of materials from molecular to macroscopic length scale.[8] To date, a wide variety of supramolecular structures have been prepared by self-assembly of the corresponding building blocks, e.g., micelles,[9-13] vesicles,[14-16] fibers,[17-19] sheets,[20-22] and DNA origami et al.[23-24] These resulting structures show enticing applications in different fields, such as biotherapy,[25-26] electronics,[27-29] catalysis,[30-31] and biomimetic engineering.[32-34]

1.2 Multicomponent self-assembly and self-sorting

Supramolecular self-assembly is widespread in nature, for example, living cell is a complex system that is entirely constructed by self-assembly of biomolecules. One typical characteristic of the self-assembly in living cell is the use of multiple subunits, such as lipids, proteins, and sugars.[35] Such multicomponent self-assembly endows the cell with complex structures and sophisticated physiological functions. Therefore, to achieve such multicomponent self-assembly in synthetic scenario would not only benefit to our understanding of the biological system, but also enrich the diversity of manmade functional supramolecular objects.[36]

In recent years, synthetic scientists have already explored multicomponent self-assembly in artificial system and some beautiful examples have been successfully developed.[19, 37] On the one extreme case of multicomponent self-assembly, the different building blocks show high affinity for each other, and as a result all components (functionalities) are integrated into a single supramolecular product through cooperative assembly (co-assembly).[38] For instant, by performing the co-assembly of two kinds of peptide building blocks (FF and Boc-FF, Figure 1.1a) bearing the same self-assembling moiety, nanotubes consisting of both two types of peptides have been prepared.[39] The resulting nanotubes present extended physical properties, such as photoluminescence, semiconductivity and thermo-electrical responsiveness, due to their composition of two kinds of functional peptides.[40] In

another example, upon co-assembly of multicomponent molecular monomers, random supramolecular copolymers have been obtained (Figure 1.1b).[41-42] Some of these multicomponent supramolecular polymers with combined properties of each individual monomer have been used to mimic extracellular matrix (ECM) for applications in tissue engineering,[19] and to construct drug delivery platforms for applications in biomedicine.[43] In addition to this random co-assembly, sequential self-assembly of different monomers has been successfully performed and leads to supramolecular block copolymers (Figure 1.1c).[44-46] This controlled multicomponent self-assembly offers a powerful "bottom-up" approach to fabricate supramolecular structures with well-defined repetitive sequences which are expected to find applications in, e.g., nanoplasmonics,[47] and nanoelectronics.[48]

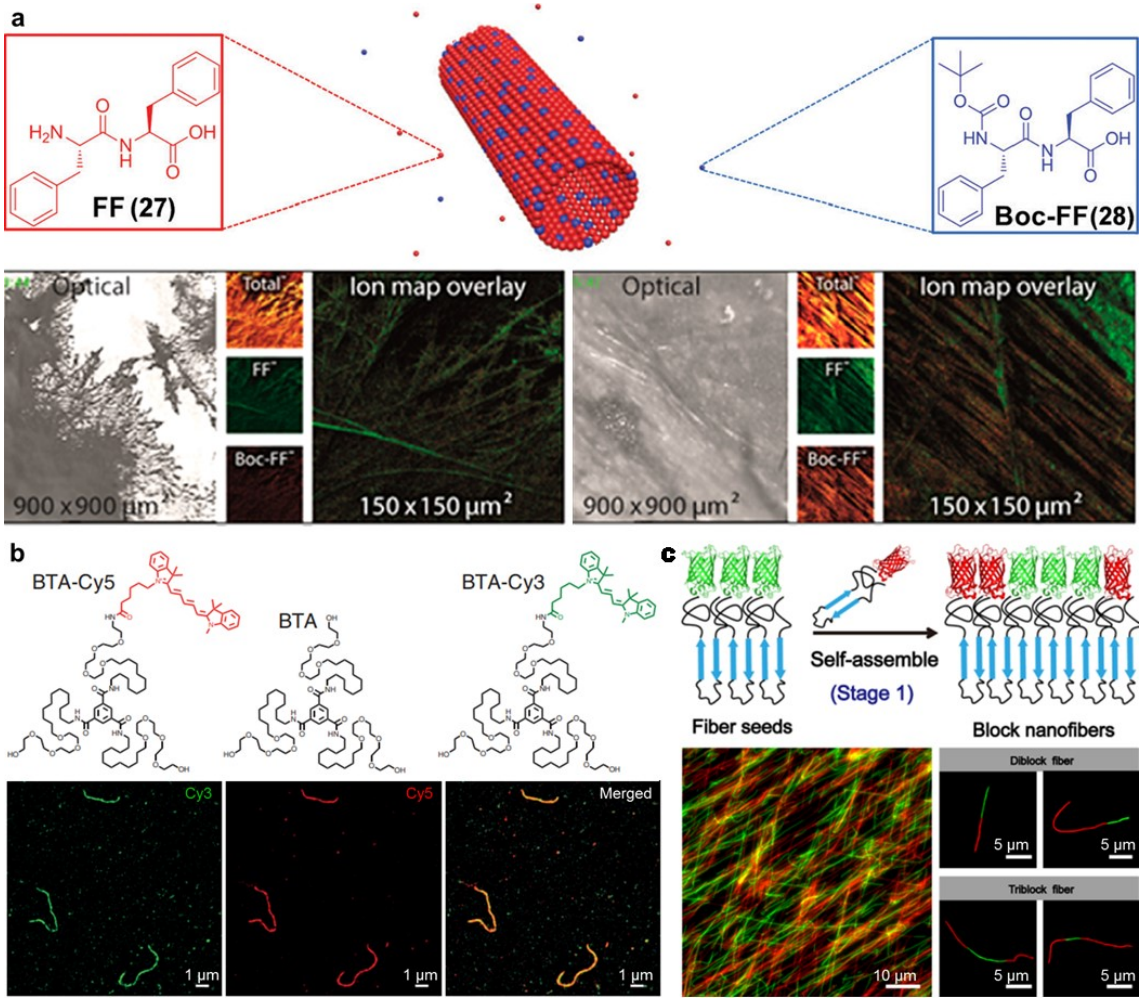

Figure 1.1 Supramolecular structures formed by multicomponent self-assembly. a) Co-assembly of FF and Boc-FF (top), and ToF-SIMS analysis of the resulting nanotubes, FF:Boc-FF = 10:1 (bottom left) and FF:Boc-FF = 5:1 (bottom right);[39-40] **b**) co-assembly of different BTA derived monomers, chemical structures of the monomers (top), and fluorescent images of the self-assembled supramolecular polymers (bottom);[41] and **c**) illustration of the formation of multisegment supramolecular nanofibers by sequential assembly of different monomers (top), and fluorescent images of the resultant block nanofibers.[44]

On the other extreme of multicomponent self-assembly, one has so called self-sorting[38, 49] or orthogonal self-assembly.[50] Here, different components self-assemble independently into different architectures within one system which possesses integrated properties of each single architecture. Self-sorting is widespread in nature and is crucial for the function of life. Even the living cell can be seen as a complex supramolecular object that is composed of many different coexisting functional supramolecular structures, each of which is assembled from one or more biomolecular building blocks.[35, 51] Inspired by nature, some synthetic self-sorting examples have been developed in recent years. For example, gelled liquid crystalline crystals consisting of a supramolecular gel networks inside a liquid crystalline phase have been prepared by the self-sorting of molecular gelators and liquid crystalline molecules, giving rise to crystal materials with improved optical performance and ionic conductivity (Figure 1.2a).[52-53] In another example, self-sorting of molecular gelators and amphiphiles has led to supramolecular gels composed of gel fibers and micelles or vesicles (Figure 1.2b),[54-57] which are much closer mimics of biological structures and present interesting applications in biomedicine.[58] Furthermore, supramolecular gel networks composed of distinct gel fibers have been created by the self-sorting of different molecular gelators,[59-61] showing tunable mechanical properties (Figure1.2c).[62-63]

Despite these advances, the established synthetic multicomponent self-assembly systems are still lagging behind their biological counterparts in terms of, not limited to, complexity of the self-assembled structures and the length scale of the self-sorting. For example, people have made remarkable progresses in the mimics of ECM through the self-assembly of multicomponent synthetic molecules. Additionally, some of these synthetic ECM have reached the clinic.[19] However, these artificial ECM are still fairly simple compared to the biological ECM in terms of chemical structures, diversities of monomers and functionalities.[19] In another example, although the implementation of self-sorting at molecular level has been achieved in synthetic case, there is still a large gap between the synthetic systems and their biological counterparts. For instance, in living cell different biological subunits self-sort into different supramolecular structures which in turn undergo a higher level self-sorting, leading to hierarchical macroscopic structures. However, the accomplishment of such multilevel self-sorting in synthetic case remains a formidable task.[37]

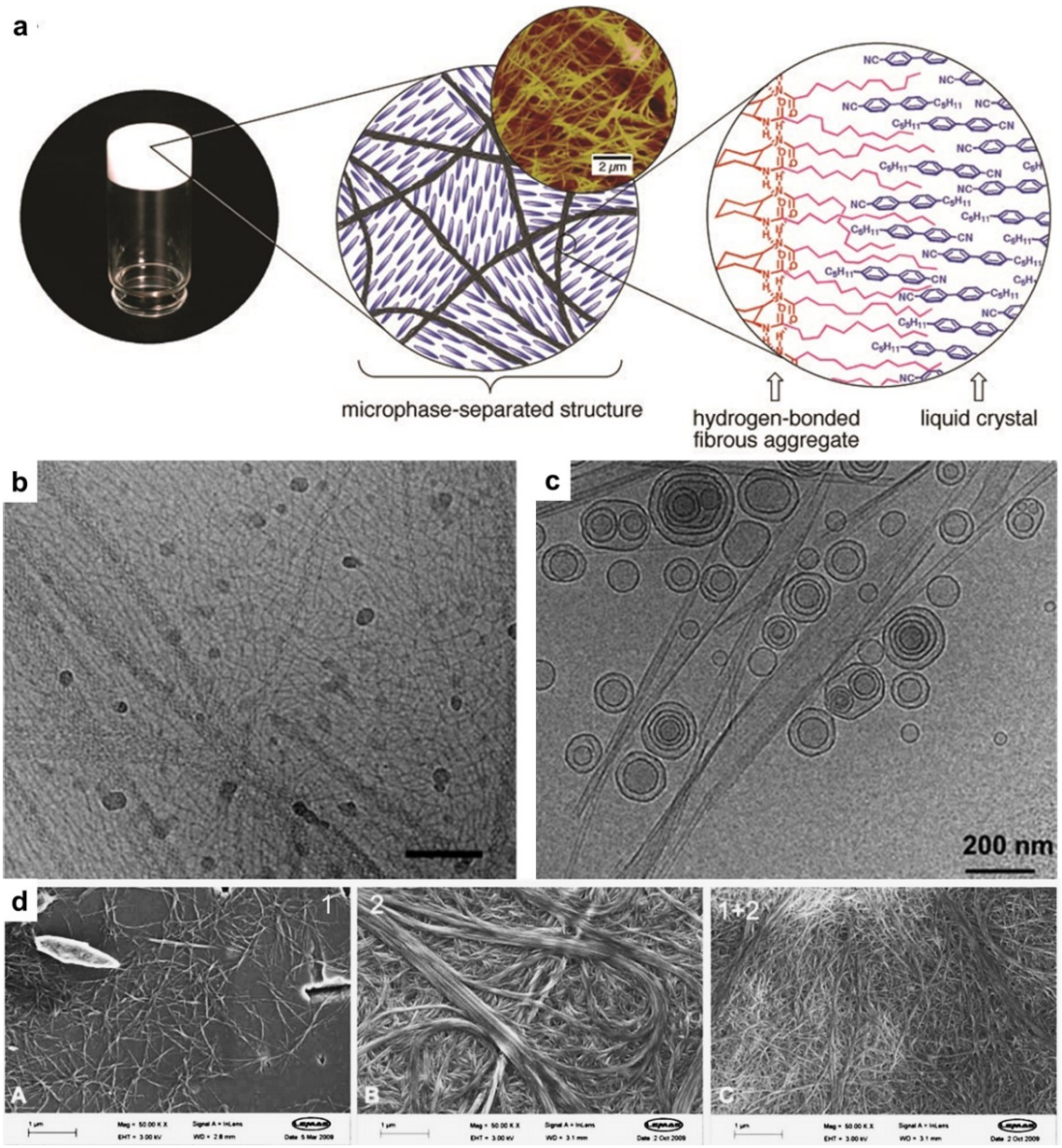

Figure 1.2 Supramolecular structures formed by molecular self-sorting. **a**) Hierarchical structures consisting of coexisted supramolecular fibers and liquid crystals;[52] **b**, **c**) complex supramolecular structures consisting of coexisted gel fibers and **b**) cylindrical micelles,[54] **c**) liposomes[57] prepared by the orthogonal self-assembly of gelators and the corresponding amphiphiles; and **d**) SEM images of gel networks formed by the separate self-assembly of two monocomponent gelators, respectively (left and middle), and interpenetrated gel networks consisting of two kinds of gel fibers formed by the self-sorting of the two distinct gelators (right).[61]

1.3 Directed molecular self-assembly

In addition to the above described involvement of multiple building blocks, another important characteristic of the self-assembly in biological system is the evolution of free energy during the self-assembly process.[64] The self-assembly in

nature is usually performed out-of-equilibrium (Figure 1.3a and b),[65] endowing the resulting supramolecular structures with unique properties that are inaccessible by thermodynamic self-assembly, such as adaptation,[66-68] intracellular transportation,[69-71] and autonomous regeneration.[72-74] In contrast, the vast majority of synthetic self-assembly systems function under thermodynamic equilibrium (Figure 1.3c). In recent years, the achievement of out-of-equilibrium self-assembly in the lab has received considerable attention.[75] In this thesis, we define the control of molecular self-assembly leading to an out-of-equilibrium system as directed molecular self-assembly (DMSA).

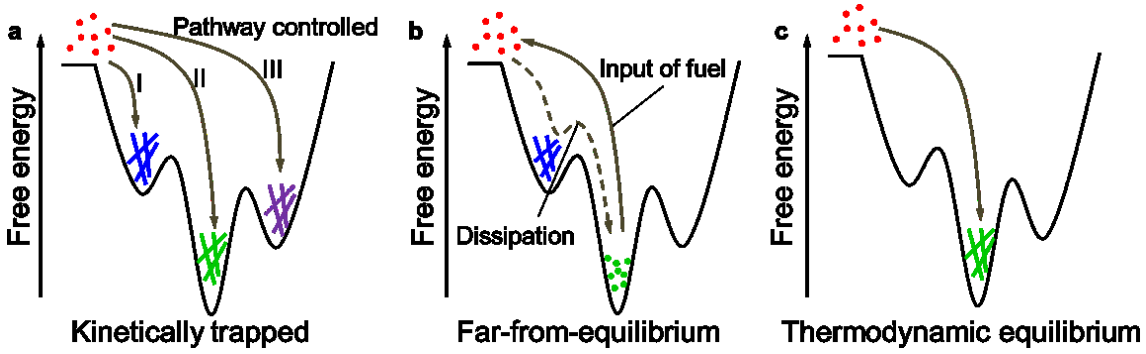

Figure 1.3 Energy landscape of different types of self-assembly. a) molecular self-assembly through different pathways leading to different kinetically favored outcomes; **b**) far-from-equilibrium system where self-assembly is driven by the dissipation of high energy fuels; and **c**) molecular self-assembly under thermodynamic equilibrium.[65, 76]

A first scenario of DMSA is kinetically controlled self-assembly. In this case, the self-assembly is forced to proceed along a kinetically controlled pathway, leading to kinetically favored outcomes which are permanently or temporarily stabilized at a local minimum of the free energy landscape.[76] The permanently stabilized product is in a so called kinetically trapped state, while the temporarily stabilized one is in a metastable state which can convert into the thermodynamic state over time. The kinetically favored supramolecular product usually presents different structures and properties from the thermodynamic counterpart, though they have the same compositions. In this context, in recent years kinetically controlled DMSA has received great interest and some impressive examples have been developed. For instance, kinetically trapped supramolecular gels have been prepared by controlling the self-assembly rate of gelators using external stimuli, e.g., catalysts (enzymes). Consequently, gels with distinct structures and mechanical properties can be prepared by controlling the self-assembly rate of gelators.[77-79] Additionally, upon activating the molecular self-assembly at different rates in different areas by using some external triggers, such as light,[80-82] pH,[83] and enzymes,[84-85] the growth of the supramolecular structures can be spatiotemporally controlled. For example, on the

basis of an enzyme catalyzed self-assembly system, the conversion of non-assembling gelator precursors into gelators can be dramatically accelerated in the presence of the catalysis of enzyme. As a result, the gel fibers mostly grown from the enzyme areas due to the local catalysis formation of gelators (Figure 1.4a and b).[78, 84] Another example involves the employment of a proton sensitive gelator system in which the self-assembly of gelators into gel fibers can be activated by protons. On the basis of this proton responsiveness, spatiotemporal formation of gel fibers has been achieved by controlling the spatial distribution and local concentration of protons (Figure 1.4c).[86-87] In addition to the above described kinetically trapped supramolecular products, metastable supramolecular structures have been achieved as well.[88] For instance, a pathway dependent supramolecular system has been systematically investigated by a stopped-flow experiement.[89] In that system *S*-chiral oligo(p-phenylenevinylene) (SOPV) was used as monomers. Supramolecular polymers with different helicities, thermodynamically stable *M*-SOPV and metastable *P*-SOPV, can be achieved by controlling the initial concentrations of SOPV. Furthermore, the metastable *P*-SOPV can convert into the thermodynamic *M*-SOPV spontaneously over time (Figure 1.4d).

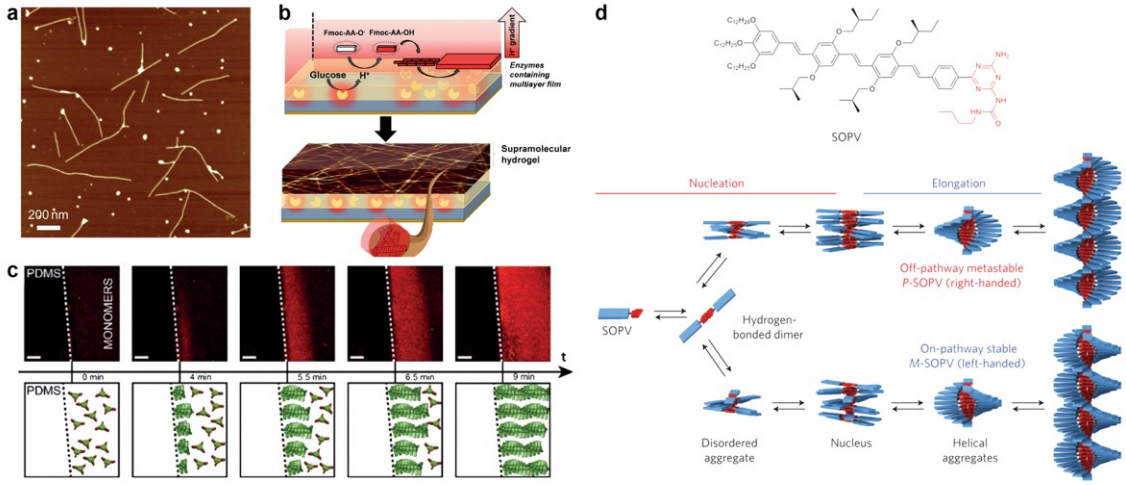

Figure 1.4 Spatiotemporally controlled molecular self-assembly. a) Growing of Fmoc-peptide gel fibers from the enzyme area (white dots) led by biocatalytic self-assembly;[78, 84] **b**) enzymatic oxidation of glucose by GOx generated local proton gradient leading to localized self-assembly of Fmoc-AA-OH dipeptide;[86] and **c**) growing of gel layer from the PDMS surface through the local self-assembly of gelators triggered by the rich proton environment in the vicinity of the acid soaked PDMS surface, scale bars = 200 mm;[87] and **d**) schematic representation of the aggregation pathways of SOPV control over the hand of resulting supramolecular helices.[89]

Another scenario of out-of-equilibrium self-assembly is associated with the consumption of high-energy fuels. In this scenario, the addition of fuels activate the

building blocks from a non-assembling state into assembling state, leading to the occurrence of self-assembly. Meanwhile, the generated assembling building blocks spontaneously and continuously transform back into the non-assembling state, thereby leading to the occurrence of disassembly.[90] Therefore the self-assembled structures can only exist through the continuous consumption of fuels (Figure 1.3b). The unique property of such transient out-of-equilibrium self-assembled structures is that they are highly dynamic and under kinetic control determined by fuel levels. This kind of fuel driven out-of-equilibrium self-assembly is common in biological system. For example, microfilaments are formed by the self-assembly of actin driven by adenosine triphosphate (ATP), while microtubules are formed by the self-assembly of tubulin driven by guanosine triphosphate (GTP).[73-74, 91] In recent years, to mimic such a fuel driven out-of-equilibrium self-assembly in lab has been an interesting topic in the field of supramoleuclar chemistry.[75-76, 90] It has been demonstrated that far-from-equilibrium supramolecular structures can be produced by using chemical fuels. For example, transient supramolecular gels have been prepared using alkylation or dehydration reagents as fuels.[92-94] The life time and material properties of the resulting gels can be easily controlled by adjusting the input of fuels (Figure 1.5a and b). In another case, GTP has been successfully used to power the self-assembly of FtsZ protein (a bacterial homologue of tubulin) under artificial circumstance, leading to far-from-equilibrium fibrils with highly dynamic behaviors of growing, shrinking, bending, and fusing (Figure 1.5c).[95]

Overall, it is clear that DMSA has emerged as a key and useful area in supramolecular chemistry. It would provide a competitive "bottom-up" route for the fabrication of sophisticated functional supramolecular objects which present intriguing applications in a broad fields, such as artificial life, smart materials, microelectronics, energy, and biotherapy. Moreover, the development of DMSA may also add to our understanding of the complex biological world. Although in recent years some important achievements have been made, there are still numerous questions that remain to be addressed. For example, the diversity of synthetic DMSA systems is still scarce, and therefore new approaches towards DMSA are desired. Furthermore, the control of the parameters of the resulting structures, such as the architectures, spatial dimensions, and length scale, remains limited.

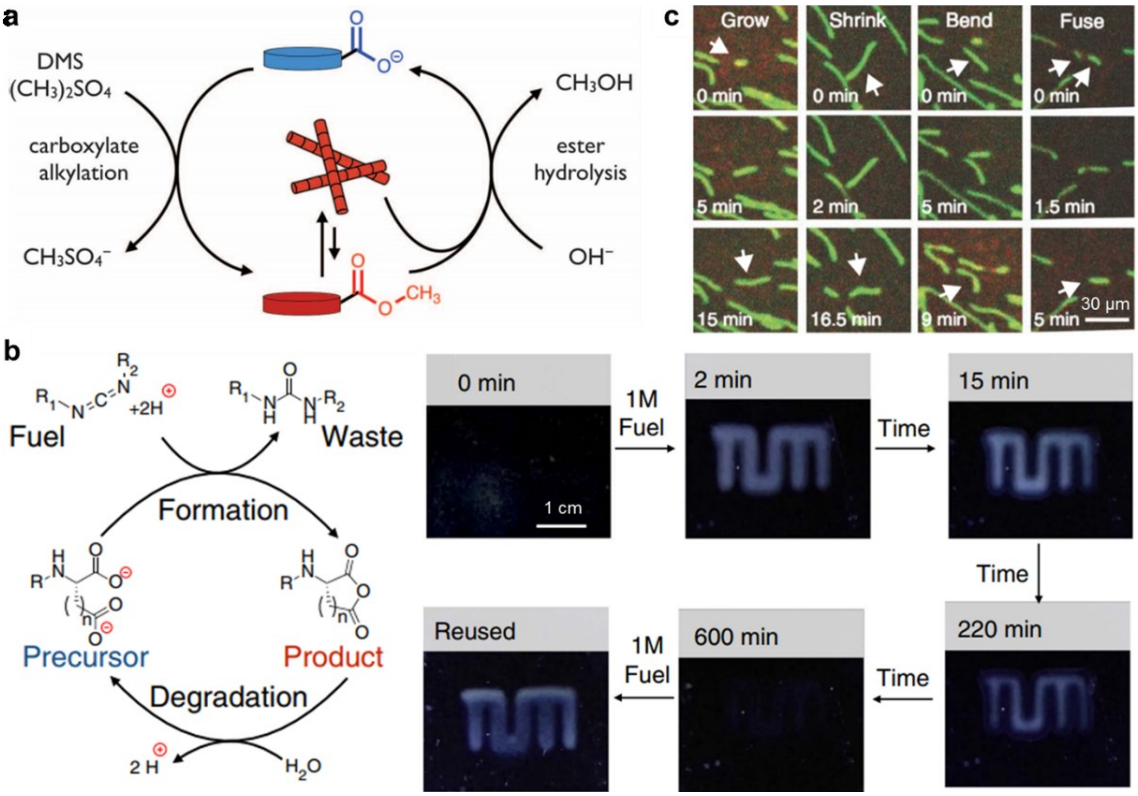

Figure 1.5 Fuel driven molecular self-assembly. a) Schematic of dimethyl sulfate (DMS) fueled transient self-assembly;[96] **b**) anhydride formation driven by dissipation of carbodiimide leading to transient self-assembly of supramolecular gels;[94] and **c**) GTP fueled formation of Fibrils showing dynamic behavior of growth, shrinkage, bending and fusion.[95]

1.4 Challenges and research aim

Inspired by biological system, self-sorting has been successfully applied in synthetic scenario, giving rise to complex supramolecular structures bearing enriched functions. However, these developed artificial systems are still limited to the molecular level. Self-sorting at multilevel is ubiquitous in nature, but is still a big challenge in lab. To make further advances, access to self-sorting at higher level is necessary, whereby more complex structures with richer functions can be unlocked. In this thesis, we aim to develop new synthetic multicomponent self-assembly systems and explore the possibility of self-sorting at higher level. The achievement of such a goal would not only pave the way to perform multilevel self-sorting in manmade systems and promote the development of new functional soft materials, but also add to our understanding of biological system.

DMSA, molecular self-assembly that functions under out-of-equilibrium, has emerged as a competitive strategy to fabricate functional materials that are usually unachievable by thermodynamic self-assembly. Up to now, some remarkable progresses have been made in the development of synthetic DMSA systems.

However, there are still some key problems need to be addressed in this field. For instance, the diversity is still lacking due to the complex design and tedious synthesis process. Moreover, the parameters, like length scale, dimensions, and architectures, in a given DMSA system is still lacking of control. In this thesis, I will focus on: 1) developing versatile routes towards new DMSA systems; 2) finding access to control the parameters of the DMSA systems. The achievements obtained from these investigations would provide more useful information for the design and control of synthetic DMSA systems.

1.5 Outline of thesis

This thesis entitled "Self-Sorting and Directed Molecular Self-Assembly towards New Soft Materials" is organized in six chapters.

In Chapter 1, the research background of the work that performed in this thesis is described.

In Chapter 2, a rare example of spontaneous multilevel self-sorting system based on multicomponent molecular gelators is described. We have found that distinct gel fibers are formed through the self-sorting of the different molecular gelators driven by their different self-assembly rates. Interestingly, these different fibers can further self-sort into different separated microdomains, leading to hierarchically compartmentalized supramolecular gels. This rare spontaneous multilevel self-sorting example can serve as a starting point for the design of multilevel self-sorting systems in synthetic scenario and advance our understanding of both synthetic and natural self-sorting systems.

In Chapter 3, we employed seeds to interfere in the nucleation step of the gelators that have been investigated in Chapter 2, aiming at forcing the self-assembly along a kinetically favored pathway. We have found that the addition of seeds gives rise to supramolecular gels with completely different structures and material properties compared to the hierarchically compartmentalized gels described in Chapter 2. Importantly, these seeding-driven gels are metastable and can spontaneously convert into the hierarchically compartmentalized gels state over time.

In Chapter 4, we have surprisingly found that one of the gelator precursor molecules used in this thesis (hydrazide) is able to self-assemble in water. Importantly, the resulting tiny aggregates of the precursor molecules exhibit similar seeding effects on the self-assembly of the multicomponent gelators, leading to the metastable gels as well. This finding demonstrates a new out-of-equilibrium supramolecular system driven by a self-seeding self-assembly process.

In Chapter 5, micropatterned catalytic surfaces were employed to direct the self-

assembly of molecular gelators on the basis of a catalysis-responsive gelator system. It has shown that the gel fibers can be locally formed at the catalytic areas. Moreover, the shapes, spatial dimensions and growing direction of the gel patterns can be easily controlled by tuning the content of the catalyst in the templates. This work shows a feasible approach to control the parameters of a DMSA system, which would promote the practical applications of the DMSA products.

In Chapter 6, we have devoted to extending the microscale DMSA system described in Chapter 5 to the nanoscale by using catalytic nanoparticles as the templates. The gel fibers were found to be selectively formed around the nanoparticles. Additionally, we have shown how the local formation of gel fibers in the vicinity of the catalytic nanoparticles can be used to selectively trap catalytic nanoparticles. This selective trapping of nano-sized objects is expecting to find some high-tech applications, such as separation of nanoparticles, virus prevention, and biotherapy.

Overall, upon the work performed in this thesis, a series of new synthetic self-sorting and DMSA examples have been created and studied. We expect that the work performed in this thesis would enrich the library of synthetic self-sorting and DMSA systems and provide valuable information for the design of new self-sorting and DMSA systems under artificial conditions.

1.6 References

1. Whitesides, G. M.; Ismagilov, R. F., Complexity in chemistry. *Science* **1999,** *284*, 89-92.
2. Whitesides, G. M.; Grzybowski, B., Self-assembly at all scales. *Science* **2002,** *295*, 2418-2421.
3. Pelesko, J. A., *Self assembly: the science of things that put themselves together*. CRC Press: 2007.
4. Schalley, C. A., *Analytical methods in supramolecular chemistry*. John Wiley & Sons: 2012.
5. Werner, A., Coordination chemistry. *Zeitschr. Anorg. Chem* **1893,** *3*, 267.
6. Behr, J.-P., *The lock-and-key principle: the state of the art--100 years on*. John Wiley & Sons: 2008; Vol. 17.
7. Villiers, A., Sur la fermentation de la fécule par l'action du ferment butyrique. *Compt. Rend. Acad. Sci* **1891,** *112*, 536-538.
8. Zhang, S.; Greenfield, M. A.; Mata, A.; Palmer, L. C.; Bitton, R.; Mantei, J. R.; Aparicio, C.; de la Cruz, M. O.; Stupp, S. I., A self-assembly pathway to aligned monodomain gels. *Nat. Mater.* **2010,** *9*, 594-601.
9. You, J.; Hu, F. Q.; Du, Y. Z.; Yuan, H., Improved cytotoxicity of doxorubicin by enhancing its nuclear delivery mediated via nanosized micelles. *Nanotechnology* **2008,** *19*, 255103.
10. Hu, F. Q.; Meng, P.; Dai, Y. Q.; Du, Y. Z.; You, J.; Wei, X. H.; Yuan, H., PEGylated chitosan-based polymer micelle as an intracellular delivery carrier for anti-tumor targeting therapy. *Eur. J. Pharm. Biopharm.* **2008,** *70*, 749-57.

11. Wang, Y. M.; Wang, J.; Wang, T. S.; Xu, Y. S.; Shi, L.; Wu, Y. T.; Li, L.; Guo, X. H., Pod-Like Supramicelles with Multicompartment Hydrophobic Cores Prepared by Self-Assembly of Modified Chitosan. *Nano-Micro Lett* **2016,** *8*, 151-156.
12. Nomoto, T.; Fukushima, S.; Kumagai, M.; Machitani, K.; Arnida; Matsumoto, Y.; Oba, M.; Miyata, K.; Osada, K.; Nishiyama, N.; Kataoka, K., Three-layered polyplex micelle as a multifunctional nanocarrier platform for light-induced systemic gene transfer. *Nat. Commun.* **2014,** *5*.
13. Zhao, Y., Photocontrollable block copolymer micelles: what can we control? *J. Mater. Chem.* **2009,** *19*, 4887-4895.
14. Du, J. Z.; O'Reilly, R. K., Advances and challenges in smart and functional polymer vesicles. *Soft Matter* **2009,** *5*, 3544-3561.
15. Xing, P. Y.; Sun, T.; Hao, A. Y., Vesicles from supramolecular amphiphiles. *Rsc Adv.* **2013,** *3*, 24776-24793.
16. Tanner, P.; Baumann, P.; Enea, R.; Onaca, O.; Palivan, C.; Meier, W., Polymeric Vesicles: From Drug Carriers to Nanoreactors and Artificial Organelles. *Accounts Chem. Res.* **2011,** *44*, 1039-1049.
17. van Bommel, K. J. C.; van der Pol, C.; Muizebelt, I.; Friggeri, A.; Heeres, A.; Meetsma, A.; Feringa, B. L.; van Esch, J., Responsive cyclohexane-based low-molecular-weight hydrogelators with modular architecture. *Angew. Chem. Int. Edit.* **2004,** *43*, 1663-1667.
18. Roy, S.; Ulijn, R. V., Exploiting Biocatalysis in the Synthesis of Supramolecular Polymers. *Adv. Polym. Sci.* **2010,** *237*, 127-143.
19. Goor, O.; Hendrikse, S. I. S.; Dankers, P. Y. W.; Meijer, E. W., From supramolecular polymers to multi-component biomaterials. *Chem. Soc. Rev.* **2017,** *46*, 6621-6637.
20. Tang, Z. Y.; Zhang, Z. L.; Wang, Y.; Glotzer, S. C.; Kotov, N. A., Self-assembly of CdTe nanocrystals into free-floating sheets. *Science* **2006,** *314*, 274-278.
21. Fukui, T.; Kawai, S.; Fujinuma, S.; Matsushita, Y.; Yasuda, T.; Sakurai, T.; Seki, S.; Takeuchi, M.; Sugiyasu, K., Control over differentiation of a metastable supramolecular assembly in one and two dimensions. *Nat. Chem.* **2017,** *9*, 493-499.
22. Fukui, T.; Takeuchi, M.; Sugiyasu, K., Impact of a subtle structural difference on the kinetic behavior of metastable supramolecular assemblies. *Polymer* **2017,** *128*, 311-316.
23. Rothemund, P. W. K., Folding DNA to create nanoscale shapes and patterns. *Nature* **2006,** *440*, 297-302.
24. Douglas, S. M.; Dietz, H.; Liedl, T.; Hogberg, B.; Graf, F.; Shih, W. M., Self-assembly of DNA into nanoscale three-dimensional shapes. *Nature* **2009,** *459*, 414-418.
25. Vader, P.; Breakefield, X. O.; Wood, M. J. A., Extracellular vesicles: emerging targets for cancer therapy. *Trends Mol. Med.* **2014,** *20*, 385-393.
26. Xu, R.; Rai, A.; Chen, M.; Suwakulsiri, W.; Greening, D. W.; Simpson, R. J., Extracellular vesicles in cancer — implications for future improvements in cancer care. *Nat. Rev. Clin. Oncol.* **2018**.
27. Ma, H.; Kang, S. H.; Kim, M. S.; Kim, K. S.; Zin, M. T.; Zareie, M. H.; Sarikaya, M.; Jen, A. K. Y., Functional self-assemblies with nanoscale ordering for molecular electronics and

biomaterials. *Abstr. Pap. Am. Chem. S.* **2003,** *226*, U389-U389.
28. Nguyen, H. D., Role of electrostatics in designing nanoscale biomaterials through self-assembly. *Abstr. Pap. Am. Chem. S.* **2013,** *246*.
29. Galland, R.; Leduc, P.; Guerin, C.; Peyrade, D.; Blanchoin, L.; Thery, M., Fabrication of three-dimensional electrical connections by means of directed actin self-organization. *Nat. Mater.* **2013,** *12*, 416-421.
30. Brown, C. J.; Toste, F. D.; Bergman, R. G.; Raymond, K. N., Supramolecular catalysis in metal-ligand cluster hosts. *Chem. Rev.* **2015,** *115*, 3012-35.
31. Qiao, Y.; Zhang, L.; Li, J.; Lin, W.; Wang, Z., Switching on Supramolecular Catalysis via Cavity Mediation and Electrostatic Regulation. *Angew. Chem. Int. Edit.* **2016,** *55*, 12778-82.
32. Kokkoli, E.; Mardilovich, A.; Wedekind, A.; Rexeisen, E. L.; Garg, A.; Craig, J. A., Self-assembly and applications of biomimetic and bioactive peptide-amphiphiles. *Soft Matter* **2006,** *2*, 1015-1024.
33. Aliprandi, A.; Mauro, M.; De Cola, L., Controlling and imaging biomimetic self-assembly. *Nat. Chem.* **2016,** *8*, 10-15.
34. Mytnyk, S.; Olive, A. G.; Versluis, F.; Poolman, J. M.; Mendes, E.; Eelkema, R.; van Esch, J. H., Compartmentalizing Supramolecular Hydrogels Using Aqueous Multi‐phase Systems. *Angew. Chem. Int. Edit.* **2017,** *56*, 14923-14927.
35. Alberts, B.; Johnson, A.; Lewis, J.; Raff, M.; Roberts, K.; Walter, P., Molecular Biology of the Cell, 4th Ed. Garland Science: New York, 2002.
36. Lehn, J. M., Toward self-organization and complex matter. *Science* **2002,** *295*, 2400-2403.
37. Raeburn, J.; Adams, D. J., Multicomponent low molecular weight gelators. *Chem. Commun.* **2015,** *51*, 5170-80.
38. Wu, A.; Isaacs, L., Self-sorting: the exception or the rule? *J. Am. Chem. Soc.* **2003,** *125*, 4831-4835.
39. Adler-Abramovich, L.; Marco, P.; Amon, Z. A.; Creasey, R. C. G.; Michaels, T. C. T.; Levin, A.; Scurr, D. J.; Roberts, C. J.; Knowles, T. P. J.; Tendler, S. J. B.; Gazit, E., Controlling the Physical Dimensions of Peptide Nanotubes by Supramolecular Polymer Coassembly. *Acs Nano* **2016,** *10*, 7436-7442.
40. Makam, P.; Gazit, E., Minimalistic peptide supramolecular co-assembly: expanding the conformational space for nanotechnology. *Chem. Soc. Rev.* **2018,** *47*, 3406-3420.
41. Albertazzi, L.; van der Zwaag, D.; Leenders, C. M. A.; Fitzner, R.; van der Hofstad, R. W.; Meijer, E. W., Probing Exchange Pathways in One-Dimensional Aggregates with Super-Resolution Microscopy. *Science* **2014,** *344*, 491-495.
42. Baker, M. B.; Gosens, R. P. J.; Albertazzi, L.; Matsumoto, N. M.; Palmans, A. R. A.; Meijer, E. W., Exposing Differences in Monomer Exchange Rates of Multicomponent Supramolecular Polymers in Water. *Chembiochem* **2016,** *17*, 207-213.
43. Bakker, M. H.; Lee, C. C.; Meijer, E. W.; Dankers, P. Y.; Albertazzi, L., Multicomponent Supramolecular Polymers as a Modular Platform for Intracellular Delivery. *Acs Nano* **2016,** *10*, 1845-52.
44. An, B. L.; Wang, X. Y.; Cui, M. K.; Gui, X. R.; Mao, X. H.; Liu, Y.; Li, K.; Chu, C. F.; Pu, J.

H.; Ren, S. S.; Wang, Y. Y.; Zhong, G. S.; Lu, T. K.; Liu, C.; Zhong, C., Diverse Supramolecular Nanofiber Networks Assembled by Functional Low-Complexity Domains. *Acs Nano* **2017,** *11*, 6985-6995.

45. Adelizzi, B.; Aloi, A.; Van Zee, N. J.; Palmans, A. R. A.; Meijer, E. W.; Voets, I. K., Painting Supramolecular Polymers in Organic Solvents by Super-resolution Microscopy. *Acs Nano* **2018,** *12*, 4431-4439.
46. Beun, L. H.; Albertazzi, L.; van der Zwaag, D.; de Vries, R.; Stuart, M. A. C., Unidirectional Living Growth of Self Assembled Protein Nanofibrils Revealed by Super-resolution Microscopy. *Acs Nano* **2016,** *10*, 4973-4980.
47. Ding, S. Y.; Yi, J.; Li, J. F.; Ren, B.; Wu, D. Y.; Panneerselvam, R.; Tian, Z. Q., Nanostructure-based plasmon-enhanced Raman spectroscopy for surface analysis of materials. *Nature Reviews Materials* **2016,** *1*.
48. Kagan, C. R.; Lifshitz, E.; Sargent, E. H.; Talapin, D. V., Building devices from colloidal quantum dots. *Science* **2016,** *353*.
49. Safont-Sempere, M. M.; Fernandez, G.; Wurthner, F., Self-Sorting Phenomena in Complex Supramolecular Systems. *Chem. Rev.* **2011,** *111*, 5784-5814.
50. Heeres, A.; van der Pol, C.; Stuart, M.; Friggeri, A.; Feringa, B. L.; van Esch, J., Orthogonal self-assembly of low molecular weight hydrogelators and surfactants. *J. Am. Chem. Soc.* **2003,** *125*, 14252-3.
51. Mendes, A. C.; Baran, E. T.; Reis, R. L.; Azevedo, H. S., Self-assembly in nature: using the principles of nature to create complex nanobiomaterials. *Wiley Interdiscip Rev Nanomed Nanobiotechnol* **2013,** *5*, 582-612.
52. Kato, T., Self-assembly of phase-segregated liquid crystal structures. *Science* **2002,** *295*, 2414-8.
53. Kumar, D. K.; Steed, J. W., Supramolecular gel phase crystallization: orthogonal self-assembly under non-equilibrium conditions. *Chem. Soc. Rev.* **2014,** *43*, 2080-2088.
54. Brizard, A.; Stuart, M.; van Bommel, K.; Friggeri, A.; de Jong, M.; van Esch, J., Preparation of nanostructures by orthogonal self-assembly of hydrogelators and surfactants. *Angew. Chem. Int. Edit.* **2008,** *47*, 2063-2066.
55. Boekhoven, J.; Koot, M.; Wezendonk, T. A.; Eelkema, R.; van Esch, J. H., A Self-Assembled Delivery Platform with Post-production Tunable Release Rate. *J. Am. Chem. Soc.* **2012,** *134*, 12908-12911.
56. Himmelein, S.; Lewe, V.; Stuart, M. C. A.; Ravoo, B. J., A carbohydrate-based hydrogel containing vesicles as responsive non-covalent cross-linkers. *Chem. Sci.* **2014,** *5*, 1054-1058.
57. Boekhoven, J.; Brizard, A. M.; Stuart, M. C. A.; Florusse, L.; Raffy, G.; Del Guerzo, A.; van Esch, J. H., Bio-inspired supramolecular materials by orthogonal self-assembly of hydrogelators and phospholipids. *Chem. Sci.* **2016,** *7*, 6021-6031.
58. Boekhoven, J.; Koot, M.; Wezendonk, T. A.; Eelkema, R.; van Esch, J. H., A self-assembled delivery platform with post-production tunable release rate. *J. Am. Chem. Soc.* **2012,** *134*, 12908-11.
59. Moffat, J. R.; Smith, D. K., Controlled self-sorting in the assembly of 'multi-gelator' gels.

Chem. Commun. **2009**, 316-318.
60. Cornwell, D. J.; Daubney, O. J.; Smith, D. K., Photopatterned Multidomain Gels: Multi-Component Self-Assembled Hydrogels Based on Partially Self-Sorting 1,3:2,4-Dibenzylidene-D-sorbitol Derivatives. *J. Am. Chem. Soc.* **2015,** *137*, 15486-92.
61. Smith, M. M.; Smith, D. K., Self-sorting multi-gelator gels-mixing and ageing effects in thermally addressable supramolecular soft nanomaterials. *Soft Matter* **2011,** *7*, 4856-4860.
62. Colquhoun, C.; Draper, E. R.; Eden, E. G. B.; Cattoz, B. N.; Morris, K. L.; Chen, L.; McDonald, T. O.; Terry, A. E.; Griffiths, P. C.; Serpell, L. C.; Adams, D. J., The effect of self-sorting and co-assembly on the mechanical properties of low molecular weight hydrogels. *Nanoscale* **2014,** *6*, 13719-13725.
63. Shigemitsu, H.; Fujisaku, T.; Tanaka, W.; Kubota, R.; Minami, S.; Urayama, K.; Hamachi, I., An adaptive supramolecular hydrogel comprising self-sorting double nanofibre networks. *Nat. Nanotechnol.* **2018,** *13*, 165-+.
64. Pascal, R.; Pross, A.; Sutherland, J. D., Towards an evolutionary theory of the origin of life based on kinetics and thermodynamics. *Open Biol.* **2013,** *3*.
65. Mattia, E.; Otto, S., Supramolecular systems chemistry. *Nat. Nanotechnol.* **2015,** *10*, 111-119.
66. Mattheck, C., *Design in nature: learning from trees*. Springer Science & Business Media: 1998.
67. Weinkamer, R.; Dunlop, J. W. C.; Brechet, Y.; Fratzl, P., All but diamonds Biological materials are not forever. *Acta Mater.* **2013,** *61*, 880-889.
68. Halley, J. D.; Winkler, D. A., Consistent Concepts of Self-organization and Self-assembly. *Complexity* **2008,** *14*, 10-17.
69. Lasek, R. J.; Brady, S. T., Attachment of Transported Vesicles to Microtubules in Axoplasm Is Facilitated by Amp-Pnp. *Nature* **1985,** *316*, 645-647.
70. Vale, R. D.; Reese, T. S.; Sheetz, M. P., Identification of a Novel Force-Generating Protein, Kinesin, Involved in Microtubule-Based Motility. *Cell* **1985,** *42*, 39-50.
71. Schroer, T. A.; Steuer, E. R.; Sheetz, M. P., Cytoplasmic Dynein Is a Minus End-Directed Motor for Membranous Organelles. *Cell* **1989,** *56*, 937-946.
72. Birnbaum, K. D.; Sanchez Alvarado, A., Slicing across kingdoms: regeneration in plants and animals. *Cell* **2008,** *132*, 697-710.
73. Nedelec, F. J.; Surrey, T.; Maggs, A. C.; Leibler, S., Self-organization of microtubules and motors. *Nature* **1997,** *389*, 305-8.
74. Korn, E. D.; Carlier, M. F.; Pantaloni, D., Actin Polymerization and Atp Hydrolysis. *Science* **1987,** *238*, 638-644.
75. van Esch, J. H.; Klajn, R.; Otto, S., Chemical systems out of equilibrium. *Chem. Soc. Rev.* **2017,** *46*, 5474-5475.
76. Sorrenti, A.; Leira-Iglesias, J.; Markvoort, A. J.; de Greef, T. F. A.; Hermans, T. M., Non-equilibrium supramolecular polymerization. *Chem. Soc. Rev.* **2017,** *46*, 5476-5490.
77. Wang, Q. G.; Yang, Z. M.; Gao, Y.; Ge, W. W.; Wang, L.; Xu, B., Enzymatic hydrogelation to immobilize an enzyme for high activity and stability. *Soft Matter* **2008,** *4*, 550-553.
78. Hirst, A. R.; Roy, S.; Arora, M.; Das, A. K.; Hodson, N.; Murray, P.; Marshall, S.; Javid, N.;

Sefcik, J.; Boekhoven, J.; van Esch, J. H.; Santabarbara, S.; Hunt, N. T.; Ulijn, R. V., Biocatalytic induction of supramolecular order. *Nat. Chem.* **2010,** *2*, 1089-94.

79. Boekhoven, J.; Poolman, J. M.; Maity, C.; Li, F.; van der Mee, L.; Minkenberg, C. B.; Mendes, E.; van Esch, J. H.; Eelkema, R., Catalytic control over supramolecular gel formation. *Nat. Chem.* **2013,** *5*, 433-7.
80. Haines, L. A.; Rajagopal, K.; Ozbas, B.; Salick, D. A.; Pochan, D. J.; Schneider, J. P., Light-activated hydrogel formation via the triggered folding and self-assembly of a designed peptide. *J. Am. Chem. Soc.* **2005,** *127*, 17025-17029.
81. Song, B. L.; Zhao, J. X.; Wang, B. X.; Jiang, R., Synthesis and self-assembly of new light-sensitive Gemini surfactants containing an azobenzene group. *Colloid Surface A* **2009,** *352*, 24-30.
82. Kundu, P. K.; Samanta, D.; Leizrowice, R.; Margulis, B.; Zhao, H.; Borner, M.; Udayabhaskararao, T.; Manna, D.; Klajn, R., Light-controlled self-assembly of non-photoresponsive nanoparticles. *Nat. Chem.* **2015,** *7*, 646-52.
83. Ziemecka, I.; Koper, G. J. M.; Olive, A. G. L.; van Esch, J. H., Chemical-gradient directed self-assembly of hydrogel fibers. *Soft Matter* **2013,** *9*, 1556-1561.
84. Williams, R. J.; Smith, A. M.; Collins, R.; Hodson, N.; Das, A. K.; Ulijn, R. V., Enzyme-assisted self-assembly under thermodynamic control. *Nat. Nanotechnol.* **2009,** *4*, 19-24.
85. Rodon Fores, J.; Martinez Mendez, M. L.; Mao, X.; Wagner, D.; Schmutz, M.; Rabineau, M.; Lavalle, P.; Schaaf, P.; Boulmedais, F.; Jierry, L., Localized Supramolecular Peptide Self-Assembly Directed by Enzyme-Induced Proton Gradients. *Angew. Chem. Int. Edit.* **2017,** *56*, 15984-15988.
86. Rodon Fores, J.; Martinez Mendez, M. L.; Mao, X.; Wagner, D.; Schmutz, M.; Rabineau, M.; Lavalle, P.; Schaaf, P.; Boulmedais, F.; JIERRY, L., Localized Supramolecular Peptide Self‐Assembly Directed by Enzyme‐Induced Proton‐Gradients. *Angew. Chem. Int. Edit.* **2017**.
87. Spitzer, D.; Marichez, V.; Formon, G.; Besenius, P.; Hermans, T., Surface‐assisted self‐assembly of a hydrogel by proton diffusion. *Angew. Chem. Int. Edit.* **2018**.
88. Debnath, S.; Roy, S.; Ulijn, R. V., Peptide nanofibers with dynamic instability through nonequilibrium biocatalytic assembly. *J. Am. Chem. Soc.* **2013,** *135*, 16789-92.
89. Korevaar, P. A.; George, S. J.; Markvoort, A. J.; Smulders, M. M.; Hilbers, P. A.; Schenning, A. P.; De Greef, T. F.; Meijer, E. W., Pathway complexity in supramolecular polymerization. *Nature* **2012,** *481*, 492-6.
90. van Rossum, S. A. P.; Tena-Solsona, M.; van Esch, J. H.; Eelkema, R.; Boekhoven, J., Dissipative out-of-equilibrium assembly of man-made supramolecular materials. *Chem. Soc. Rev.* **2017,** *46*, 5519-5535.
91. Hess, H.; Ross, J. L., Non-equilibrium assembly of microtubules: from molecules to autonomous chemical robots. *Chem. Soc. Rev.* **2017,** *46*, 5570-5587.
92. Boekhoven, J.; Brizard, A. M.; Kowlgi, K. N.; Koper, G. J.; Eelkema, R.; van Esch, J. H., Dissipative self-assembly of a molecular gelator by using a chemical fuel. *Angew. Chem. Int. Edit.* **2010,** *49*, 4825-8.

93. Boekhoven, J.; Hendriksen, W. E.; Koper, G. J.; Eelkema, R.; van Esch, J. H., Transient assembly of active materials fueled by a chemical reaction. *Science* **2015,** *349*, 1075-9.
94. Tena-Solsona, M.; Riess, B.; Grotsch, R. K.; Lohrer, F. C.; Wanzke, C.; Kasdorf, B.; Bausch, A. R.; Muller-Buschbaum, P.; Lieleg, O.; Boekhoven, J., Non-equilibrium dissipative supramolecular materials with a tunable lifetime. *Nat. Commun.* **2017,** *8*, 15895.
95. Te Brinke, E.; Groen, J.; Herrmann, A.; Heus, H. A.; Rivas, G.; Spruijt, E.; Huck, W. T. S., Dissipative adaptation in driven self-assembly leading to self-dividing fibrils. *Nat. Nanotechnol.* **2018**.
96. Boekhoven, J.; Hendriksen, W. E.; Koper, G. J. M.; Eelkema, R.; van Esch, J. H., Transient assembly of active materials fueled by a chemical reaction. *Science* **2015,** *349*, 1075-1079.

Chapter 2

Hierarchically compartmentalized supramolecular gels through multilevel self-sorting

Abstract: Hierarchical compartmentalization through bottom-up approach is ubiquitous in living cells, but remains a formidable task in synthetic systems. Here we report on hierarchically compartmentalized supramolecular gels that are spontaneously formed by multilevel self-sorting. Two types of molecular gelators are formed in situ from non-assembling building blocks and self-sort into distinct gel fibers due to their different self-assembly rates; interestingly, these distinct fibers further self-sort into separated microdomains, leading to microscale compartmentalized gel networks. Such spontaneously multilevel self-sorting systems provide a "bottom-up" approach towards hierarchically structured functional materials, and may play a role in intracellular organization.

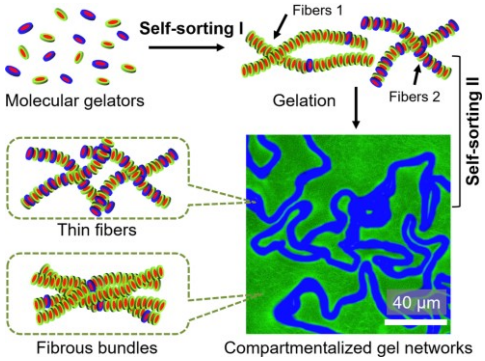

The content of this chapter is based on:

Yiming Wang, Matija Lovrak, Qian Liu, Chandan Maity, Vincent A. A. le Sage, Xuhong Guo, Rienk Eelkema, Jan H. van Esch*, Hierarchically compartmentalized supramolecular gels through multilevel self-sorting. *J. Am. Chem. Soc.* **2019**, *141*, 2847.

2.1 Introduction

The archetype example of compartmentalized systems are living cells,[1] in which hierarchical compartmentalization at the level of organelles followed by their intracellular organization enables complex physiological functions.[2-4] Interestingly, the spatial organization and functions of cells are entirely created through self-assembly of multicomponent biological subunits. Although the self-sorting of these different components into biological supramolecular structures is well known, the processes that lead to higher-level organization of these structures into different compartments remain poorly understood. To mimic the intracellular compartmentalization can not only improve our understanding on the intracellular scenario, but also inspire the design and construction of hierarchically compartmentalized functional objects,[5, 6] such as artificial cells,[7, 8] and microreactors.[9]

In recent years, much progress has been made towards the development and understanding of multicomponent self-assembly in synthetic systems.[10, 11] Especially self-sorting or orthogonal self-assembly, i.e. the independent self-assembly of different building blocks into distinct supramolecular structures,[12, 13] is a viable route towards complex systems composed of different coexisting supramolecular structures, such as fibers,[14-18] micelles or vesicles,[19-21] and liquid crystals.[22] Despite these advances, self-sorting in synthetic systems is still limited to the molecular level, and multilevel organization towards hierarchical supramolecular architectures remains an elusive goal.

Here we present a rare example of hierarchical compartmentalization at both nanoscale and microscale that has resulted exclusively by self-assembly of different synthetic molecules. We found that molecular gelators bearing a common self-assembling motif first self-sort into distinct nanofibers, which further self-sort into separated microdomains, resulting in hierarchically compartmentalized supramolecular gels. Our findings suggest that subtle variations in interactions can also enable self-sorting. Importantly, such hierarchically compartmentalized systems are formed spontaneously, without consumption of fuels, thereby contributing to our understanding on self-sorting and compartmentalization in both synthetic and natural systems.

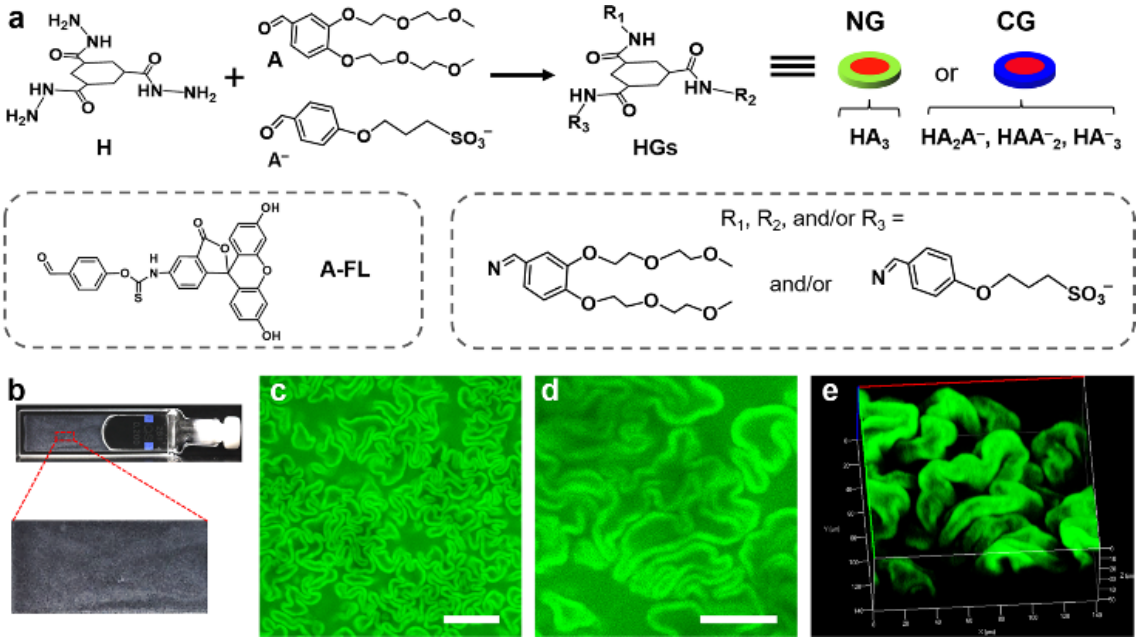

Figure 2.1. a) Schematic of formation of **HGs** from the precursors of **H**, **A**, and **A**$^-$; **A-FL** was used as a fluorescence label for self-assembled structures; b) photograph of the gel sample; c) CLSM image of the gel networks; d) magnified 2D and e) the corresponding 3D CLSM images (transparent mode) of the gel networks. 30 µM **A-FL** were added in c-e).

2.2 Results and discussion

In this work we used a modular supramolecular gel system with tunable properties, based on *in situ* formation of tris-hydrazone gelators (**HGs**) from soluble hydrazide (**H**) and aldehyde derivatives.[23-25] By combining a charged (**A**$^-$) and a neutral aldehyde (**A**) we obtained a multicomponent gelator system consisting of neutral (**NGs**: **HA$_3$**) and negatively charged gelators (**CGs**: **HA$_2$A**$^-$, **HAA**$^-_2$, and **HA**$^-_3$) (Figure 2.1a). We anticipated that the introduction of charges may prevent fiber bundling, thereby influencing the viscoelastic properties of the gels.[23-25]

In a typical experiment, a mixture of **H** (20 mM) and aldehydes **A** and **A**$^-$ (120 mM, 30 mol% **A**$^-$) dissolved in a phosphate buffer (0.1 M, pH 7.0) was allowed to react and self-assemble at room temperature. After 24 hours, a turbid gel was formed as determined by tube inversion test (Figure 2.1b). Surprisingly, CLSM investigation showed that the resulted gel consisted of worm-like microstructures (Figure 2.1c and d), which are very different from the typical fibrous networks observed in pure **HA$_3$** gels (Figure S2.1)[23-25] and other supramolecular gels.[26, 27] Three dimensional (3D) CLSM revealed that the gels consisted of closely packed crumpled sheets (Figure 2.1e and Movie S2.1), and the worm-like structures appeared to be 2D cross-sections of these sheets.

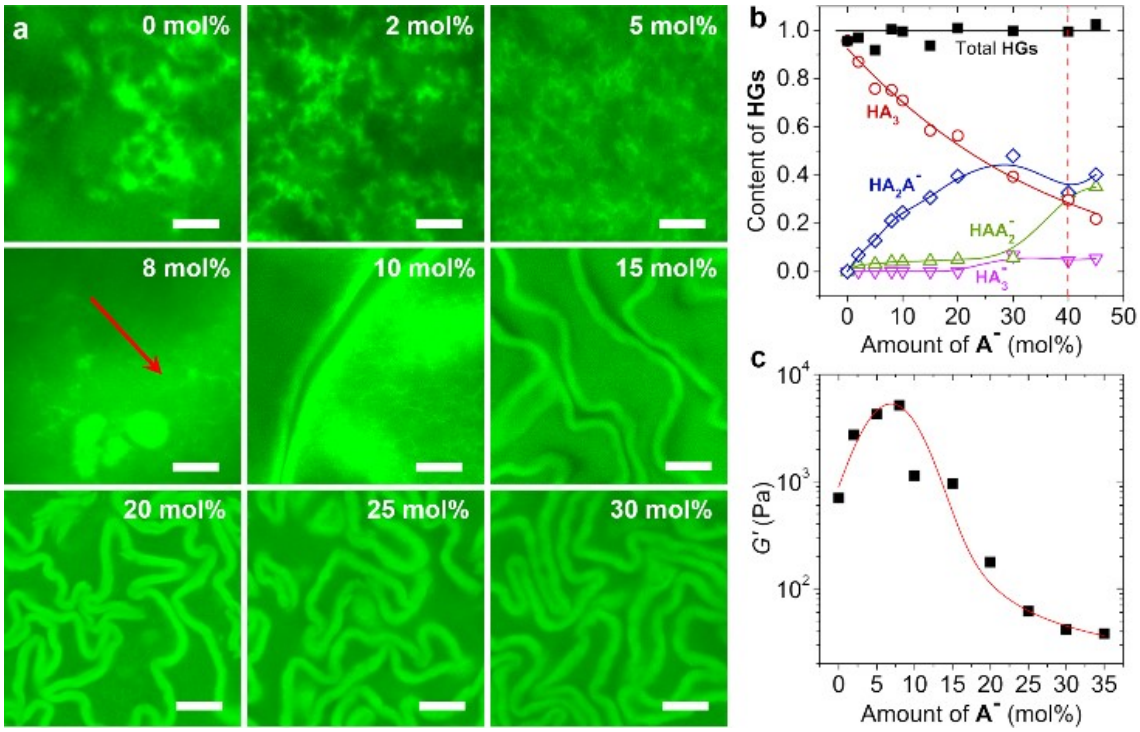

Figure 2.2. a) CLSM images of the gel networks formed with different mol% **A**$^-$, scale bars = 40 µm; b) gelator composition of the gels, the amount was normalized by the initial concentration of **H**; c) influences of mol% **A**$^-$ on the gel stiffness. All samples: [**H**] = 20 mM, [**A**] + [**A**$^-$] = 120 mM (different mol% **A**$^-$); and [**A-FL**] = 30 µM in a).

To investigate whether the appearance of the crumbled sheets are caused by the presence of **A**$^-$ we varied the amount of **A**$^-$ and explored its effects on the gel morphology (Figure 2.2a and S2.2). We found that gels were only formed if less than 40 mol% **A**$^-$ was added. Furthermore, the addition of small amounts of **A**$^-$ already led to a marked decrease in the size of the fibrous clusters (Figure 2.2a, 0 to 5 mol%). Interestingly, at 8 mol% **A**$^-$ some isolated structures were formed (arrowed area in Figure 2.2a), and further increasing the amount of **A**$^-$ led to crumpled sheets. Importantly, the density of the crumpled sheets increases with the amount of **A**$^-$, indicating that their appearance is related to the charged species. Analysis of the gel composition by high performance liquid chromatography (HPLC) confirmed that the gels consisted of the two types of gelators, i.e. **NGs** and **CGs**, as was expected (Figure 2.2b and S2.3). In each sample **H** was fully converted to **HGs** and the amount of **CGs** was increased with mol% **A**$^-$. This confirms the aforementioned correlation between the crumpled sheets and **CGs**. When the content of **A**$^-$ was > 40 mol%, the molar fraction of **CGs** was exceeded 0.75. Most likely, these high concentrations of **CGs** hinder either the self-assembly of gelators or crosslinking of fibers because of the electrostatic repulsion, with both scenarios explaining the lack of gel formation in samples with more than 40 mol% **A**$^-$.

After studying the gel structures, we applied oscillatory rheology to investigate the effects of the content of **A**$^-$ on the viscoelastic properties of the gels. We found that the addition of small amounts of **A**$^-$ from 0 up to 8 mol% led to an increase of *G'* from ~700 Pa to 5.0 kPa, but larger mol% **A**$^-$ caused a dramatic decrease of *G'*, from ~5.0 kPa (8 mol% **A**$^-$) to ~40 Pa (35 mol% **A**$^-$) (Figure 2.2c and S2.4). This *G'* maximum at 8 mol% **A**$^-$ coincides with the initial reduction of fiber cluster sizes followed by appearance of crumpled sheets as observed in the CLSM tests. Apparently, the reduction in cluster sizes leads to an increase in gel stiffness, whereas the formation of crumpled sheets weakens the gels.

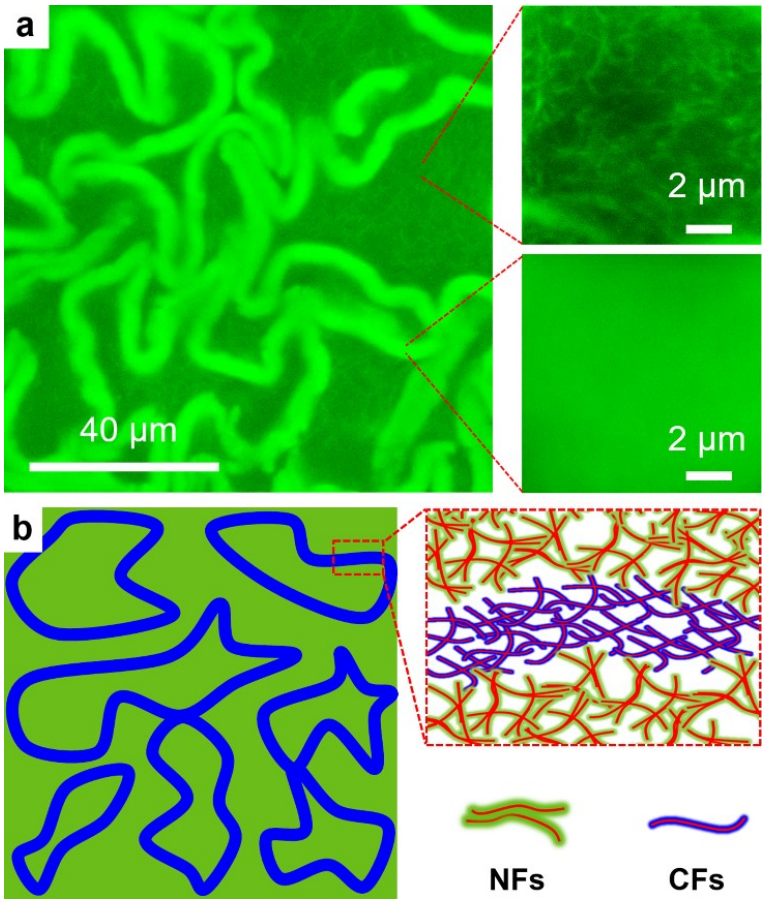

Figure 2.3. a) Morphologies of the gel networks in crumpled sheets and the areas in between the sheets; and b) possible composition of the gel networks. Sample: [**H**] = 20 mM, [**A**] + [**A**$^-$] = 120 mM (30 mol% **A**$^-$), and [**A-FL**] = 30 μM.

In the subsequent experiments, we are keen to unveil how these gel networks can be formed. Closer inspection of the gel networks by CLSM revealed that the areas in between the sheets displayed typical fibrous networks (right top in Figure 2.3a), similar to the morphology of **HA$_3$** gels,[23] while the crumpled sheets showed uniform fluorescence without any visible fibrous structures (right bottom in Figure 2.3a). Bleaching experiments revealed that the fluorescence only recovered slowly, indicating that the self-assembled structures in both areas were crosslinked (Figure

S2.5). Cryo-TEM confirmed that the gels are composed of two differently sized fibers, i.e. thin fibers with a diameter of ~5.3 nm, and thick fibrous bundles with a size of ~31 nm (Figure S2.6). In previous studies, we have found that single hydrazone fibers showed a typical diameter of ~ 5.5 nm.[23, 28] Moreover, polarized light microscopy showed that neither the crumpled sheets nor the fibrous networks are birefringent (Figure S2.7), indicating the random orientation of the fibers in these areas. We therefore conclude that the coarse network between the sheets consist of a randomly oriented fibrous bundles which are visible by CLSM, while the crumpled sheets consist of finer dispersed and randomly oriented thin fibers which cannot be resolved by optical microscopy.

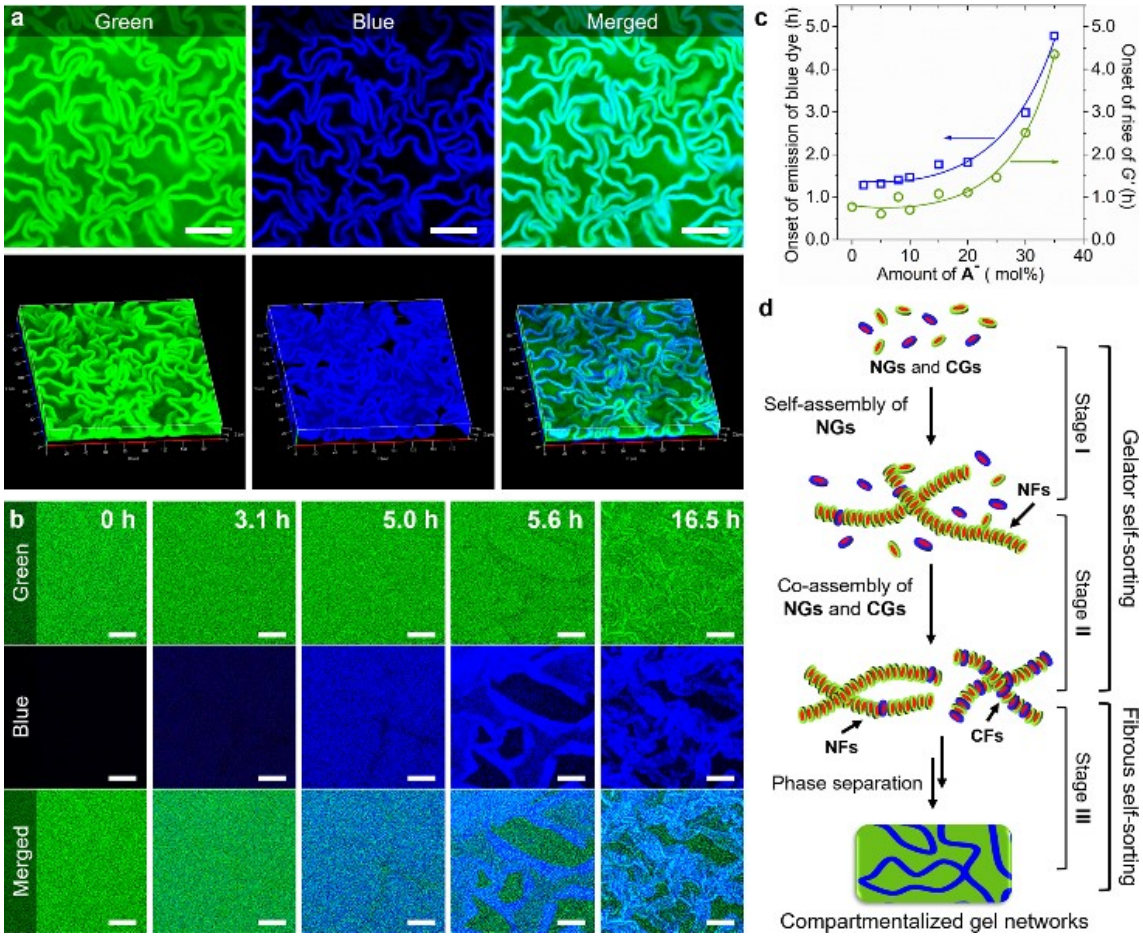

Figure 2.4. a) Split 2D (top) and the corresponding 3D (bottom) CLSM images of the gel networks; b) formation process of the gel networks; c) critical formation time of fibers as a function of mol% A^-; d) illustration of the multilevel self-sorting process. Samples in a-c): [H] = 20 mM, [A] + [A^-] = 120 mM (a, b including 30 mol% A^-), [A-FL] = 30 µM, and [Hoechst 33342] = 20 µM; Scale bars = 40 µm.

We were wondering how the formation of these different types of fibrous networks is related to the molecular composition of the gelators. Clearly, the appearance of the crumpled sheets is related to the presence of $\mathbf{A}^-$, while the regions

of coarser fibers in between the sheets are more prominent at lower mol% $\mathbf{A}^-$ (Figure 2.2a). Therefore, it seems likely that the fibrous bundles in the coarse networks are composed of neutral fibers (**NFs**) formed from **NGs** as they are prone to form fiber bundles.[23] In contrast, the finer fibers in the crumpled sheets are negatively charged fibers (**CFs**) formed from **CGs**, which can effectively prevent occurrence of bundling relying on the interfibrous electrostatic repulsion (Figure 2.3b). Most interestingly, the formation of fibers with different molecular composition and their subsequent organization into different macroscopic domains starting from a mixture of gelator molecules would involve the self-sorting of the fiber components first at the supramolecular level and subsequently at the macroscopic level.

To investigate the above hypothesis, we first investigated the distribution of **CFs** in the gel networks using CLSM by selectively staining the **CFs** with a cationic dye **Hoechst 33342** (blue, Figure S2.8). Simultaneously **A-FL** (green) was used to stain all fibers. CLSM showed again in the green channel the gel networks with the crumpled sheets, indicating that the presence of **Hoechst 33342** does not affect the gel morphology (Figure 2.4a). However, in the blue channel only the crumpled sheets appeared to be stained by the blue dye (Figure 2.4a and S2.2, Movie S2.2). Additionally, $\mathbf{HA_3}$ gel was not stained by **Hoechst 33342** (Figure S2.9), indicating no appreciable interactions between **NFs** and **Hoechst 33342**. These results unambiguously confirm that the crumpled sheets consist of **CFs** while the coarse networks are formed by **NFs**.

To investigate how self-sorting of a molecular mixture leads to different macroscopic domains, we monitored the formation of these gel networks over time by CLSM and rheology, while analyzing the molecular composition over time by HPLC. HPLC experiments showed that both **A** and $\mathbf{A}^-$ reacted with **H** at similar rates and complete conversion within 5 h (Figure S2.10), in line with a previous study.[23] This result confirms that the proposed self-sorting of **NGs** and **CGs** is not simply due to their different formation rates. We also employed rheology to monitor the network formation over time. We found that after ~40 min to ~4.3 h, depending on the amount of $\mathbf{A}^-$, *G'* started to rise, indicating the onset of fiber formation (Figure 2.4c and S2.4), and then gradually increased until reaching the final strengths.

Then, we followed the formation of the gel networks over time using CLSM by labeling the samples with both **A-FL** and **Hoechst 33342** to distinguish **CFs** from **NFs** (Figure 2.4b and Movie S2.3). Initially the sample only displayed green fluorescence, however, after ~1.3 to ~4.9 h, depending on the amount of $\mathbf{A}^-$, a homogenous blue fluorescence start to appear (Figure 2.4b, c). We assign the development of the blue fluorescence to the formation of **CFs**, and interestingly, its development is markedly

delayed compared to the onset of fiber formation as observed by rheology. Apparently, the onset of fiber formation as observed by rheology marks the formation of **NFs**, which precede the formation of **CFs**. The CLSM experiments showed that over the next two hours, the intensity of the blue fluorescence gradually increased but remained homogeneous. However, after ~5 h the blue fluorescence became inhomogeneous and after ~5.6 h blue stained sheet structures became visible and separated from the bulk area, gradually collapsing into a crumpled state. A control sample without addition of **Hoechst 33342** gave rise to the same gel formation process (Figure S2.11 and Movie S2.4), indicating the lack of impacts of the addition of **Hoechst 33342** on the gel formation process.

Altogether, these results clearly reveal that the formation of the gel networks with crumpled sheets proceed through three stages (Figure 2.4d). During the first stage, characterized by a rise of *G'* and absence of blue fluorescence, **NFs** are formed through self-assembly of **NGs**. Then, during the second stage, marked by the development of a homogeneous blue fluorescence, **CFs** start to form and remain homogeneously mixed with **NFs**. Most likely, the delayed formation of **CFs** compared to **NFs** is related to a higher critical assembly concentration (CAC) of **CGs** compared to **NGs**, caused by electrostatic repulsions between **CGs** (Figure S2.12). While **NGs** and **CGs** are formed at the same rate, **NGs** reach their CAC prior to **CGs**, leading to the kinetic self-sorting of **NGs** and **CGs** at the supramolecular level into **NFs** and **CFs**.[29] Finally, during the third stage, characterized by macroscopic phase separation, a second self-sorting process takes place at the macroscopic level, in which the **NFs** and **CFs** phase separate and form different macroscopic domains consisting of a coarse network of **NFs** and the crumpled sheets consisting of a fine network of **CFs**, respectively. Although the mechanism of this second self-sorting process remains unclear, it should be noted also in aqueous two phase systems, polyethylene glycol (PEG) polymers and anionic polyelectrolytes are prone to form separated phases.[30]

2.3 Conclusions

In summary, we have shown how multilevel self-sorting processes can lead to the spontaneous formation of hierarchically compartmentalized supramolecular gels. This finding would accelerate our understanding on both the natural and synthetic self-sorting systems, and can serve as a starting point for the "bottom-up" fabrication of hierarchically compartmentalized structures for applications in, such as synthetic biology,[7, 8] catalysis,[31, 32] and drug delivery.[33, 34]

2.4 References

1. Hurtley, S., Spatial cell biology. Location, location, location. Introduction. *Science* **2009,** *326*, 1205.
2. Brangwynne, C. P.; Tompa, P.; Pappu, R. V., Polymer physics of intracellular phase transitions. *Nat. Phys.* **2015,** *11*, 899-904.
3. Devos, D. P.; Graf, R.; Field, M. C., Evolution of the nucleus. *Curr. Opin. Cell. Biol.* **2014,** *28*, 8-15.
4. Nott, T. J.; Petsalaki, E.; Farber, P.; Jervis, D.; Fussner, E.; Plochowietz, A.; Craggs, T. D.; Bazett-Jones, D. P.; Pawson, T.; Forman-Kay, J. D.; Baldwin, A. J., Phase transition of a disordered nuage protein generates environmentally responsive membraneless organelles. *Mol. Cell* **2015,** *57*, 936-47.
5. Ahmed, R.; Patra, S. K.; Chabanne, L.; Faul, C. F. J.; Manners, I., Hierarchical Organometallic Materials: Self-Assembly of Organic-Organometallic Polyferrocenylsilane Block Polyelectrolyte-Surfactant Complexes in Bulk and in Thin Films. *Macromolecules* **2011,** *44*, 9324-9334.
6. Faul, C. F. J., Ionic Self-Assembly for Functional Hierarchical Nanostructured Materials. *Accounts Chem. Res.* **2014,** *47*, 3428-3438.
7. Deng, N. N.; Yelleswarapu, M.; Zheng, L.; Huck, W. T., Microfluidic Assembly of Monodisperse Vesosomes as Artificial Cell Models. *J. Am. Chem. Soc.* **2017,** *139*, 587-590.
8. Weiss, M.; Frohnmayer, J. P.; Benk, L. T.; Haller, B.; Janiesch, J. W.; Heitkamp, T.; Borsch, M.; Lira, R. B.; Dimova, R.; Lipowsky, R.; Bodenschatz, E.; Baret, J. C.; Vidakovic-Koch, T.; Sundmacher, K.; Platzman, I.; Spatz, J. P., Sequential bottom-up assembly of mechanically stabilized synthetic cells by microfluidics. *Nat. Mater.* **2018,** *17*, 89-96.
9. Hosta-Rigau, L.; Shimoni, O.; Stadler, B.; Caruso, F., Advanced Subcompartmentalized Microreactors: Polymer Hydrogel Carriers Encapsulating Polymer Capsules and Liposomes. *Small* **2013,** *9*, 3573-3583.
10. Safont-Sempere, M. M.; Fernandez, G.; Wurthner, F., Self-Sorting Phenomena in Complex Supramolecular Systems. *Chem. Rev.* **2011,** *111*, 5784-5814.
11. Kumar, D. K.; Steed, J. W., Supramolecular gel phase crystallization: orthogonal self-assembly under non-equilibrium conditions. *Chem. Soc. Rev.* **2014,** *43*, 2080-2088.
12. Kato, T., Self-assembly of phase-segregated liquid crystal structures. *Science* **2002,** *295*, 2414-8.
13. Heeres, A.; van der Pol, C.; Stuart, M.; Friggeri, A.; Feringa, B. L.; van Esch, J., Orthogonal self-assembly of low molecular weight hydrogelators and surfactants. *J. Am. Chem. Soc.* **2003,** *125*, 14252-3.
14. Cornwell, D. J.; Daubney, O. J.; Smith, D. K., Photopatterned Multidomain Gels: Multi-Component Self-Assembled Hydrogels Based on Partially Self-Sorting 1,3:2,4-Dibenzylidene-D-sorbitol Derivatives. *J. Am. Chem. Soc.* **2015,** *137*, 15486-92.
15. Moffat, J. R.; Smith, D. K., Controlled self-sorting in the assembly of 'multi-gelator' gels. *Chem. Commun.* **2009**, 316-318.

16. Colquhoun, C.; Draper, E. R.; Eden, E. G. B.; Cattoz, B. N.; Morris, K. L.; Chen, L.; McDonald, T. O.; Terry, A. E.; Griffiths, P. C.; Serpell, L. C.; Adams, D. J., The effect of self-sorting and co-assembly on the mechanical properties of low molecular weight hydrogels. *Nanoscale* **2014,** *6*, 13719-13725.
17. Draper, E. R.; Eden, E. G.; McDonald, T. O.; Adams, D. J., Spatially resolved multicomponent gels. *Nat. Chem.* **2015,** *7*, 848-52.
18. Singh, N.; Zhang, K.; Angulo-Pachon, C. A.; Mendes, E.; van Esch, J. H.; Escuder, B., Tandem reactions in self-sorted catalytic molecular hydrogels. *Chem. Sci.* **2016,** *7*, 5568-5572.
19. Brizard, A.; Stuart, M.; van Bommel, K.; Friggeri, A.; de Jong, M.; van Esch, J., Preparation of nanostructures by orthogonal self-assembly of hydrogelators and surfactants. *Angew. Chem. Int. Edit.* **2008,** *47*, 2063-6.
20. Boekhoven, J.; Brizard, A. M.; Stuart, M. C. A.; Florusse, L.; Raffy, G.; Del Guerzo, A.; van Esch, J. H., Bio-inspired supramolecular materials by orthogonal self-assembly of hydrogelators and phospholipids. *Chem. Sci.* **2016,** *7*, 6021-6031.
21. Vieira, V. M. P.; Hay, L. L.; Smith, D. K., Multi-component hybrid hydrogels - understanding the extent of orthogonal assembly and its impact on controlled release. *Chem. Sci.* **2017,** *8*, 6981-6990.
22. Kato, T.; Hirai, Y.; Nakaso, S.; Moriyama, M., Liquid-crystalline physical gels. *Chem. Soc. Rev.* **2007,** *36*, 1857-1867.
23. Boekhoven, J.; Poolman, J. M.; Maity, C.; Li, F.; van der Mee, L.; Minkenberg, C. B.; Mendes, E.; van Esch, J. H.; Eelkema, R., Catalytic control over supramolecular gel formation. *Nat. Chem.* **2013,** *5*, 433-7.
24. Poolman, J. M.; Boekhoven, J.; Besselink, A.; Olive, A. G.; van Esch, J. H.; Eelkema, R., Variable gelation time and stiffness of low-molecular-weight hydrogels through catalytic control over self-assembly. *Nat. Protoc.* **2014,** *9*, 977-88.
25. Poolman, J. M.; Maity, C.; Boekhoven, J.; van der Mee, L.; le Sage, V. A. A.; Groenewold, G. J. M.; van Kasteren, S. I.; Versluis, F.; van Esch, J. H.; Eelkema, R., A toolbox for controlling the properties and functionalisation of hydrazone-based supramolecular hydrogels. *J. Mater. Chem. B* **2016,** *4*, 852-858.
26. Du, X.; Zhou, J.; Shi, J.; Xu, B., Supramolecular Hydrogelators and Hydrogels: From Soft Matter to Molecular Biomaterials. *Chem. Rev.* **2015,** *115*, 13165-307.
27. Draper, E. R.; Adams, D. J., Low-Molecular-Weight Gels: The State of the Art. *Chem* **2017,** *3*, 390-410.
28. Wang, Y.; Versluis, F.; Oldenhof, S.; Lakshminarayanan, V.; Zhang, K.; Wang, Y.; Wang, J.; Eelkema, R.; Guo, X.; van Esch, J. H., Directed Nanoscale Self-Assembly of Low Molecular Weight Hydrogelators Using Catalytic Nanoparticles. *Adv. Mater.* **2018,** *30*, 1707408.
29. Raeburn, J.; Adams, D. J., Multicomponent low molecular weight gelators. *Chem. Commun.* **2015,** *51*, 5170-80.

30. Mace, C. R.; Akbulut, O.; Kumar, A. A.; Shapiro, N. D.; Derda, R.; Patton, M. R.; Whitesides, G. M., Aqueous multiphase systems of polymers and surfactants provide self-assembling step-gradients in density. *J. Am. Chem. Soc.* **2012,** *134*, 9094-7.
31. Shi, J. F.; Du, X. W.; Huang, Y. B.; Zhou, J.; Yuan, D.; Wu, D. D.; Zhang, Y.; Haburcak, R.; Epstein, I. R.; Xu, B., Ligand-Receptor Interaction Catalyzes the Aggregation of Small Molecules To Induce Cell Necroptosis. *J. Am. Chem. Soc.* **2015,** *137*, 26-29.
32. Tang, X. Y.; Huang, Z. H.; Chen, H.; Kang, Y. T.; Xu, J. F.; Zhang, X., Supramolecularly Catalyzed Polymerization: From Consecutive Dimerization to Polymerization. *Angew. Chem. Int. Edit.* **2018,** *57*, 8545-8549.
33. Boekhoven, J.; Koot, M.; Wezendonk, T. A.; Eelkema, R.; van Esch, J. H., A self-assembled delivery platform with post-production tunable release rate. *J. Am. Chem. Soc.* **2012,** *134*, 12908-11.
34. Majumder, P.; Baxa, U.; Walsh, S. T.; Schneider, J. P., Design of a multicompartment hydrogel that facilitates time‐resolved delivery of combination therapy and synergized killing of glioblastoma. *Angew. Chem. Int. Edit.* **2018**.

2.5 Supplementary information

Materials

Molecule **H**, **A**, **A**$^{-}$, and **A-FL** were synthesized as reported.[1-3] All commercial chemicals were purchased from Sigma Aldrich.

Experimental

CLSM measurement

CLSM measurements were performed on a Zeiss LSM 710 confocal laser scanning microscope equipped with a Zeiss Axio Observer inverted microscope and 40x PlanFluor oil immersion objective lens (NA 1.3). Incident laser with a wavelength of 488 nm and 405 nm was used to excite the fluorescein probe and **Hoechst 33342**, respectively. The pinhole was set to 1.0 airy unit during the measurements and the data were processed using ZEN 2009 software. Each sample was prepared in well-sealed imaging chambers (CoverWell PCI-0.5) and incubated at room temperature.

Rheological test

The Oscillatory rheological results were collected from a AR G2 TA rheometer equipped with a parallel-plate made of stainless steel (diameter is 40 mm) and a solvent trap to prevent the evaporation of solvent from the samples. All the measurements were performed in a strain controlled mode at 25 ^{o}C. The strain and the frequency for the time sweep measurements were set to 0.05% and 1.0 Hz, respectively. All the samples were prepared in 0.1 M phosphate buffer at pH 7.0. After mixing the stock solutions of the building blocks to the target concentration, the sample solution was transferred immediately onto the rheometer plate for the measurement.

Determination of the gel composition

The composition of the tris-hydrazone products in the gel was analyzed by high performance liquid chromatography (HPLC) using a gradient eluent flow of H_2O:(MeOH+0.4% triethylamine (TEA)) linearly varied from a ratio of 8:2 to 2:8, referring to a previous study.[1] The samples for the HPLC measurements were prepared by adding 80 µL gel sample into a mixture solution of 400 µL THF and 400 µL TEA saturated H_2O. The ratio of various HGs was calculated using the UV absorbance at the isosbestic point (275 nm). HPLC-MS (Figure S2.3): **A**, elution time = 9.0 min, MS (ESI, positive) m/z = 365.4 $(M+Na)^{+}$; **A**$^{-}$, elution time = 1.45 min, MS (ESI, negative) m/z = 243.0 $(M-H)^{-}$; **HA$_3$**, elution time = 15.3 min, MS (ESI, positive) m/z =

1253.55 $(M+Na)^+$; **HA_2A^-**, elution time = 10.5 min, MS (ESI, negative) m/z = 584.3 $(M+2H_2O-2H)^{2-}$; **HAA^-_2**, elution time = 2.4 min, MS (ESI, negative) m/z = 517.3 $(M-2H)^{2-}$, 534.0 $(M+2H_2O-2H)^{2-}$; **HA^-_3**, elution time = 1.2 min, MS (ESI, negative) m/z = 317.0 $(M+H_2O-3H)^{3-}$.

Cryo-TEM measurements

A Gatan model 626 cryo-stage in a JEOL JEM 1400 Plus electron microscope was employed to characterize the morphologies of the gel networks. The operating voltage was 120 kV. For the measurements, 5 µL of the gel samples were carefully deposited on a Quantifoil R 1.2/1.3 100 Holey carbon films coated Cu 200 mesh grid. After blotting, the grid was rapidly inserted into liquid ethane. The frozen-hydrated sample was always stored in liquid nitrogen before the observation. The cryo-TEM images were recorded under low-dose conditions on a slow scan CCD camera (Gatan, model 830).

Polarizing light microscope measurements

A gelator precursor solution including 20 mM H, 120 mM (**A** + **A^-**) (containing 30 mol% **A^-**) in 0.1 M phosphate buffer at pH 7.0 was prepared and transferred into a glass chamber made by two glass slides with a PDMS spacer in between. After the gel formation, the network structures of the generated gel were analyzed on a Nikon E400POL polarizing microscope.

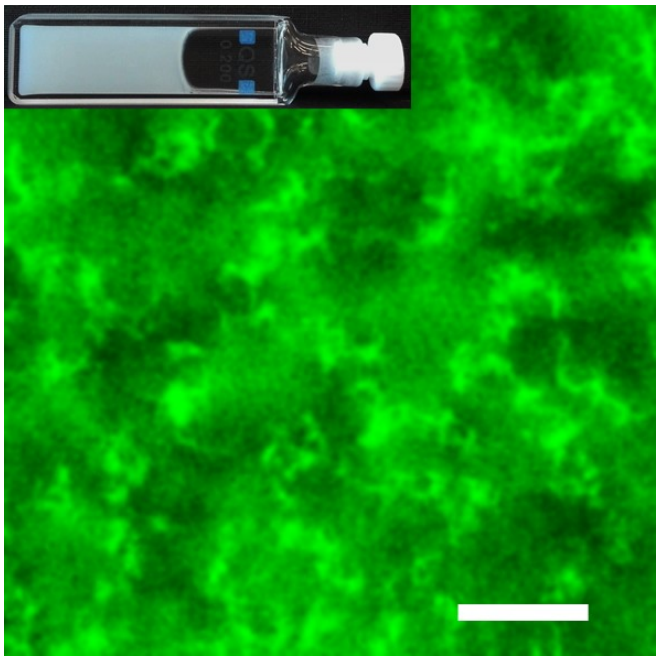

Figure S2.1. CLSM image and photograph of the gel prepared with 20 mM **H** and 120 mM **A** in 0.1 M phosphate buffer at pH 7.0, scale bar = 40 μm, 30 μM **A-FL** was added to label the gel.

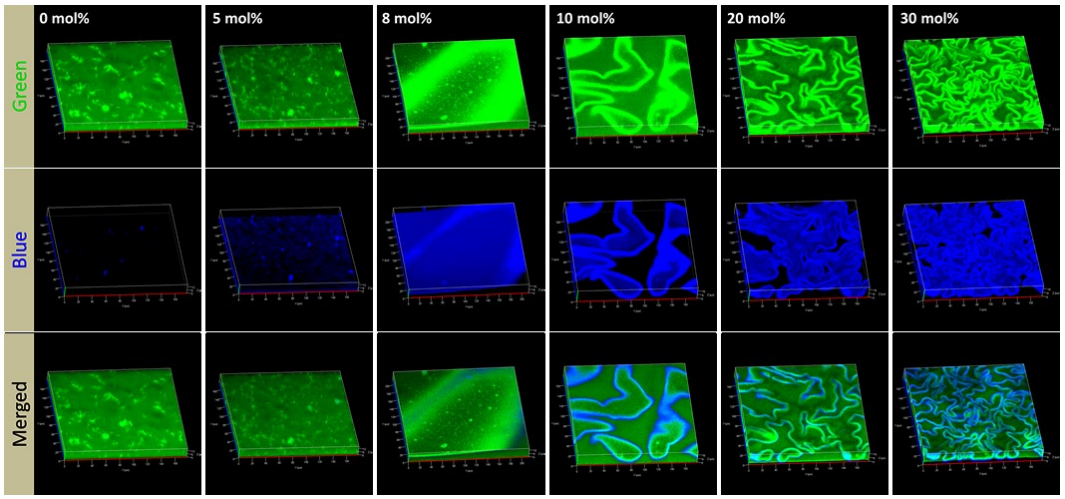

Figure S2.2. 3D CLSM images of the crumpled gel networks formed with different ratio of $\mathbf{A}^-$. Samples: [**H**] = 20 mM, [**A**] + [$\mathbf{A}^-$] = 120 mM (including different mol% $\mathbf{A}^-$), [**A-FL**] = 30 μM, [**Hoechst 33342**] = 20 μM.

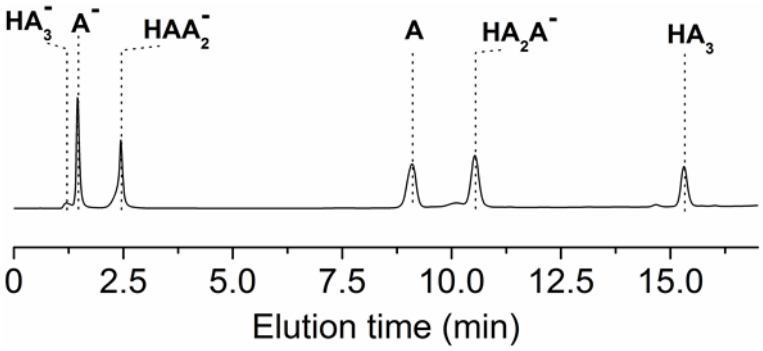

Figure S2.3. HPLC spectrum of the gel samples. The gel sample is prepared with 20 mM **H**, and 120 mM (**A** + **A**$^-$) (including 35 mol% **A**$^-$).

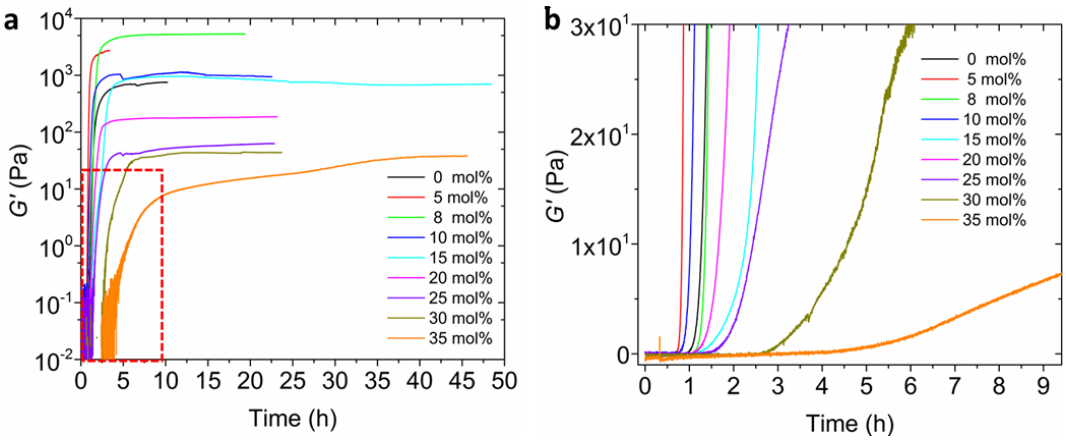

Figure S2.4. a) Evolution of *G′* against time for the samples prepared with different content of **A**$^-$, b) magnified graph corresponding to the red doted rectangle in a). Samples: [**H**] = 20 mM [**A**] + [**A**$^-$] = 120 mM (containing different mol% **A**$^-$).

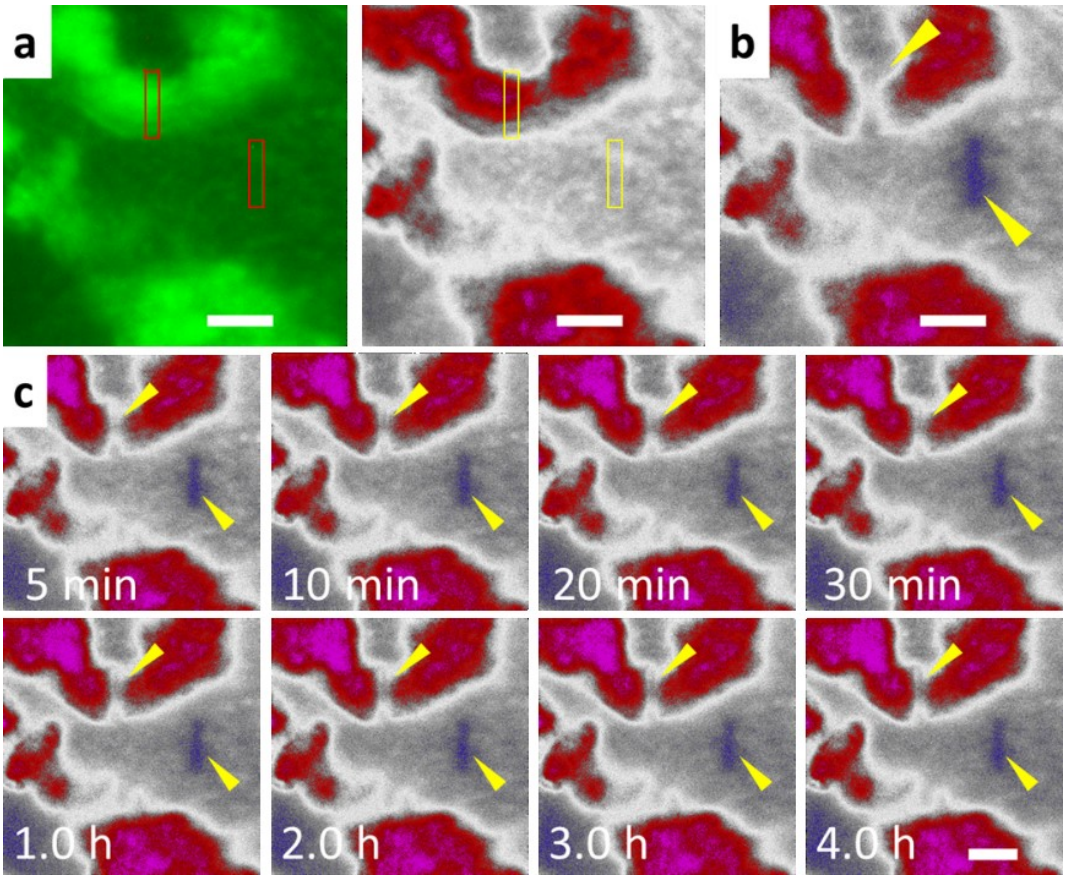

Figure S2.5. CLSM images of the gel networks a) before (rectangle areas), and b) after (yellow arrows) bleaching; c) evolution of the bleached areas over time. Sample: [**H**] = 20 mM, [**A**] + [**A**$^-$] = 120 mM (30 mol% **A**$^-$), [**A-FL**] = 30 µM, and [**Hoechst 33342**] = 20 µM. Scale bars are 10 µm. The fluorescence intensity of the bleached regions in both the crumpled sheets and the fibrous networks did not recover over a period of 4.0 h, indicating the crosslinked nature in both areas.

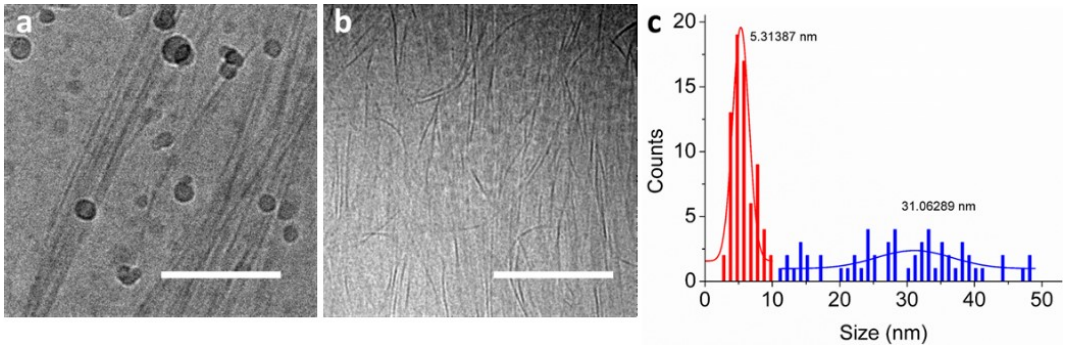

Figure S2.6. Cryo-TEM images of the gel fibers in the gel, a) area with more fibrous bundles; b) area with more thin fibers; and c) statistical size distribution of the fibers in the gel sample, 130 fibers or bundles were randomly counted. Scale bar in a and b) is 200 nm. Sample: [**H**] = 20 mM, [**A**] + [**A**$^-$] = 120 mM (including 30 mol% **A**$^-$).

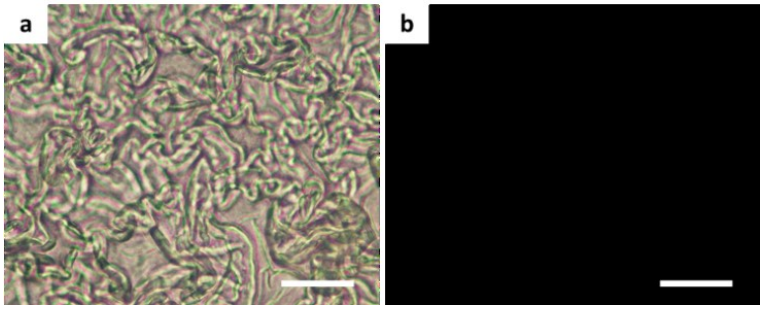

Figure S2.7. Polarizing light microscope images of the crumpled gel networks placed between a) parallel polarizer and b) crossed polarizers. Scale bars = 40 µm. Sample: [**H**] = 20 mM, [**A**] + [**A**$^-$] = 120 mM (including 30 mol% **A**$^-$).

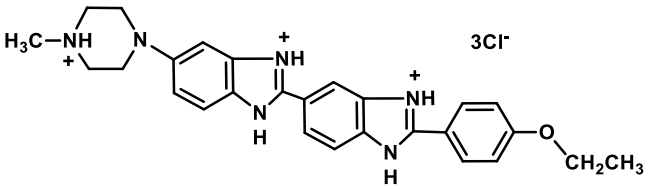

Figure S2.8. Chemical structure of **Hoechst 33342**.

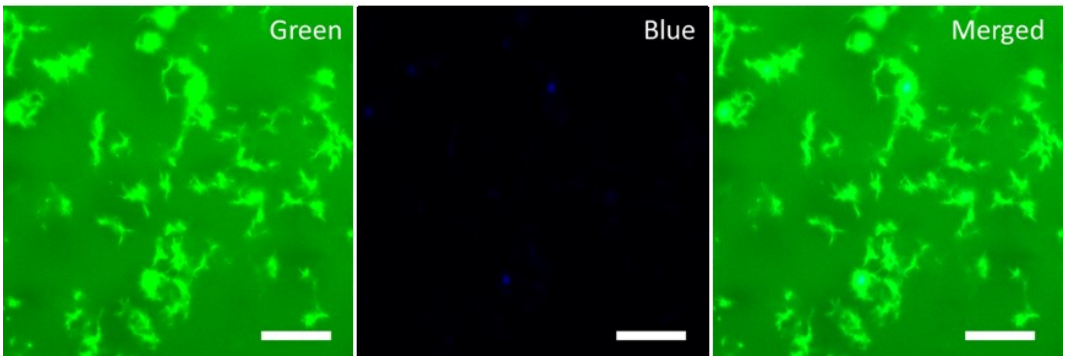

Figure S2.9. Confocal images of the gel networks prepared with pure **A**. Sample: [**H**] = 20 mM, [**A**] = 120 mM, [**A-FL**] = 30 µM (green), [**Hoechst 33342**] = 20 µM (blue). Scale bars = 40 µm.

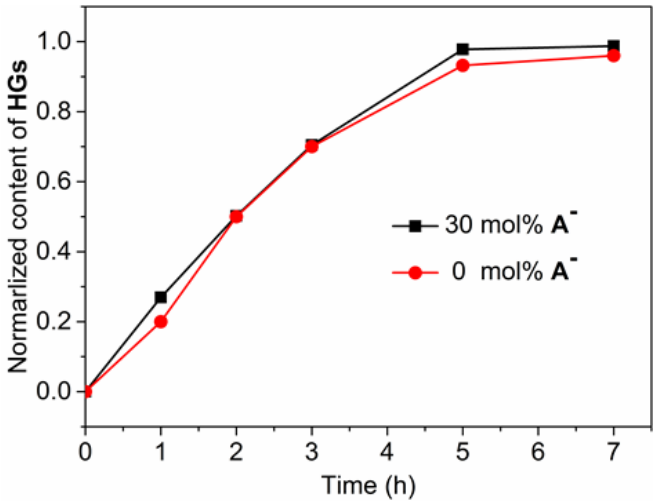

Figure S2.10. Formation of tris-hydrazone gelators (**HGs**) over time monitored by HPLC. Samples: [**H**] = 20 mM, [**A**] + [**A**$^-$] = 120 mM (including 0 and 30 mol% **A**$^-$, respectively).

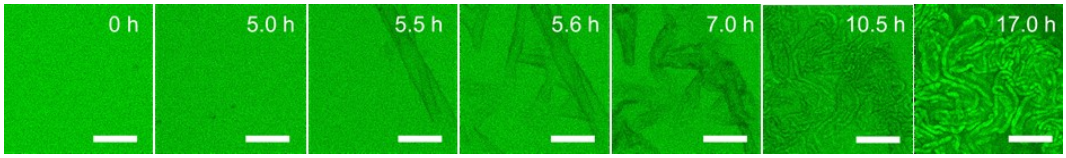

Figure S2.11. Formation of the gel networks without addition of **Hoechst 33342** over time, scale bars = 40 μm. Sample: [**H**] = 20 mM, [**A**] + [**A**$^-$] = 120 mM (30 mol% **A**$^-$), and [A-FL] = 30 μM.

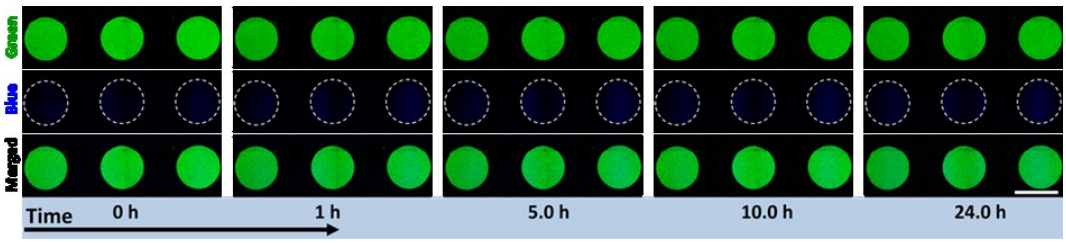

Figure S2.12. Fluorescence evolution of different channels over time. Sample: [**H**] = 20 mM [**A**] + [**A**$^-$] = 120 Mm (for each time point, the left sample 40 mol% **A**$^-$, the middle 45 and the right sample 50 mol%), [**A-FL**] = 30 μM (green), [**Hoechst 33342**] = 20 μM (blue). Scale bar for each subimage is 5 mm. The sample is prepared in a μ-Slide Angiogenesis (Ibidi) microscopy chamber with a glass bottom and sealed with grease. In the blue channel, ignorable blue fluorescence can be observed, indicating the failure of formation of **CFs**. It also demonstrates that the critical assembly concentration (CAC) of **CGs** is pretty high such that their self-assembly can only be achieved through coassembly with **NGs**, by which the strong electrostatic repulsions between **CGs** caused by immediate face-to-face stack of **CGs** would be released.

Reference

1. Boekhoven, J.; Poolman, J. M.; Maity, C.; Li, F.; van der Mee, L.; Minkenberg, C. B.; Mendes, E.; van Esch, J. H.; Eelkema, R., Catalytic control over supramolecular gel formation. *Nat. Chem.* **2013,** *5*, 433-7.
2. Poolman, J. M.; Boekhoven, J.; Besselink, A.; Olive, A. G.; van Esch, J. H.; Eelkema, R., Variable gelation time and stiffness of low-molecular-weight hydrogels through catalytic control over self-assembly. *Nat. Protoc.* **2014,** *9*, 977-88.
3. Suzuka, T.; Kimura, K.; Nagamine, T., Reusable Polymer-Supported Terpyridine Palladium Complex for Suzuki-Miyaura, Mizoroki-Heck, Sonogashira, and Tsuji-Trost Reaction in Water. *Polymers* **2011,** *3*, 621-639.

Chapter 3

Access to metastable gel states using seeded self-assembly of low molecular weight gelators

Abstract: Here we report on how metastable supramolecular gels can be formed through seeded self-assembly of multicomponent gelators. Hydrazone-based gelators decorated with non-ionic and anionic groups are formed in situ from hydrazide and aldehyde building blocks, and lead through multiple self-sorting processes to the formation of heterogeneous gels at thermodynamic equilibrium. Interestingly, the addition of seeds composing of oligomers of gelators bypasses the self-sorting processes and accelerate the gelation along a kinetically favored pathway, resulting in homogeneous gels of which the network morphologies and gel stiffness are markedly different from the thermodynamic gel products. Importantly, over time, these metastable homogeneous gel networks are capable of converting into the thermodynamically stable state. This seeding-driven formation of non-equilibrium supramolecular structures is expected to serve as a simple approach towards functional materials with pathway-dependent properties.

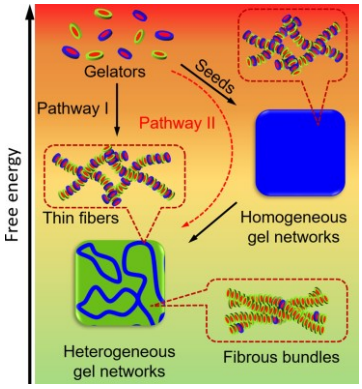

The content of this chapter is based on:
Yiming Wang, Robin de Kruijff, Matija Lovrak, Xuhong Guo, Rienk Eelkema, Jan H. van Esch*, Access to metastable gel states using seeded self-assembly of low molecular weight gelators. *Angew. Chem. Int. Ed.* **2019**. DOI: 10.1002/anie.201812412.

3.1 Introduction

Out-of-equilibrium supramolecular self-assembly is widespread in nature and endows biological system with extraordinary functions such as adaptation,[1-3] intracellular transport,[4-6] self-replication,[7-9] and autonomous self-healing,[10-12] that are rare in inanimate world. Inspired by biological system, research interests in supramolecular chemistry are now shifting to the implementation of out-of-equilibrium self-assembly in artificial scenario.[13-19] An important focus of out-of-equilibrium self-assembly is the selection of specific self-assembly pathways along a corrugated self-assembly energy landscape, that leads to products temporarily or permanently retained in a local rather than the global minimum. In recent efforts, specific pathways are selected through the employment of, e.g., rationally designed molecules,[20-22] or catalysts,[23-27] and features the formation of different out-of-equilibrium structures bearing different material properties while still employing the same building blocks. Despite these prospects, the current approaches towards kinetically controlled self-assembly remain scarce.[15]

In this work, we present how the formation of supramolecular gels can be guided towards a metastable state through seeded self-assembly of multicomponent gelators. The employment of seeds has been realized as an effective way to accelerate and direct the self-assembly processes,[28-33] and different kinds of well-defined supramolecular structures have been prepared.[34-38] Nevertheless, most cases of seeded self-assembly give rise to the thermodynamic products, and only few examples of seeded self-assembly have been reported that lead to the formation of supramolecular structures that are temporarily stabilized at a metastable state.[39-40] Recently, we have reported on a multicomponent tris-hydrazone gelator (**HGs**) system in which two kinds of gelators, neutral (**NGs**) and charged ones (**CGs**), are formed *in situ* from the building blocks consisting of the hydrazide (**H**) and a mixture of a neutral aldehyde (**A**) and negatively charged aldehyde ($\mathbf{A}^-$) (Figure 3.1a).[41] Previous studies have shown that the resulting **NGs** and **CGs** undergo a kinetic self-sorting process into neutral fibers (**NFs**) and negatively charged fibers (**CFs**), which in turn can further self-sort into compartmentalized gel networks composed of **CFs**-rich crumpled sheets with **NFs**-rich coarse fibrous networks in between (Figure 3.1b and S3.1).[41] Here, we show our approaches to control the self-assembly of **NGs** and **CGs** through interfering with the nucleation step, thereby yielding a handle to control the structures and the corresponding material properties of the resulting gels.

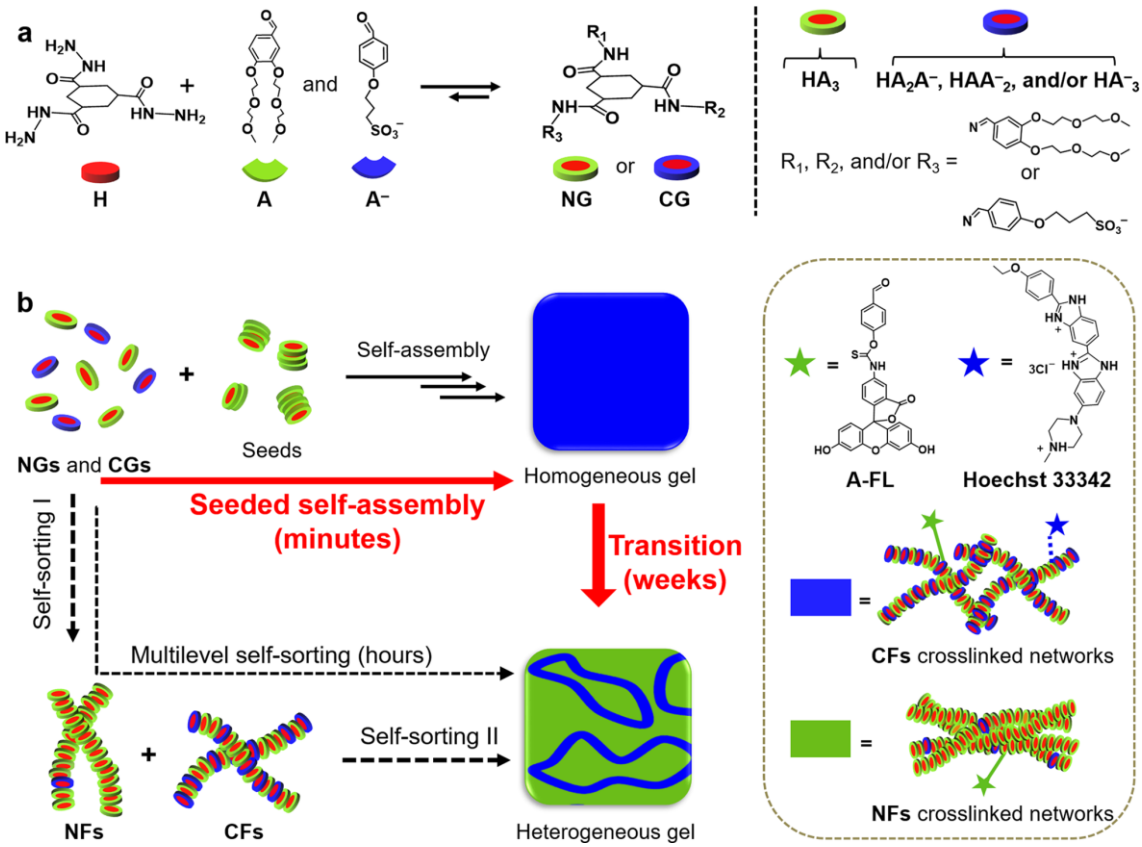

Figure 3.1. a) Scheme of the formation of **NGs** (HA_3) and **CGs** (HA_2A^-, HAA^-_2, and HA^-_3) from the building blocks of **H**, **A**, and A^-; b) illustration of the self-assembly of **NGs** and **CGs** along different pathways controlled by seeds leading to different gel products. Fluorescent probes of **A-FL** and **Hoechst 33342** are used to label all the gel fibers and **CFs**, respectively.

It has been well established that seeds can act as nucleation centers for crystallization and other types of nucleated self-assembly, and hence the addition of seeds effectively bypasses the energy barrier of nucleation.[42] Here, we exploit this feature and use seeds consisting of preformed hydrazone gelators to control the nucleation of **NGs** and **CGs**, and subsequently to control the self-assembly and gelation processes (Figure 3.1b). We find that the addition of seeds can dramatically accelerate the gelation process and enhance the gel stiffness. Importantly, the acceleration achieved by seeded self-assembly bypasses the self-sorting of **NGs** and **CGs** observed during unseeded self-assembly, because self-sorting is due to the different nucleation rates of **NGs** and **CGs**.[41] Instead, seeded self-assembly leads to co-assembly of **NGs** and **CGs**, and ultimately to a homogeneous gel network consisting of a high density of crosslinked thin **CFs** (Figure 3.1b). Interestingly, these homogeneous gels have a finite life time, and over time (weeks) slowly convert into the compartmentalized gels consisting of domains of **CFs** and **NFs**, thus further underpinning their metastable state and equilibrium state, respectively.

3.2 Results and discussion

In this study, unless mentioned otherwise, all the samples are prepared using phosphate-buffered (0.1 M, pH 7.0) stock solutions of **H**, **A**, and **A**$^-$; the concentration of aldehyde (**A** + **A**$^-$) is kept at six times higher than **H** to ensure a full conversion of **H** into **HGs**.[25, 43] Aldehyde tailored fluorescein (**A-FL**) dye (green, 30 μM) and cationic **Hoechst 33342** (blue, 20 μM) are added to label the self-assembled structures for confocal laser scanning microscopy (CLSM) observations (Figure 3.1b). The seed solution consists of a dispersion of short hydrazone fibers with length of ~30 nm and diameter of ~5.6 nm that are prepared by sonication of pre-formed **NFs** (see supporting information, Figure S3.2), and the concentration of seeds is expressed by the total concentration of gelators.

To explore the influence of seeds on the gel formation, we first performed oscillatory rheology measurements. We found that the addition of seeds can dramatically accelerate the gelation process. The gelation time (the time at which the storage modulus *G′* starts to exceed the loss modulus *G″*) showed a drop from ~2.7 h to ~0.7 h (30 mol% **A**$^-$) or from~0.75 h to ~3.5 min (0 mol% **A**$^-$) upon addition of seeds from 0 to 1.5 mM (Figure 3.2a). Moreover, the stiffness of the resulting gels increased from ~40 Pa to ~3.0 kPa (30 mol% **A**$^-$) or from ~700 Pa to ~20.0 kPa (0 mol% **A**$^-$), upon increasing the concentration of seeds from 0 to 1.5 mM (Figure 3.2b). These observations clearly demonstrate that the addition of seeds facilitates the gelation process and alters the mechanical properties of the resulting gels. Moreover, the measurements of critical gelation concentration (CGC) of **H**, equal to the final concentration of **HGs**, showed that the addition of seeds remarkably decreased the CGC (see supporting information, Figure 3.2c), leading to a drop from ~20 mM (no seeds) to less than 3 mM (1.5 mM seeds), which further verifies that the addition of seeds can accelerate the self-assembly of gelators.[25, 44] On the basis of these results, it is likely that the addition of seeds facilitates the nucleation of **HGs** by bypassing the nucleation energy barriers, which activates an earlier occurrence of the elongation and branching of the gel fibers, thereby leading to the faster gelation, higher gel stiffness and lower CGC.

However, the effect of seeding on gelation times, gel stiffness, and CGC levels off when the concentration of added seeds was > 1.0 mM (Figure 3.2a-c). This observation suggests that at these seed concentrations gel formation has become so fast that the formation of **HGs** from the precursors rather than nucleation has become rate-limiting. Previously, we have found that the formation rate of gelators also presents significant effects on the self-assembly and the subsequent gelation process.[25, 44] Therefore, we investigated the rate of gelator formation and the effect of

seeding thereon in more detail by following gelator formation over time by high performance liquid chromatography (HPLC). The results showed that the **H** was fully converted to **HGs** within 5.0 h, which is nicely in line with previous studies (Figure S3.3).[25, 41] Importantly, the hydrazone products, including the main components $\mathbf{HA_3}$ and $\mathbf{HA_2A^-}$, are formed at very similar rates, and are not affected by the presence of seeds. It therefore demonstrates that the seeds facilitate the gel formation through accelerating the nucleation rather than the formation of the gelators.

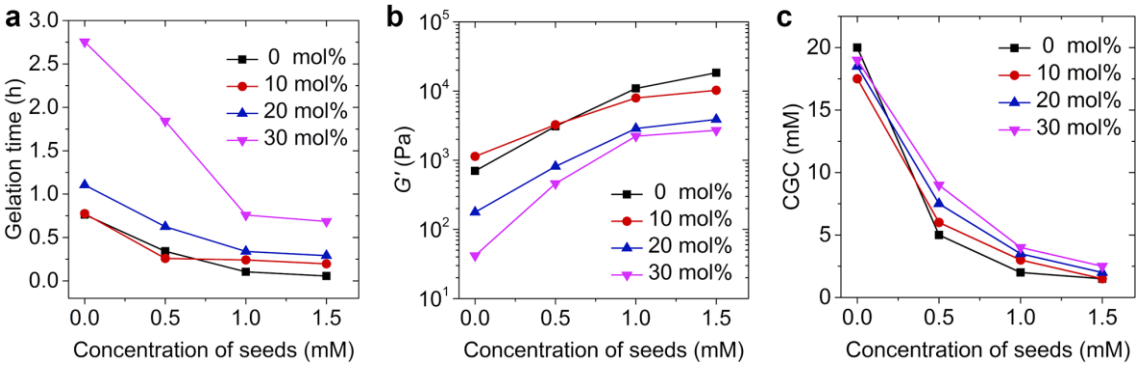

Figure 3.2. Effects of seeds on a) gelation time; b) gel stiffness; and c) CGC for the samples containing different mol% $\mathbf{A^-}$. Samples in a, b): [**H**] = 20 mM, [**A** + $\mathbf{A^-}$] = 120 mM.

The preceding rheological and CGC measurements lead us to investigate how the addition of seeds impact the morphologies of the gel networks. For this purpose, gel samples with different concentration of seeds were prepared and observed by CLSM. We found that the addition of seeds presented dramatic effects on the morphologies of the gel networks (Figure 3.3). For the sample without **CGs** (Figure 3.3, 0 mol% $\mathbf{A^-}$), the morphology changed from large clusters to densely crosslinked thin bundles upon increasing the concentration of seeds from 0 to 1.5 mM. For the samples with increasing amounts of **CGs** (Figure 3.3, 10 to 30 mol% $\mathbf{A^-}$), without the addition of seeds, compartmentalized gel networks composed of **CFs**-rich crumpled sheets with **NFs**-rich coarse networks in between are formed (Figure S3.4), in line with the previous study.[41] Interestingly, upon the addition of seeds, the crumpled sheet structures gradually disappeared, and instead, homogeneous networks composed of dense thin fibrous bundles are formed. Apparently, the decrease in the dimension of the fibrous structures with the addition of seeds enhances the crosslinking degree of the resulted gel networks, which explains the above CGC and rheological results. When the concentration of added seeds was higher than 1.0 mM, completely uniform fluorescence without any fibrous structures were observed in the gel networks (Figure 3.3, 10 to 30 mol% $\mathbf{A^-}$), and the transparency of the gel samples increased with the content of $\mathbf{A^-}$, giving rise to a complete transparent gel for the

sample prepared with 30 mol% **A**$^-$ (Figure S3.5). Cryo-TEM test revealed that these uniform gel networks consisted of single nanofibers with a diameter of ~5.5 nm with very few large bundles (Figure S3.6). The small diameters of the fibers are consistent with the homogeneity of the gel networks observed on CLSM. Also after the addition of cationic **Hoechst 33342** dye, these gel networks exhibit uniform blue fluorescence (Figure S3.4), which indicates that the uniform gel networks are composed of **CFs**. These results strongly suggest that the seeds bypass the nucleation energy barrier of **NGs** and **CGs**, and reduce the difference in the nucleation rates of **NGs** and **CGs**, thereby leading to co-assembly of **NGs** and **CGs** at the expense of self-sorting. As a result, **CFs** are exclusively formed and crosslink into the homogeneous gel networks. The electrostatic repulsion between **CFs** is thought to effectively prevent the occurrence of bundling which explains the small diameters of the fibers and homogeneity of the gels.

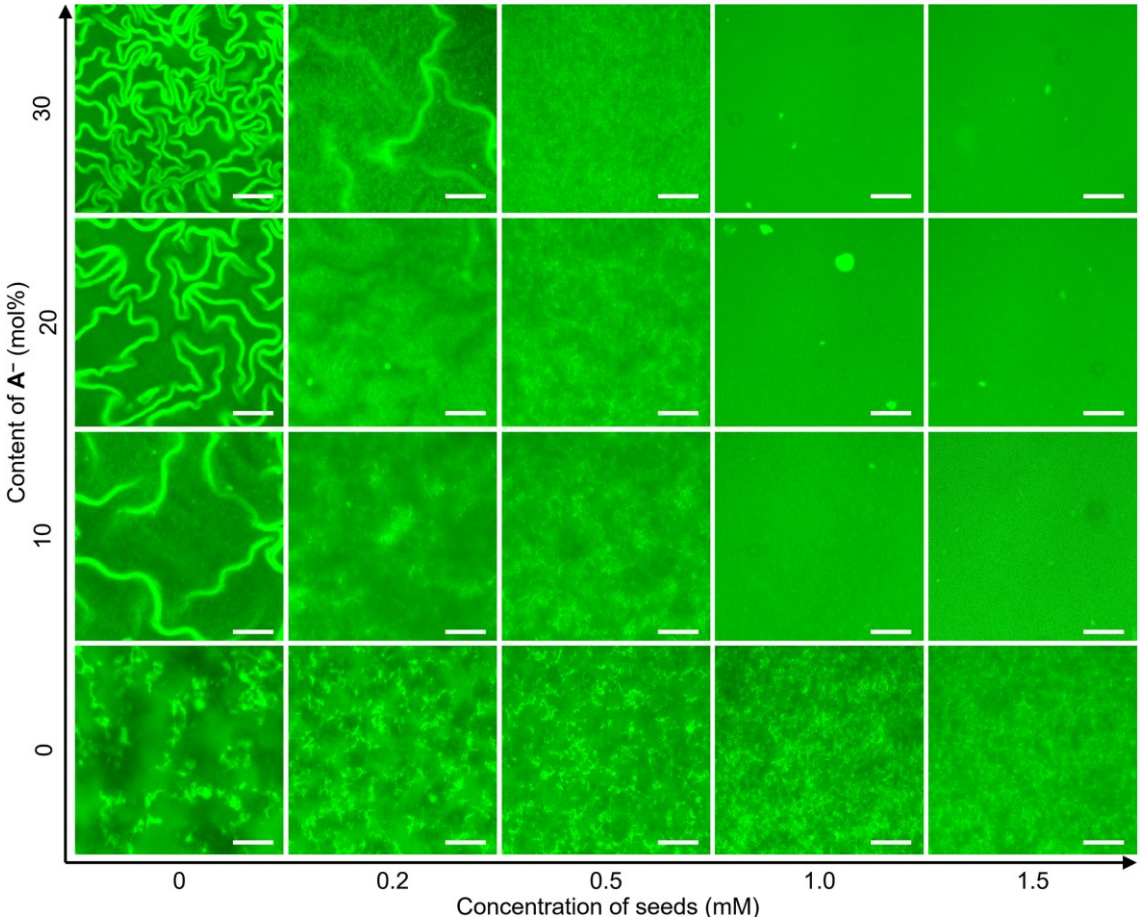

Figure 3.3. CLSM images of the gel networks formed with different concentration of seeds and different mol% **A**$^-$. Samples: [**H**] = 20 mM, [**A** + **A**$^-$] = 120 mM (different mol% **A**$^-$), [**A-FL**] = 30 µM. Scale bars = 40 µm.

Interestingly, after storing the gel samples for 3 weeks at room temperature, we found that the transparent gel prepared with 30 mol% **A**$^-$ became turbid (Figure 3.4a).

We studied the morphological changes by CLSM. To our surprise, the previously obtained homogeneous gel network transformed into a heterogeneous state (Figure 3.4a and b). These heterogeneous gels contained crumpled sheet structures that are separated from the bulk networks, with the overall morphology very similar to the gel obtained from unseeded samples (Figure 3.3 and S3.1). Indeed, after addition of **Hoechst 33342**, we found that the crumpled structures emitted strong blue fluorescence, indicating that the crumpled sheets are negatively charged. Moreover, some small clusters were observed and showed lower intensity of blue fluorescence, indicating the formation of bundling fibers with low dose of charges. These observations are consistent with the previous study,[41] and it can be concluded that over time the initially formed homogenous gels transformed into compartmentalized gel networks composed of separated charged crumpled sheets and less charged coarse networks. Similar structure transformations in the other uniform gels prepared with different mol% $\mathbf{A}^-$ were observed as well after three-week incubation (Figure S3.7).

These observations clearly indicate that in the initially formed uniform gel networks, the **CFs** consisting of **NGs** and **CGs** are dynamic at the time scale of weeks. Most interestingly, the transformation from a homogenous to a heterogeneous network appeared to be a spontaneous process implying that the heterogeneous network is the thermodynamically favored gel structure, while the homogenous network is in a metastable state. Moreover, the formation of the gels can follow multiple pathways, which point to a complex energy landscape (Figure 3.4c). Without seeding, gel formation typically follows pathway I: a self-sorting of **NGs** and **CGs** driven by their different self-assembly rates results in the formation of a mixture of **NFs** and **CFs**. These mixed fibers undergo a higher-level self-sorting leading to the thermodynamically more stable heterogeneous gels composed of **CFs**-rich crumpled sheets with **NFs**-rich coarse networks in between.[41] However the addition of seeds leads the system to follow pathway II: here, the addition of seed bypasses the nucleation barrier of **NGs** and **CGs** and eliminates the difference in their self-assembly rates. As a result, a co-assembly of **NGs** and **CGs** instead of self-sorting is achieved and leads to the exclusive formation of **CFs** which in turn crosslink into metastable homogeneous gels. Importantly, these metastable gels are temporarily stablized at a local energy minimum state and convert into the thermodynamically more stable gel states over a period of several weeks (Figure 3.4c).

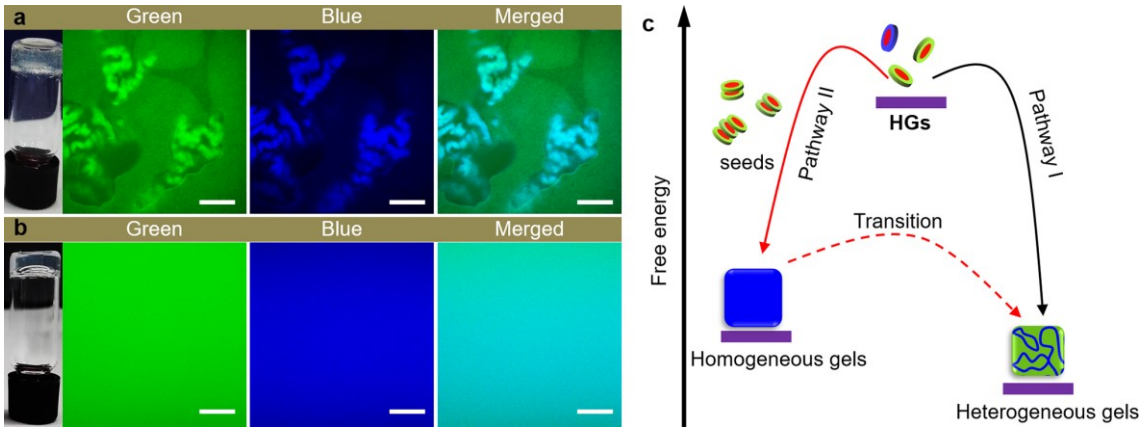

Figure 3.4. Photograph and CLSM images of a) the homogeneous gels after an incubation of three weeks and b) the freshly prepared gels; c) illustration of the energy landscape of the gel formation through **different** pathways. Samples in a, b): [**H**] = 20 mM, [**A** + **A**$^-$] = 120 mM (30 mol% **A**$^-$), [**A-FL**] = 30 μM (green) and [**Hoechst 33342**] = 20 μM (blue). Scale bars = 40 μm.

3.3 Conclusions

In conclusion, we have shown how metastable supramolecular gels can be prepared by using seeds to interfere in the nucleation step of the molecular gelators. These resulting metastable gels can spontaneously convert into the thermodynamically more stable gel states over a period of several weeks. Out-of-equilibrium self-assembly has been regarded as a prospective route towards novel supramolecular structures and functions, but its accomplishment in lab is still a challenging task. We believe such a seeding-driven out-of-equilibrium supramolecular self-assembly can serve as a simple and versatile approach towards synthetic out-of--equilibrium supramolecular systems and benefit the development of new functional materials, such as adaptive materials.[45, 46]

3.4 References

1. Mattheck, C., *Design in nature: learning from trees*. Springer Science & Business Media: 1998.
2. Weinkamer, R.; Dunlop, J. W. C.; Brechet, Y.; Fratzl, P., All but diamonds Biological materials are not forever. *Acta Mater.* **2013,** *61*, 880-889.
3. Halley, J. D.; Winkler, D. A., Consistent Concepts of Self-organization and Self-assembly. *Complexity* **2008,** *14*, 10-17.
4. Lasek, R. J.; Brady, S. T., Attachment of Transported Vesicles to Microtubules in Axoplasm Is Facilitated by Amp-Pnp. *Nature* **1985,** *316*, 645-647.

5. Vale, R. D.; Reese, T. S.; Sheetz, M. P., Identification of a Novel Force-Generating Protein, Kinesin, Involved in Microtubule-Based Motility. *Cell* **1985,** *42*, 39-50.
6. Schroer, T. A.; Steuer, E. R.; Sheetz, M. P., Cytoplasmic Dynein Is a Minus End-Directed Motor for Membranous Organelles. *Cell* **1989,** *56*, 937-946.
7. Wu, M.; Higgs, P. G., Origin of Self-Replicating Biopolymers: Autocatalytic Feedback Can Jump-Start the RNA World. *J. Mol. Evol.* **2009,** *69*, 541-554.
8. Robertson, M. P.; Joyce, G. F., The origins of the RNA world. *Cold Spring Harb Perspect Biol.* **2012,** *4*, a003608.
9. Pross, A.; Pascal, R., The origin of life: what we know, what we can know and what we will never know. *Open Biol.* **2013,** *3*, 120190.
10. Birnbaum, K. D.; Sanchez Alvarado, A., Slicing across kingdoms: regeneration in plants and animals. *Cell* **2008,** *132*, 697-710.
11. Nedelec, F. J.; Surrey, T.; Maggs, A. C.; Leibler, S., Self-organization of microtubules and motors. *Nature* **1997,** *389*, 305-8.
12. Korn, E. D.; Carlier, M. F.; Pantaloni, D., Actin Polymerization and Atp Hydrolysis. *Science* **1987,** *238*, 638-644.
13. Merindol, R.; Walther, A., Materials learning from life: concepts for active, adaptive and autonomous molecular systems. *Chem. Soc. Rev.* **2017,** *46*, 5588-5619.
14. van Rossum, S. A. P.; Tena-Solsona, M.; van Esch, J. H.; Eelkema, R.; Boekhoven, J., Dissipative out-of-equilibrium assembly of man-made supramolecular materials. *Chem. Soc. Rev.* **2017,** *46*, 5519-5535.
15. van Esch, J. H.; Klajn, R.; Otto, S., Chemical systems out of equilibrium. *Chem. Soc. Rev.* **2017,** *46*, 5474-5475.
16. Mattia, E.; Otto, S., Supramolecular systems chemistry. *Nat. Nanotechnol.* **2015,** *10*, 111-119.
17. Sorrenti, A.; Leira-Iglesias, J.; Markvoort, A. J.; de Greef, T. F. A.; Hermans, T. M., Non-equilibrium supramolecular polymerization. *Chem. Soc. Rev.* **2017,** *46*, 5476-5490.
18. Hess, H.; Ross, J. L., Non-equilibrium assembly of microtubules: from molecules to autonomous chemical robots. *Chem. Soc. Rev.* **2017,** *46*, 5570-5587.
19. Solis Munana, P.; Ragazzon, G.; Dupont, J.; Ren, C.; Chen, J.; Prins, L. J., Substrate‐Induced Self‐Assembly of Cooperative Catalysts. *Angew. Chem. Int. Edit.*
20. Korevaar, P. A.; George, S. J.; Markvoort, A. J.; Smulders, M. M.; Hilbers, P. A.; Schenning, A. P.; De Greef, T. F.; Meijer, E. W., Pathway complexity in supramolecular polymerization. *Nature* **2012,** *481*, 492-6.
21. Ogi, S.; Fukui, T.; Jue, M. L.; Takeuchi, M.; Sugiyasu, K., Kinetic control over pathway complexity in supramolecular polymerization through modulating the energy landscape by rational molecular design. *Angew. Chem. Int. Edit.* **2014,** *53*, 14363-7.
22. Greciano, E. E.; Matarranz, B.; Sanchez, L., Pathway Complexity Versus Hierarchical Self-Assembly in N-Annulated Perylenes: Structural Effects in Seeded Supramolecular Polymerization. *Angew. Chem. Int. Edit.* **2018,** *57*, 4697-4701.
23. Wang, Q. G.; Yang, Z. M.; Gao, Y.; Ge, W. W.; Wang, L.; Xu, B., Enzymatic hydrogelation to immobilize an enzyme for high activity and stability. *Soft Matter* **2008,** *4*, 550-553.

24. Hirst, A. R.; Roy, S.; Arora, M.; Das, A. K.; Hodson, N.; Murray, P.; Marshall, S.; Javid, N.; Sefcik, J.; Boekhoven, J.; van Esch, J. H.; Santabarbara, S.; Hunt, N. T.; Ulijn, R. V., Biocatalytic induction of supramolecular order. *Nat. Chem.* **2010,** *2*, 1089-94.
25. Boekhoven, J.; Poolman, J. M.; Maity, C.; Li, F.; van der Mee, L.; Minkenberg, C. B.; Mendes, E.; van Esch, J. H.; Eelkema, R., Catalytic control over supramolecular gel formation. *Nat. Chem.* **2013,** *5*, 433-7.
26. Pappas, C. G.; Sasselli, I. R.; Ulijn, R. V., Biocatalytic Pathway Selection in Transient Tripeptide Nanostructures. *Angew. Chem. Int. Edit.* **2015,** *54*, 8119-23.
27. Trausel, F.; Versluis, F.; Maity, C.; Poolman, J. M.; Lovrak, M.; van Esch, J. H.; Eelkema, R., Catalysis of Supramolecular Hydrogelation. *Accounts Chem. Res.* **2016,** *49*, 1440-7.
28. Ogi, S.; Sugiyasu, K.; Manna, S.; Samitsu, S.; Takeuchi, M., Living supramolecular polymerization realized through a biomimetic approach. *Nat. Chem.* **2014,** *6*, 188-195.
29. Boott, C. E.; Nazemi, A.; Manners, I., Synthetic Covalent and Non-Covalent 2D Materials. *Angew. Chem. Int. Edit.* **2015,** *54*, 13876-13894.
30. Ogi, S.; Stepanenko, V.; Sugiyasu, K.; Takeuchi, M.; Wurthner, F., Mechanism of Self-Assembly Process and Seeded Supramolecular Polymerization of Perylene Bisimide Organogelator. *J. Am. Chem. Soc.* **2015,** *137*, 3300-3307.
31. Kang, J.; Miyajima, D.; Mori, T.; Inoue, Y.; Itoh, Y.; Aida, T., A rational strategy for the realization of chain-growth supramolecular polymerization. *Science* **2015,** *347*, 646-651.
32. Endo, M.; Fukui, T.; Jung, S. H.; Yagai, S.; Takeuchi, M.; Sugiyasu, K., Photoregulated Living Supramolecular Polymerization Established by Combining Energy Landscapes of Photoisomerization and Nucleation-Elongation Processes. *J. Am. Chem. Soc.* **2016,** *138*, 14347-14353.
33. Ogi, S.; Matsumoto, K.; Yamaguchi, S., Seeded Polymerization through the Interplay of Folding and Aggregation of an Amino-Acid-based Diamide. *Angew. Chem. Int. Edit.* **2018,** *57*, 2339-2343.
34. Qiu, H. B.; Hudson, Z. M.; Winnik, M. A.; Manners, I., Multidimensional hierarchical self-assembly of amphiphilic cylindrical block comicelles. *Science* **2015,** *347*, 1329-1332.
35. Li, X. Y.; Jin, B. X.; Gao, Y.; Hayward, D. W.; Winnik, M. A.; Luo, Y. J.; Manners, I., Monodisperse Cylindrical Micelles of Controlled Length with a Liquid-Crystalline Perfluorinated Core by 1D "Self-Seeding". *Angew. Chem. Int. Edit.* **2016,** *55*, 11392-11396.
36. Qiu, H. B.; Gao, Y.; Boott, C. E.; Gould, O. E. C.; Harniman, R. L.; Miles, M. J.; Webb, S. E. D.; Winnik, M. A.; Manners, I., Uniform patchy and hollow rectangular platelet micelles from crystallizable polymer blends. *Science* **2016,** *352*, 697-701.
37. Wagner, W.; Wehner, M.; Stepanenko, V.; Ogi, S.; Wurthner, F., Living Supramolecular Polymerization of a Perylene Bisimide Dye into Fluorescent J-Aggregates. *Angew. Chem. Int. Edit.* **2017,** *56*, 16008-16012.
38. Jin, X. H.; Price, M. B.; Finnegan, J. R.; Boott, C. E.; Richter, J. M.; Rao, A.; Menke, S. M.; Friend, R. H.; Whittell, G. R.; Manners, I., Long-range exciton transport in conjugated polymer nanofibers prepared by seeded growth. *Science* **2018,** *360*, 897-900.

39. Fukui, T.; Kawai, S.; Fujinuma, S.; Matsushita, Y.; Yasuda, T.; Sakurai, T.; Seki, S.; Takeuchi, M.; Sugiyasu, K., Control over differentiation of a metastable supramolecular assembly in one and two dimensions. *Nat. Chem.* **2017,** *9*, 493-499.
40. Fukui, T.; Takeuchi, M.; Sugiyasu, K., Autocatalytic Time-Dependent Evolution of Metastable Two-Component Supramolecular Assemblies to Self-Sorted or Coassembled State. *Sci. Rep.* **2017,** *7*, 2425.
41. Wang, Y.; Lovrak, M.; Liu, Q.; Maity, C.; le Sage, V. A. A.; Eelkema, R.; van Esch, J. H., Hierarchically compartmentalized supramolecular gels through multilevel self-sorting. *Submitted for publication*.
42. Kumar, D. K.; Steed, J. W., Supramolecular gel phase crystallization: orthogonal self-assembly under non-equilibrium conditions. *Chem. Soc. Rev.* **2014,** *43*, 2080-2088.
43. Poolman, J. M.; Boekhoven, J.; Besselink, A.; Olive, A. G.; van Esch, J. H.; Eelkema, R., Variable gelation time and stiffness of low-molecular-weight hydrogels through catalytic control over self-assembly. *Nat. Protoc.* **2014,** *9*, 977-88.
44. Eelkema, R.; van Esch, J. H., Catalytic control over the formation of supramolecular materials. *Org. Biomol. Chem.* **2014,** *12*, 6292-6.
45. Rybtchinski, B., Adaptive Supramolecular Nanomaterials Based on Strong Noncovalent Interactions. *Acs Nano* **2011,** *5*, 6791-6818.
46. Shigemitsu, H.; Fujisaku, T.; Tanaka, W.; Kubota, R.; Minami, S.; Urayama, K.; Hamachi, I., An adaptive supramolecular hydrogel comprising self-sorting double nanofibre networks (vol 13, pg 165, 2018). *Nat. Nanotechnol.* **2018,** *13*, 267-267.

3.5 Supplementary information

Materials

All commercial chemicals were purchased from Sigma Aldrich. Compound **H**, **A**, **A**$^-$, and **A-FL** were synthesized according to methods described in our previous work.[1-3]

Experimental

Preparation of seeds

The seeds were prepared by sonicating already formed gel fibers using a Branson 2510E-MTH sonicator with an output frequency of 42 kHz. Briefly, 200 µL fibers suspension formed from the precursor solution including 10 mM **H** and 60 mM **A** in 0.1 M phosphate buffer at pH 7.0 was added into a vial and sonicated for at least 20 min. This freshly obtained solution was then used for the seeding experiments.

Determination of the critical gelation concentration (CGC)

A series of samples include different concentration of **H** and (**A** + **A**$^-$) was prepared and kept at room temperature for one week to ensure a complete formation and self-assembly of **HGs**; different ratio of **A**$^-$ was investigated as well, and the molar ratio of (**A** + **A**$^-$) was constantly maintained at six times higher than **H**. After that, the gel formation was determined by vial inversion test. Typically, a sample that can resist flow for at least 30 seconds was then regarded as a gel in this study. The lowest concentration of **H** at which the sample would form a gel was defined as the corresponding CGC.

Rheological test

The oscillatory rheological measurements were performed on a AR G2 TA rheometer equipped with a parallel-plate made of stainless steel (diameter is 40 mm) and a solvent trap to prevent the evaporation of water from the samples. All the measurements were performed in a strain controlled mode at 25 ^{o}C. The strain and the frequency for the time sweep measurements were set to 0.05% and 1.0 Hz, respectively. All the samples were prepared in 0.1 M phosphate buffer at pH 7.0. After mixing the stock solutions of the building blocks to the target concentration, 400 µL of the solution was transferred immediately onto the rheometer plate and the gap was set to be 290 µm for the measurements with a solvent trap.

CLSM measurement

In this work, CLSM measurements were performed on a Zeiss LSM 710 confocal laser scanning microscope equipped with a Zeiss Axio Observer inverted microscope and 40x PlanFluor oil immersion objective lens (NA 1.3). Incident laser with a wavelength of 488 nm and 405 nm was used to excite the fluorescein probe and Hoechst, respectively. The pinhole was set to 1.0 airy unit during the measurements and the data were processed using ZEN 2009 software. To preserve the gel samples for longer time without dehydration, samples were prepared in sealed homemade PDMS chambers.

High performance liquid chromatography (HPLC)

The gelator composition of the gels was analyzed by high performance liquid chromatography (HPLC) using a gradient eluent flow of H_2O:(MeOH+0.4% triethylamine (TEA)) linearly varied from a ratio of 8:2 to 2:8, referring to the previous study.[1, 3] The samples for the HPLC measurements were prepared by adding 80 µL gel sample into a mixture solution of 400 µL THF and 400 µL TEA saturated H_2O. The ratio of each **HGs** was calculated at an isosbestic point (275 nm). The first increase followed by a decrease in the content of $\mathbf{HAA^-_2}$ and $\mathbf{HA^-_3}$ can be ascribed to the occurrence of self-assembly; $\mathbf{HA_3}$ and $\mathbf{HA_2A^-}$ can self-assemble more easily because of their lower charge; the self-assembly of $\mathbf{HA_3}$ and $\mathbf{HA_2A^-}$ leads to the decrease of their content in water, which leads a shift of the reaction equilibrium to the formation of $\mathbf{HA_3}$ and $\mathbf{HA_2A^-}$. As a result, the $\mathbf{HAA^-_2}$ and $\mathbf{HA^-_3}$ go backward to the intermediate molecules which can convert to $\mathbf{HA_3}$ and $\mathbf{HA_2A^-}$ to supplement their decreased content in water.

Cryo-TEM

A Gatan model 626 cryo-stage in a JEOL JEM 1400 Plus electron microscope was employed to characterize the morphologies of the gel networks. The operating voltage was 120 kV. For the measurements, all the gel samples were destroyed into flow state and 3 µL of the diluted sol solutions were carefully deposited on a Quantifoil R 1.2/1.3 100 Holey carbon films coated Cu 200 mesh grid. After blotting, the grid was rapidly inserted into liquid ethane. The frozen-hydrated samples were always stored in liquid nitrogen before the observation. The cryo-TEM images were recorded under low-dose conditions on a slow scan CCD camera (Gatan, model 830).

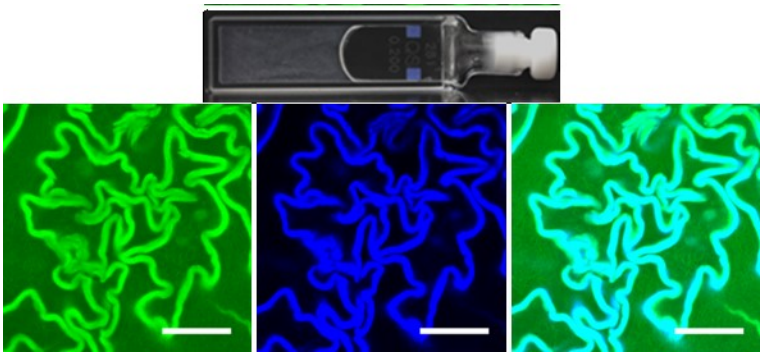

Figure S3.1. Photograph (top) and CLSM images (bottom) of the gel prepared without addition of seeds. Sample: 20 mM **H**, 120 mM (**A** + **A**$^-$) (30 mol% **A**$^-$), 30 μM **A-FL** (green) and 20 μM **Hoechst 33342** (blue). Scale bars on the CLSM images are 40 μm.

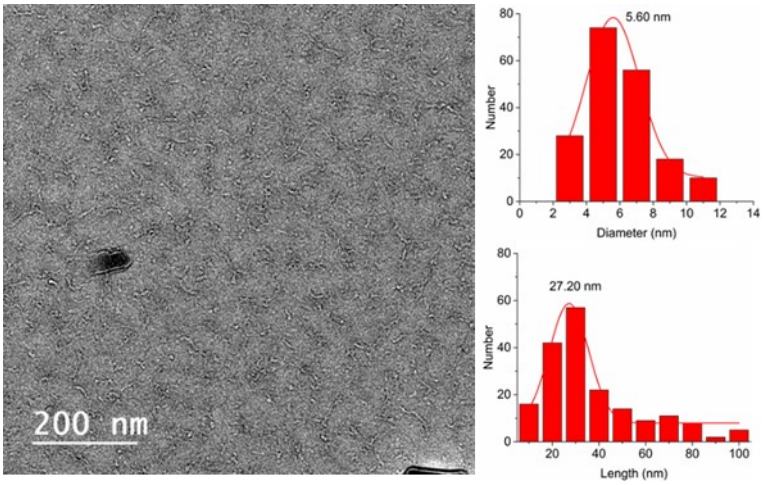

Figure S3.2. Cryo-TEM image of prepared seeds (left) and the statistical results (right) of the diameter and lengh of the seeds.

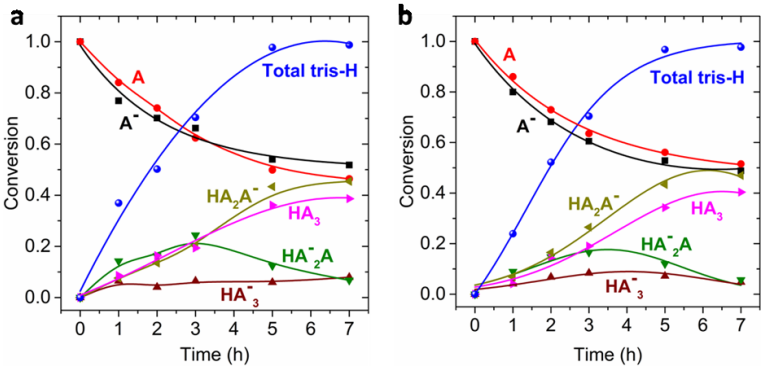

Figure S3.3. Formation of tris-hydrazone products and the consumption of aldehyde against time measured by HPLC: a) without seeds; and b) with 1.0 mM seeds. Samples: [**H**] = 20 mM, [**A** + **A**$^-$] = 120 mM (30 mol% **A**$^-$). The content of tris-hydrazone products is normalized by the initial concentration of **H**, and the content of aldehydes, including **A**$^-$ and , is respectively normalized by their initial content.

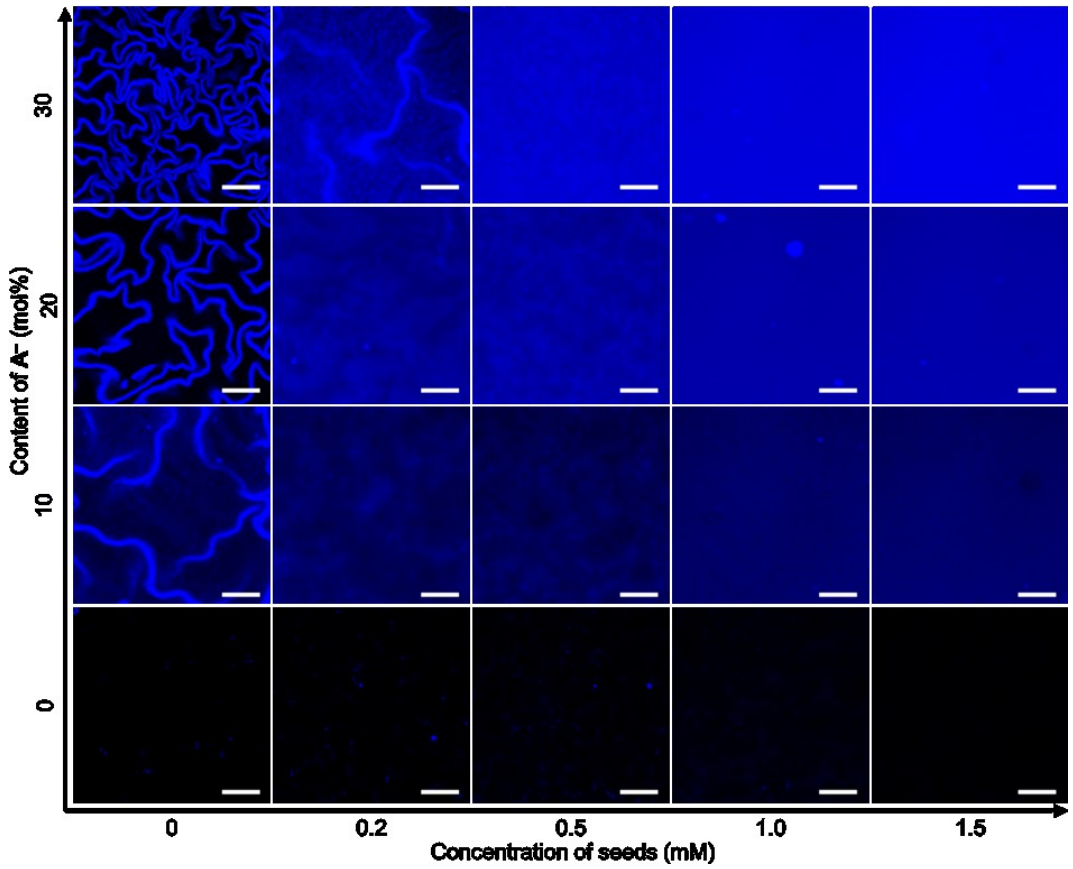

Figure S3.4. CLSM images of the gel networks formed with different concentration of seeds and different mol% **A**$^-$. Samples: [**H**] = 20 mM, [**A** + **A**$^-$] = 120 mM (different mol% **A**$^-$), [**Hoechst 33342**] = 20 μM. Scale bars = 40 μm.

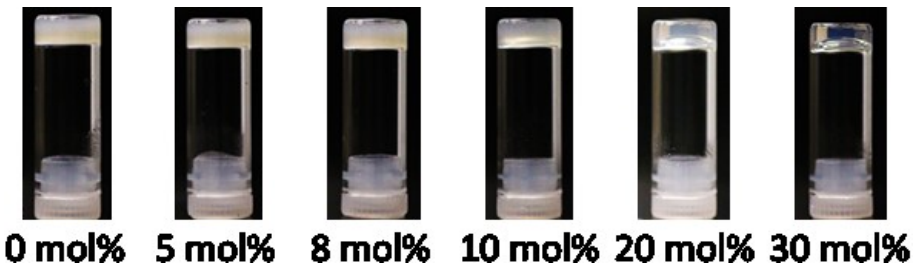

Figure S3.5. Photographs of gel samples prepared by 20 mM fresh **H**, 120 mM (**A** + **A**$^-$) (different mol% **A**$^-$) and 1.0 mM seeds.

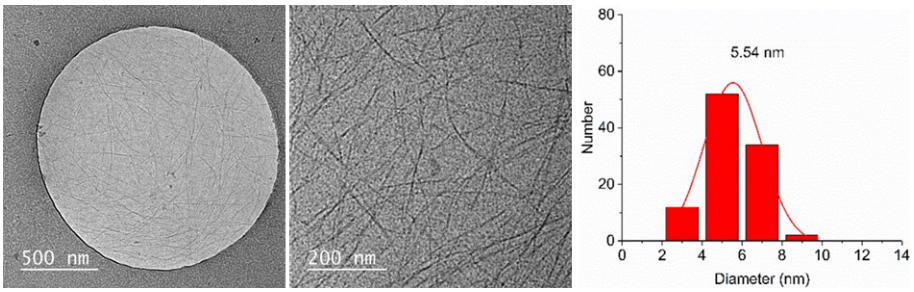

Figure S3.6. Cryo-TEM images (left and middle) of the gel sample prepared by 20 mM fresh **H**, 120 mM (**A** + **A**$^-$) (30 mol% **A**$^-$) and 1.0 mM seeds, and the statistical diameter of fibers (right).

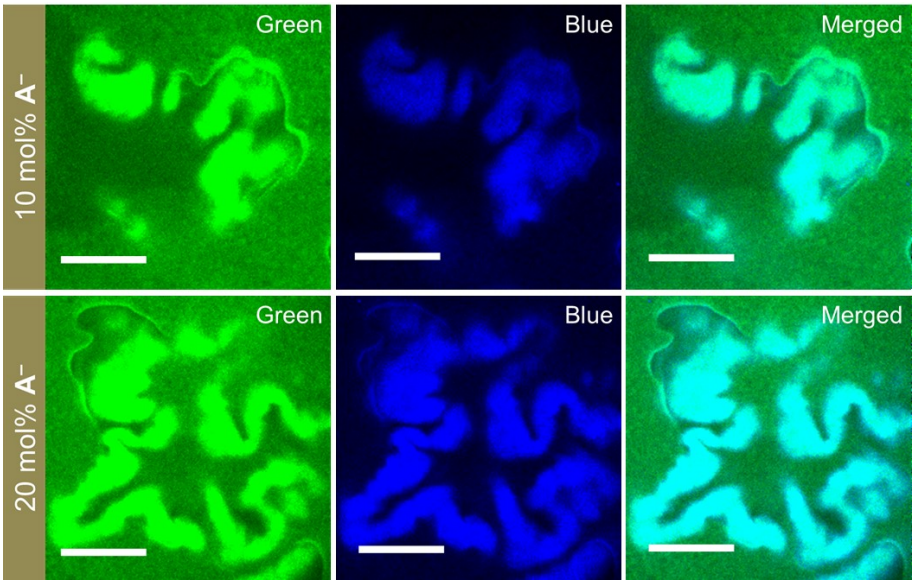

Figure S3.7. CLSM images of the homogeneous gel networks after three weeks incubation. Samples are prepared by 20 mM **H**, 120 mM (**A** + **A**$^-$) (different mol% **A**$^-$), 1.0 mM seeds, 30 μM **A-FL** (green) and 20 μM **Hoechst 33342** (blue). Scale bars = 30 μm.

References

1. Boekhoven, J.; Poolman, J. M.; Maity, C.; Li, F.; van der Mee, L.; Minkenberg, C. B.; Mendes, E.; van Esch, J. H.; Eelkema, R., Catalytic control over supramolecular gel formation. *Nat. Chem.* **2013,** *5*, 433-7.
2. Poolman, J. M.; Boekhoven, J.; Besselink, A.; Olive, A. G.; van Esch, J. H.; Eelkema, R., Variable gelation time and stiffness of low-molecular-weight hydrogels through catalytic control over self-assembly. *Nat. Protoc.* **2014,** *9*, 977-88.
3. Y. Wang, M. Lovrak, Q. Liu, C. Maity, V. A. A. le Sage, X. Guo, R. Eelkema, and J. H. van Esch, Hierarchically Compartmentalized supramolecular gels through multilevel self-sorting, *submitted for publication*.

Chapter 4

Self-seeding self-assembly towards out-of-equilibrium supramolecular gels

Abstract: Out-of-equilibrium supramolecular self-assembly enables the resulting products sophisticated functions, but the approach towards such a system remains limited. Here we report on metastable supramolecular gels that are formed through a facile self-seeding self-assembly process. This involves a synthetic multicomponent gelator system in which different gelators are formed from a mixture of precursor molecules and spontaneously self-assemble into thermodynamically stable gels through multilevel self-sorting processes. Here we surprisingly found that one of the precursor molecules is capable of self-assembling into nano-sized aggregates upon a gentle aging treatment. Importantly, these tiny aggregates can serve as seeds to force the self-assembly of gelators along a kinetically favored pathway, leading to metastable gels. Over time, this metastable gels can convert into the thermodynamic state spontaneously. This work adds to the route towards out-of-equilibrium supramolecular system under artificial condition.

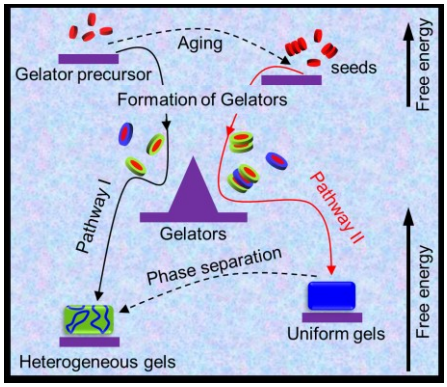

The content of this chapter is based on:

Yiming Wang, Matija Lovrak, Xuhong Guo, Eduardo Mendes, Rienk Eelkema, and Jan H. van Esch*, Self-seeding self-assembly towards out-of-equilibrium supramolecular gels, *submitted for publication.*

4.1 Introduction

In this work, we present how out-of-equilibrium supramolecular gels can be formed by a simple aging-induced self-seeding self-assembly of molecular gelators. Inspired by nature, synthetic supramolecular self-assembly performed at out-of-equilibrium state has received extensive interest in recent years,[1-3] as the implementation of such a system in manmade scenario would not only improve our understanding of the biological counterpart, but also result in supramolecular materials with numerous intriguing functions, such as adaptation,[4-7] self-replication,[8-11] and autonomous regeneration.[12-14] To date, there are some impressive examples of out-of-equilibrium self-assembly have been developed in lab. For instance, by using of (bio)catalysts,[15] the self-assembly can be guided along a specific kinetic pathway, leading to kinetically trapped or metastable supramolecular products which are permanently or temporarily stabilized in a local minimum of energy landscape.[16-23] In another example, the self-assembly system is dynamically stabilized at a far-from-equilibrium state by continuous consumption of chemical fuels, that is so called dissipative self-assembly.[24-29] Despite these advances, the route towards such out-of-equilibrium supramolecular systems remains limited. Most of the already established examples involve complex synthesis process and rigid selection of reaction-self-assembly networks, and even some of them can only be achieved under rigorous experimental conditions. Here we show an example of metastable supramolecular gels that are formed though a simple aging-induced self-seeding self-assembly at ambient temperature.

Very recently, we have described a multicomponent supramolecular self-assembly system in which tris-hydrazone gelators (**HGs**) composed of neutral (**NGs**) and negatively charged ones (**CGs**) are produced in situ by the reaction between hydrazide (**H**) and differently charged aldehydes (**A**, and **A**$^-$) (Figure 4.1a).[30] The **HGs** can self-assemble into thermodynamically stable heterogeneous gels composed of separated neutral fibers (**NFs**) rich and negatively charged fibers (**CFs**) rich microdomains through multilevel self-sorting (Figure 4.1b).[30-31] Additionally, we have found that the addition of seeds composed of **HGs** can effectively bypass the multilevel self-sorting process and guide the self-assembly of **HGs** along a kinetically favored pathway, resulting in metastable gels with different network morphologies and mechanical properties; over time, these gels convert into the thermodynamic equilibrium state.[30]

In this work, we show a different and simpler approach by which similar metastable gels can be created without necessary addition of **HG** seeds. Here we surprisingly find that in aging solutions at ambient temperature the gelator precursor

molecules, **H**, spontaneously self-assemble into nano-sized aggregates. These resulting tiny aggregates can serve as nucleation centers to direct the self-assembly of **NGs** and **CGs** along a kinetically favored pathway, giving rise to metastable gels with homogenous networks and enhanced stiffness analogous to the **HG** seeds driven gels,[30] but distinctly different from the thermodynamic heterogeneous gels (Figure 4.1b).[31] Furthermore, these gels can convert into the thermodynamic state as well against time.

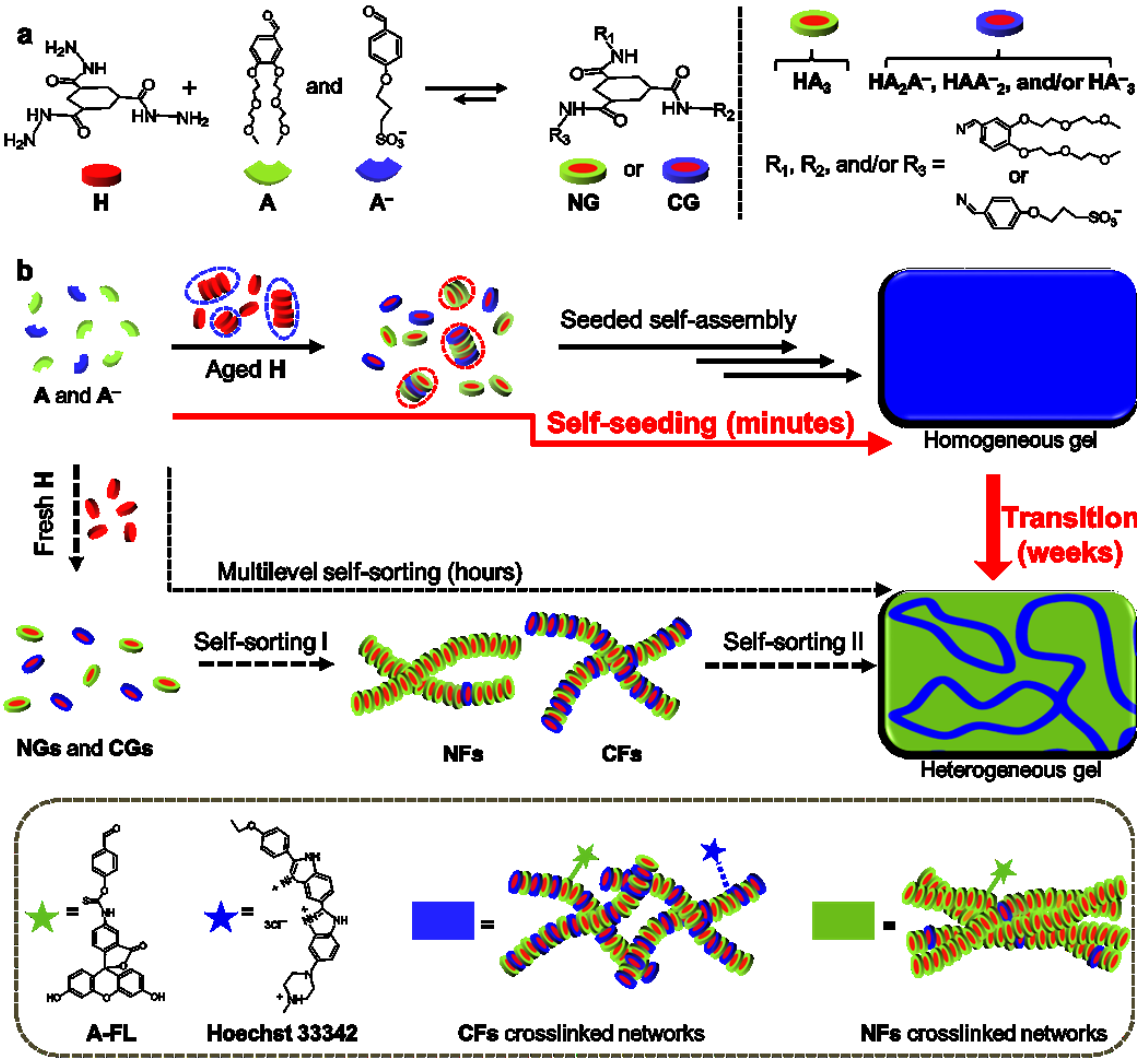

Figure 4.1. a) Scheme of the formation of **HGs** (**NGs** and **CGs**) from the building blocks of **H**, **A**, and **A**$^-$; b) illustration of the self-assembly of **NGs** and **CGs** through different pathways leading to formation of different gels, fluorescent probes of **A-FL** and **Hoechst 33342** are used to label all the gel fibers and **CFs**, respectively.

4.2 Results and discussion

All the gel samples used in this work were prepared in phosphate buffer (0.1 M, pH 7.0), and excess (**A** + **A**$^-$) (six times higher than **H**) were mixed with **H** to ensure a complete conversion of **H** into **HGs**.[32] For the aged **H** gel samples, the ages of the

used **H** solution are two weeks. To characterize the self-assembled structures using confocal laser scanning microscope (CLSM), an aldehyde tailored fluorescein (**A-FL**) and cationic dye **Hoechst 33342** are used to label the entire self-assembled structures, and the negatively charged species, respectively (Figure 4.1b).

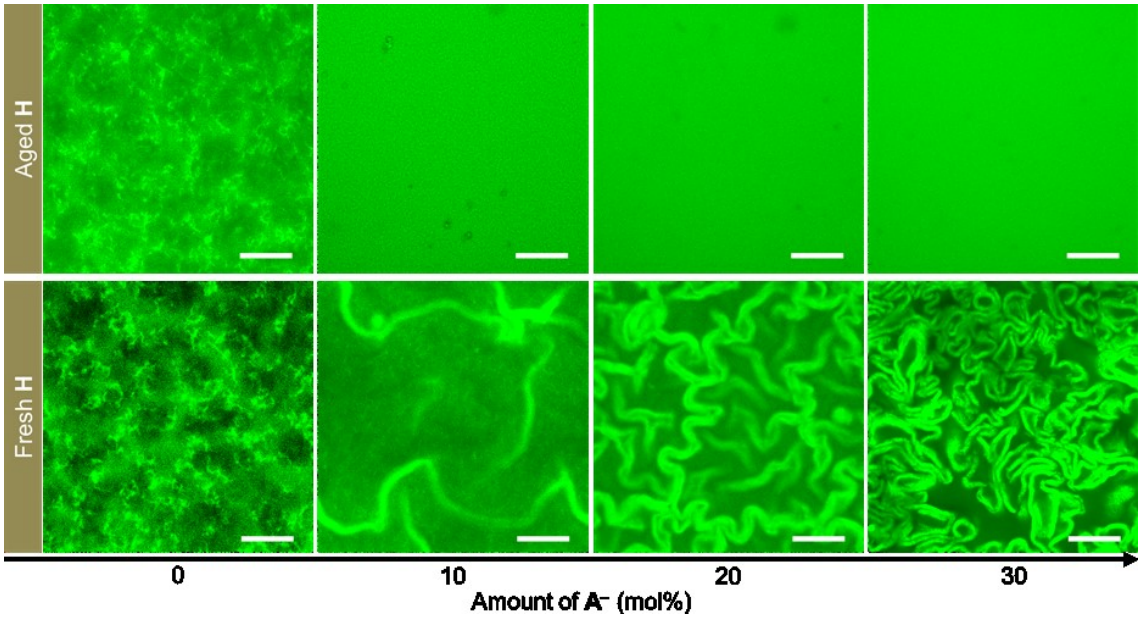

Figure 4.2. CLSM images of the gel networks prepared with aged (top) and fresh (down) **H** solutions as a function of the amount of $\mathbf{A}^-$, scale bars = 40 μm. Samples: [**H**] = 20 mM, [**A** + $\mathbf{A}^-$] = 120 mM (different mol% of $\mathbf{A}^-$), and [**A-FL**] = 30 μM.

During a preparation of gel samples, we surprisingly found that the use of an old **H** solution can lead to an increase in the transparency of the resulting gels with the amount of $\mathbf{A}^-$ (Figure S4.1), resembling the phenomena observed in previous **HG** seeds driven gels,[30] but differing from the heterogeneous gels.[31] To further insight into this unique aging effect, we performed CLSM to check the effects of aged **H** solution on the morphologies of the gel networks. In the sample with only **A**, we found that use of aged **H** solution led to a decrease in the size of the fibrous clusters compared to the fresh **H** gel sample (Figure 4.2). For the samples prepared with fresh **H** solution, increasing the content of added $\mathbf{A}^-$ led to formation of heterogeneous gel networks composed of separated **CFs**-rich crumpled sheets and **NFs**-rich coarse fibrous networks (Figure 4.2 and S4.3), which is in alignment with a previous study.[31] Interestingly, however, for the samples prepared with aged **H** solution the resulting gel networks turned to be more uniform with increasing the content of $\mathbf{A}^-$ (Figure 4.2). When the content of $\mathbf{A}^-$ was increased to be above 20 mol%, the gel networks just showed homogeneous fluorescence without any distinguishable structures. Cryo-TEM indicated that these uniform gel networks were composed of thin fibers with a diameter of ~ 5.8 nm which is comparable to the single hydarzone fibers as

reported previously (Figure S4.2).[17, 33] Furthermore, **Hoechst 33342** staining tests reveal that the thin fibers in these uniform gel networks are **CFs** (Figure S4.3). Apparently, **CFs** are not prone to form bundles due to the interfibrous electrostatic repulsions, thereby leading to the thin fibers crosslinked homogeneous networks.[31] These CLSM results clearly demonstrate that employment of aged **H** solutions completely prevents the formation of heterogeneous gel networks, instead, **CFs** crosslinked homogeneous gel networks are formed, which is very similar to the case of **HG** seeds driven gels as described in a previous study.[30]

To further insight into this unique aging effect, we performed oscillatory rheological measurements to investigate the effects of aged **H** solution on the gel formation. For the samples prepared with fresh **H** solutions, we found that the gelation time (the time at which the storage modules *G'* surpass the loss modulus *G"*) was increased from ~45 min to ~2.75 h upon an increase in the content of $\mathbf{A}^-$ from 0 to 30 mol% (Figure 4.3a), and the stiffness of the resulted gels was first increased from ~700 Pa (0 mol% $\mathbf{A}^-$) to ~1.1 kPa (10 mol% $\mathbf{A}^-$) and then decreased to ~40 Pa (30 mol% $\mathbf{A}^-$) (Figure 4.3b). These results are in line with a previous study.[31] Much to our surprise, use of aged **H** solution led to an increase in gelation time from ~9 to ~50 min with an increase in the content of $\mathbf{A}^-$ from 0 to 30 mol% (Figure 4.3a), indicating faster gelation rates compared to the fresh **H** samples. Moreover, the gel stiffness showed a slight increase from ~4.0 (0 mol% $\mathbf{A}^-$) to ~5.0 kPa (10 mol% $\mathbf{A}^-$) followed by a decrease to ~2.5 kPa (30 mol% $\mathbf{A}^-$) (Figure 4.3b), which are higher than the gel samples prepared with fresh **H** solution. These rheological results clearly demonstrate that use of aged **H** solution can markedly facilitate the gelation process. Importantly, the employment of aged **H** solution did not change the hydrazone formation rate and the resulting gelator compositions as determined by high performance liquid chromatography (HPLC) (Figure S4.4). Thus we conclude that the accelerated gelation due to use of aged **H** solutions is ascribed to the interference of aged **H** in the self-assembly rather than the formation of **HGs**, resembling previous **HG** seeds driven gelation.[30] Such an accelerated self-assembly would lead to a fractal-like growth of the gel fibers which is responsible for the higher gel stiffness, and may also contribute to the formation of the bundling free fibers.[17, 34]

A further measurement of critical gelation concentration (CGC) of **H** (see supporting information) showed that use of aged **H** solution given rise to a low CGC which slightly varies from ~2.0 mM (0 mol% $\mathbf{A}^-$) to 3.0 mM (30 mol% $\mathbf{A}^-$) (Figure 4.3c). However, for the fresh **H** samples, the CGC is much higher and varies from ~20 mM (0 mol% $\mathbf{A}^-$) to 17 mM (8 mol% $\mathbf{A}^-$). This remarkable lower CGC due to the use of aged **H** further confirms the accelerated self-assembly of **HGs**.

On the basis of these data together with previous study of **HG** seeds driven gels, we propose a self-seeding self-assembly mechanism led by use of aged **H** solutions. In this hypothesis, small aggregations consisting of **H** molecules are spontaneously formed during aging at room temperature. Analogous to the **HG** seeds driven self-assembly,[30] these small **H** aggregates play as seeds to accelerate the self-assembly of **HGs** by interfering in the nucleation step, leading to exclusive formation of **CFs** through co-assembly of **NGs** and **CGs**. As a result, homogeneous gel networks crosslinked by **CFs** are formed.

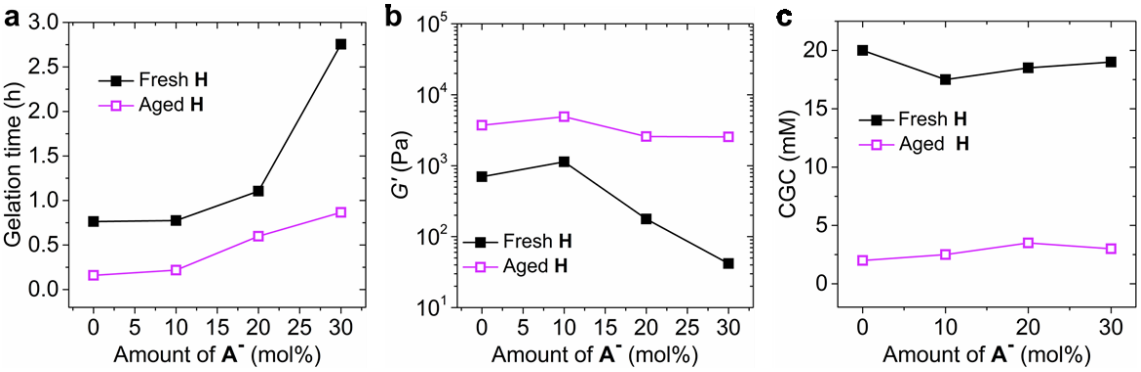

Figure 4.3. Effects of aged **H** solution on a) gelation time; b) gel stiffness; and c) CGC. Samples in a, b): [**H**] = 20 mM, [**A** + **A**$^-$] = 120 mM (different mol% **A**$^-$).

The HPLC results have shown that aging does not change the formation rates and compositions of **HGs**, which therefore suggest that the aging effects result from physical rather than chemical variations of **H**. This supports the above hypothesis. Indeed, **H** molecules do have the potential to interact with each other through hydrogen bonds between the hydrazine groups and hydrophobic interactions between the cyclohexane cores, which may drive the self-assembly of **H** molecules. To test this hypothesis, we first employed Dynamic Light Scattering (DLS) to check the aged **H** solution (see supporting information). For the control samples of blank phosphate buffer and fresh **H** solution, scattering signals at >100 nm are observed (Figure S4.5). However, for the aged **H** solution, besides the scattering signals at >100 nm, a new scattering signal at 1.28 nm was detected (Figure S4.5), indicating that some nanostructures are indeed formed. Furthermore, with addition of THF, a good solvent for **H**, into the aged **H** solution, the characteristic scattering peak at 1.28 nm disappeared (Figure S4.6), which therefore suggests that these generated nanostructures are composed of **H**. However, we cannot distinguish these nanostructures in cryo-TEM observations (Figure S4.7), which could be ascribed to the low dimension and contrast of the **H** assemblies. Furthermore, in the NMR spectra, we can observe that hydrogen peaks belonging to the cyclohexene core

partially shift or show an increase in intensity which can be explained by the assembly of **H** molecules (Figure S4.8).

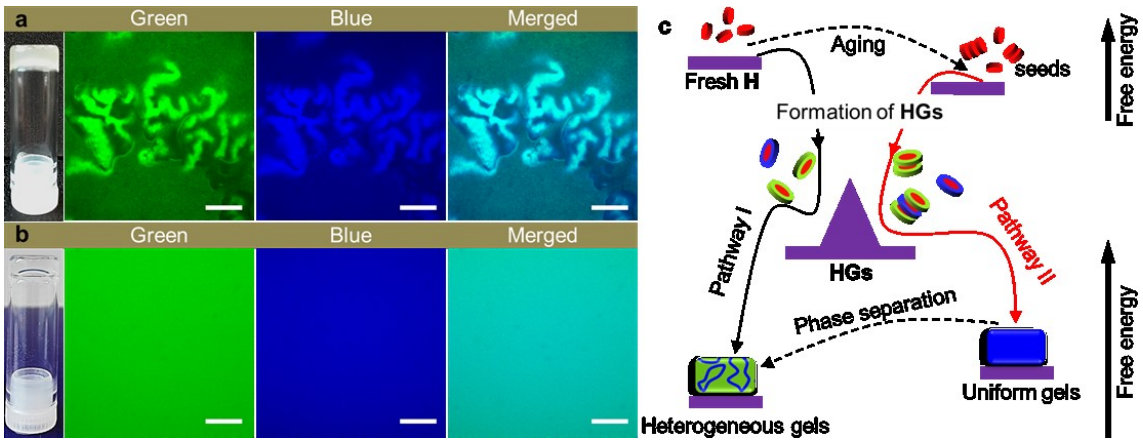

Figure 4.4. a, b) CLSM images of the aged **H** gel networks a) after an incubation of three weeks; b) at initial stage; and c) the energy landscape of the gel formation. Samples in a, b): [**H**] = 20 mM, [**A** + **A**$^-$] = 120 mM (30 mol% of **A**$^-$), [**A-FL**] = 30 μM, and [**Hoechst 33342**] = 20 μM, scale bars = 40 μm.

Form the results and discussions up to now, we can conclude that H molecules self-assemble into tiny assemblies during aging which subsequently give rise to seeding effects on the self-assembly of **HGs** resembling to the previous **HG** seeds driven self-assembly. Next, we are curious about whether the resulting homogeneous gels led by use of aged **H** solution are also temporarily stabilized at an out-of-equilibrium state as we have observed in the **HG** seeds driven gels.[30] To test this, we incubated the resulting homogeneous gels at room temperature and employed CLSM to observe the network morphologies. After an incubation of three weeks, we found that the transparent gel prepared with 30 mol% **A**$^-$ turned to be turbid (Figure 4.4a and b). CLSM observations indicate that this turbid gel present identical network morphologies with the thermodynamically stable heterogeneous gels composed with crumpled sheets surrounded by fibrous networks.[30-31] Moreover, in the blue channel we found the crumpled sheets showed higher emission of the blue fluorescence, while the fibrous networks in between these sheets showed relatively lower intensity of the blue dye (Figure 4.4a), indicating that the crumpled sheets consist of **CFs**, while the networks in between the sheets are composed of **NFs**. Similar morphologies transformations in the other gel samples prepared with different mol% **A**$^-$ were observed as well (Figure S4.9). It therefore demonstrates that these homogeneous gels led by use of aged H solutions are metastable and are capable of converting into the thermodynamic state over time.

These preceding experiments and discussions thus lead to an interesting self-seeding driven out-of-equilibrium supramolecular self-assembly system (Figure 4.4c): use of fresh H solution would lead to a multilevel self-sorting, resulting in thermodynamic heterogeneous gels (pathway I). However, use of aged **H** solution would bypass the multilevel self-sorting process and accelerate a co-assembly of **NGs** and **CGs**, leading to **CFs** crosslinked metastable homogenous gels (pathway II). Interestingly, these out-of-equilibrium gels are able to spontaneously convert into the thermodynamic gel state over time.

4.3 Conclusions

In conclusion, we have presented the formation of out-of-equilibrium supramolecular gels through an aging-induced self-seeding self-assembly. We have found that one of the hydrazone gelator precursor molecule is able to self-assemble into nano-sized aggregates which can drive the self-assembly of gelators along a kinetically favored pathway, thereby leading to metastable gels without addition of external triggers. Moreover, we have observed that these metastable gels can convert into the thermodynamic gel state over time at room temperature. We believe that such an gentle aging-induced out-of-equilibrium self-assembly provide a new simple approach toward the establishment of synthetic out-of-equilibrium systems.

4.4 References

1. van Esch, J. H.; Klajn, R.; Otto, S., Chemical systems out of equilibrium. *Chem. Soc. Rev.* **2017,** *46*, 5474-5475.
2. Mattia, E.; Otto, S., Supramolecular systems chemistry. *Nat. Nanotechnol.* **2015,** *10*, 111-119.
3. Sorrenti, A.; Leira-Iglesias, J.; Markvoort, A. J.; de Greef, T. F. A.; Hermans, T. M., Non-equilibrium supramolecular polymerization. *Chem. Soc. Rev.* **2017,** *46*, 5476-5490.
4. Mattheck, C., *Design in nature: learning from trees*. Springer Science & Business Media: 1998.
5. Weinkamer, R.; Dunlop, J. W. C.; Brechet, Y.; Fratzl, P., All but diamonds Biological materials are not forever. *Acta Mater.* **2013,** *61*, 880-889.
6. Halley, J. D.; Winkler, D. A., Consistent Concepts of Self-organization and Self-assembly. *Complexity* **2008,** *14*, 10-17.
7. Debnath, S.; Roy, S.; Ulijn, R. V., Peptide nanofibers with dynamic instability through nonequilibrium biocatalytic assembly. *J. Am. Chem. Soc.* **2013,** *135*, 16789-92.
8. Kurihara, K.; Tamura, M.; Shohda, K.; Toyota, T.; Suzuki, K.; Sugawara, T., Self-reproduction of supramolecular giant vesicles combined with the amplification of encapsulated DNA. *Nat. Chem.* **2011,** *3*, 775-81.

9. Carnall, J. M. A.; Waudby, C. A.; Belenguer, A. M.; Stuart, M. C. A.; Peyralans, J. J. P.; Otto, S., Mechanosensitive Self-Replication Driven by Self-Organization. *Science* **2010,** *327*, 1502-1506.
10. Sadownik, J. W.; Mattia, E.; Nowak, P.; Otto, S., Diversification of self-replicating molecules. *Nat. Chem.* **2016,** *8*, 264-269.
11. Altay, M.; Altay, Y.; Otto, S., Parasitic Behavior of Self-Replicating Molecules. *Angew. Chem. Int. Edit.* **2018,** *57*, 10564-10568.
12. Birnbaum, K. D.; Sanchez Alvarado, A., Slicing across kingdoms: regeneration in plants and animals. *Cell* **2008,** *132*, 697-710.
13. Nedelec, F. J.; Surrey, T.; Maggs, A. C.; Leibler, S., Self-organization of microtubules and motors. *Nature* **1997,** *389*, 305-8.
14. Korn, E. D.; Carlier, M. F.; Pantaloni, D., Actin Polymerization and Atp Hydrolysis. *Science* **1987,** *238*, 638-644.
15. Trausel, F.; Versluis, F.; Maity, C.; Poolman, J. M.; Lovrak, M.; van Esch, J. H.; Eelkema, R., Catalysis of Supramolecular Hydrogelation. *Accounts Chem. Res.* **2016,** *49*, 1440-7.
16. Korevaar, P. A.; George, S. J.; Markvoort, A. J.; Smulders, M. M.; Hilbers, P. A.; Schenning, A. P.; De Greef, T. F.; Meijer, E. W., Pathway complexity in supramolecular polymerization. *Nature* **2012,** *481*, 492-6.
17. Boekhoven, J.; Poolman, J. M.; Maity, C.; Li, F.; van der Mee, L.; Minkenberg, C. B.; Mendes, E.; van Esch, J. H.; Eelkema, R., Catalytic control over supramolecular gel formation. *Nat. Chem.* **2013,** *5*, 433-7.
18. Ogi, S.; Fukui, T.; Jue, M. L.; Takeuchi, M.; Sugiyasu, K., Kinetic control over pathway complexity in supramolecular polymerization through modulating the energy landscape by rational molecular design. *Angew. Chem. Int. Edit.* **2014,** *53*, 14363-7.
19. Vigier-Carriere, C.; Garnier, T.; Wagner, D.; Lavalle, P.; Rabineau, M.; Hemmerle, J.; Senger, B.; Schaaf, P.; Boulmedais, F.; Jierry, L., Bioactive Seed Layer for Surface-Confined Self-Assembly of Peptides. *Angew. Chem. Int. Edit.* **2015,** *54*, 10198-201.
20. Moreira, I. P.; Piskorz, T. K.; van Esch, J. H.; Tuttle, T.; Ulijn, R. V., Biocatalytic Self-Assembly of Tripeptide Gels and Emulsions. *Langmuir* **2017,** *33*, 4986-4995.
21. Vigier-Carriere, C.; Wagner, D.; Chaumont, A.; Durr, B.; Lupattelli, P.; Lambour, C.; Schmutz, M.; Hemmerle, J.; Senger, B.; Schaaf, P.; Boulmedais, F.; Jierry, L., Control of Surface-Localized, Enzyme-Assisted Self-Assembly of Peptides through Catalyzed Oligomerization. *Langmuir* **2017,** *33*, 8267-8276.
22. Greciano, E. E.; Matarranz, B.; Sanchez, L., Pathway Complexity Versus Hierarchical Self-Assembly in N-Annulated Perylenes: Structural Effects in Seeded Supramolecular Polymerization. *Angew. Chem. Int. Edit.* **2018,** *57*, 4697-4701.
23. Fukui, T.; Kawai, S.; Fujinuma, S.; Matsushita, Y.; Yasuda, T.; Sakurai, T.; Seki, S.; Takeuchi, M.; Sugiyasu, K., Control over differentiation of a metastable supramolecular assembly in one and two dimensions. *Nat. Chem.* **2017,** *9*, 493-499.
24. Boekhoven, J.; Hendriksen, W. E.; Koper, G. J.; Eelkema, R.; van Esch, J. H., Transient assembly of active materials fueled by a chemical reaction. *Science* **2015,** *349*, 1075-9.

25. Merindol, R.; Walther, A., Materials learning from life: concepts for active, adaptive and autonomous molecular systems. *Chem. Soc. Rev.* **2017,** *46*, 5588-5619.
26. Tena-Solsona, M.; Riess, B.; Grotsch, R. K.; Lohrer, F. C.; Wanzke, C.; Kasdorf, B.; Bausch, A. R.; Muller-Buschbaum, P.; Lieleg, O.; Boekhoven, J., Non-equilibrium dissipative supramolecular materials with a tunable lifetime. *Nat. Commun.* **2017,** *8*, 15895.
27. van Rossum, S. A. P.; Tena-Solsona, M.; van Esch, J. H.; Eelkema, R.; Boekhoven, J., Dissipative out-of-equilibrium assembly of man-made supramolecular materials. *Chem. Soc. Rev.* **2017,** *46*, 5519-5535.
28. De, S.; Klajn, R., Dissipative Self-Assembly Driven by the Consumption of Chemical Fuels. *Adv. Mater.* **2018**.
29. Te Brinke, E.; Groen, J.; Herrmann, A.; Heus, H. A.; Rivas, G.; Spruijt, E.; Huck, W. T. S., Dissipative adaptation in driven self-assembly leading to self-dividing fibrils. *Nat. Nanotechnol.* **2018**.
30. Wang, Y.; Lovrak, M.; Guo, X.; Mendes, E.; Eelkema, R.; van Esch, J. H., Self-seeding self-assembly towards out-of-equilibrium supramolecular gels. *Submitted for publication*.
31. Wang, Y.; Lovrak, M.; Liu, Q.; Maity, C.; le Sage, V. A. A.; Eelkema, R.; van Esch, J. H., Hierarchically compartmentalized supramolecular gels through multilevel self-sorting. *Submitted for publication*.
32. Poolman, J. M.; Boekhoven, J.; Besselink, A.; Olive, A. G.; van Esch, J. H.; Eelkema, R., Variable gelation time and stiffness of low-molecular-weight hydrogels through catalytic control over self-assembly. *Nat. Protoc.* **2014,** *9*, 977-88.
33. Wang, Y.; Versluis, F.; Oldenhof, S.; Lakshminarayanan, V.; Zhang, K.; Wang, Y.; Wang, J.; Eelkema, R.; Guo, X.; van Esch, J. H., Directed Nanoscale Self-Assembly of Low Molecular Weight Hydrogelators Using Catalytic Nanoparticles. *Adv. Mater.* **2018,** *30*, 1707408.
34. Liu, X. Y.; Sawant, P. D., Mechanism of the formation of self-organized microstructures in soft functional materials. *Adv. Mater.* **2002,** *14*, 421-+.

4.5 Supplementary information

Materials

All commercial chemicals were purchased from Sigma Aldrich. Compound **H**, **A**, **A**$^-$, and **A-FL** were synthesized according to the method proposed in our previous work.[1-3]

Experimental

Rheological test

The Oscillatory rheological measurements were performed on a AR G2 TA rheometer equipped with a parallel-plate made of stainless steel (diameter is 40 mm) and a solvent trap to prevent the evaporation of water from the samples. All the measurements were performed in a strain controlled mode at 25 ^oC. The strain and the frequency for the time sweep measurements were set to 0.05% and 1.0 Hz, respectively. All the samples were prepared in 0.1 M phosphate buffer at pH 7.0. After mixing the stock solutions of the building blocks to the target concentration, 400 µL of the solution was transferred immediately onto the rheometer plate and the gap was set to be 290 µm for the measurements with a solvent trap.

Determination of the critical gelation concentration (CGC)

A series of samples include different concentration of **H** and (**A** + **A**$^-$) was prepared and kept at room temperature for one week to ensure a complete formation and self-assembly of **HGs**; different ratio of **A**$^-$ was investigated as well, but the concentration of **H** was constantly maintained at six times higher than (**A** + **A**$^-$). After that, the gel formation was determined by vital inversion test. Typically, the resultant sample which can resist flow for at least 30 seconds was then regarded as gel in this study. The lowest concentration of **H** at which the sample was allowed to form a gel was defined as the corresponding CGC.

CLSM measurement

In this work, CLSM measurements were performed on a Zeiss LSM 710 confocal laser scanning microscope equipped with a Zeiss Axio Observer inverted microscope and 40x PlanFluor oil immersion objective lens (NA 1.3). Incident laser with a wavelength of 488 nm and 405 nm was used to excite the fluorescein probe and Hoechst, respectively. The pinhole was set to 1.0 airy unit during the measurements and the data were processed using ZEN 2009 software. To preserve the gel samples for

longer time without dehydration, samples were prepared in sealed homemade PDMS chambers.

High performance liquid chromatography (HPLC)

The gelator composition of the gels was analyzed by high performance liquid chromatography (HPLC) using a gradient eluent flow of H_2O:(MeOH+0.4% triethylamine (TEA)) linearly varied from a ratio of 8:2 to 2:8, referring to the previous study.[1, 3] The samples for the HPLC measurements were prepared by adding 80 µL gel sample into a mixture solution of 400 µL THF and 400 µL TEA saturated H_2O. The ratio of each **HGs** was calculated at isosbestic point (275 nm). The first increase followed by a decrease in the content of $\mathbf{HAA^-_2}$ and $\mathbf{HA^-_3}$ can be ascribed to the occurrence of self-assembly; $\mathbf{HA_3}$ and $\mathbf{HA_2A^-}$ are easier to self-assemble because of their less charges; the self-assembly of $\mathbf{HA_3}$ and $\mathbf{HA_2A^-}$ leads to the decrease of their content in water, which leads a shift of the reaction equilibrium to the formation of $\mathbf{HA_3}$ and $\mathbf{HA_2A^-}$. As a result, the $\mathbf{HAA^-_2}$ and $\mathbf{HA^-_3}$ go backward to the intermediate molecules which can convert to $\mathbf{HA_3}$ and $\mathbf{HA_2A^-}$ to supplement their decreased content in water.

Cryo-TEM

A Gatan model 626 cryo-stage in a JEOL JEM 1400 Plus electron microscope was employed to characterize the morphologies of the gel networks. The operating voltage was 120 kV. For the measurements, all the gel samples were destroyed into flow state and 3 µL of the diluted sol solutions were carefully deposited on a Quantifoil R 1.2/1.3 100 Holey carbon films coated Cu 200 mesh grid. After blotting, the grid was rapidly inserted into liquid ethane. The frozen-hydrated samples were always stored in liquid nitrogen before the observation. The cryo-TEM images were recorded under low-dose conditions on a slow scan CCD camera (Gatan, model 830).

Dynamic light scattering (DLS) measurement

The formation of aggregates of **H** during aging was monitored using a Malvern Nano ZS 3600 Zetasizer. For the measurements, the concentrations of aged **H** was diluted into 4 mM by phosphate buffer (0.1 M, pH 7.0). The laser wavelength was 633 nm with a scattering angle of 173°. All the samples were allowed to equilibrate for 2 min and measured at 25 °C.

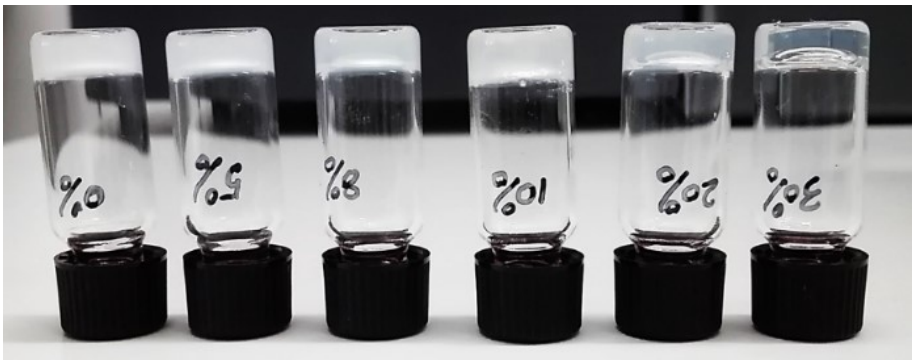

Figure S4.1. Photographs of gel samples prepared by 20 mM aged **H**, 120 mM (**A** + **A**$^-$) (different mol% **A**$^-$).

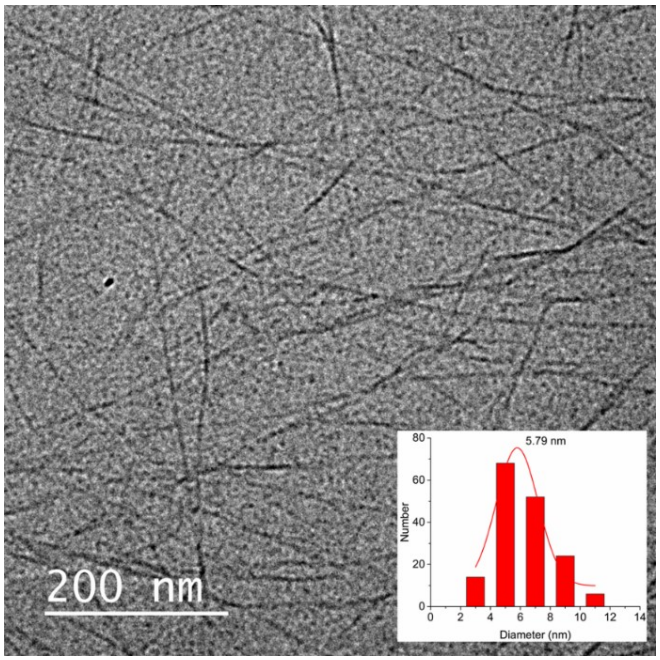

Figure S4.2. Cryo-TEM image and **statistical** diamter (inset) of the hydrazone fibers.

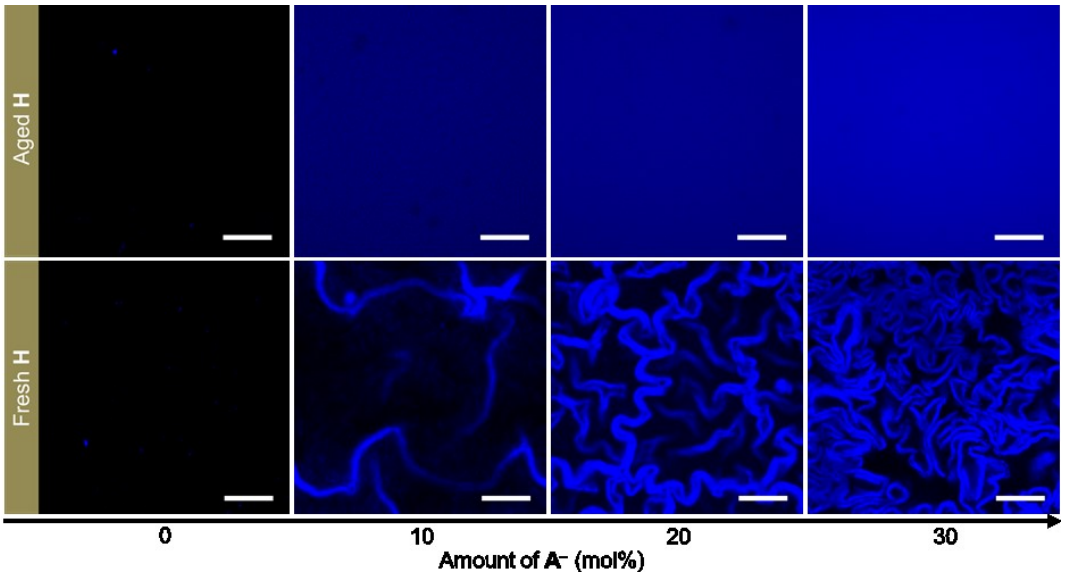

Figure S4.3. CLSM images (blue channel) of the morphologies of the gel networks prepared by aged (top) and fresh (down) **H** solutions as a **function** of the amount of **A**$^-$, scale bars = 40 μm. Samples: [**H**] = 20 mM, [**A** + **A**$^-$] = 120 mM (**different** mol% of **A**$^-$), and [**Hoechst 33342**] = 30 μM.

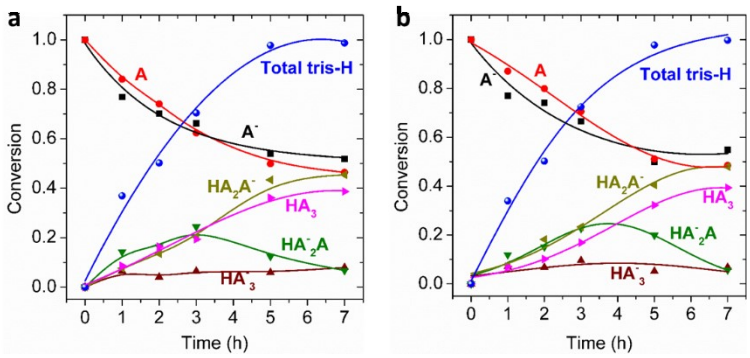

Figure S4.4. Formation of tris-hydrazone products and the consumption of aldehyde against time measured by HPLC: a) fresh **H**; and b) aged **H**. Samples: [**H**] = 20 mM, [**A** + **A**$^-$] = 120 mM (30 mol% **A**$^-$).

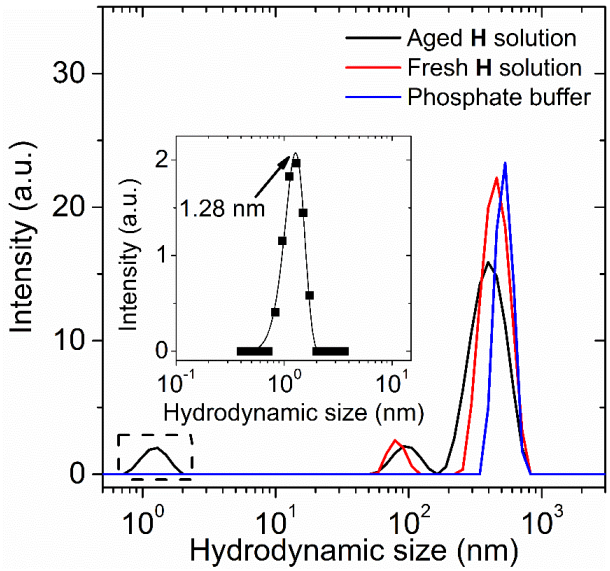

Figure S4.5. DLS measurements of a) fresh and two weeks aged H solutions; and b) THF treated two weeks aged **H** solution. The concentration of **H** used for the measureuments is 4 mM.

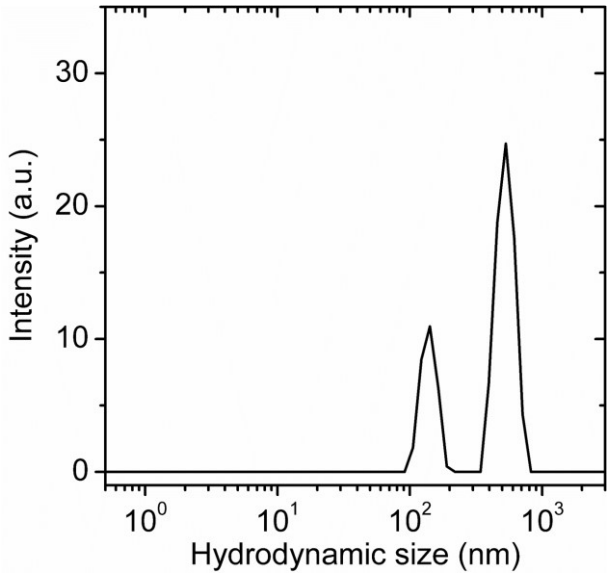

Figure S4.6. DLS measurement of THF treated two-week aged **H** solutions. The concentration of **H** used for the measureuments is 4 mM.

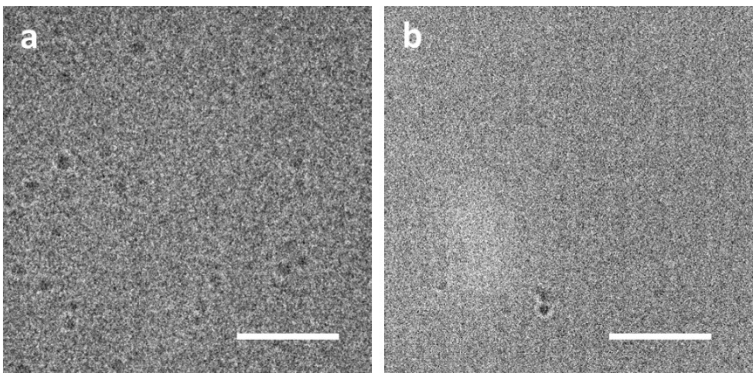

Figure S4.7. Cryo-TEM images of a) two weeks aged and b) freshly prepared **H** solution. Scale bars = 200 nm. The dark dots on these images are contaminations of ice crystals.

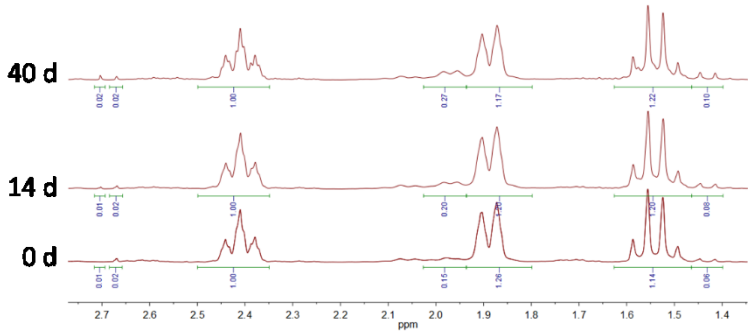

Figure S4.8. ^{1}H NMR spectra of **H** at different incubation time. The solvent for the measurement was D_2O.

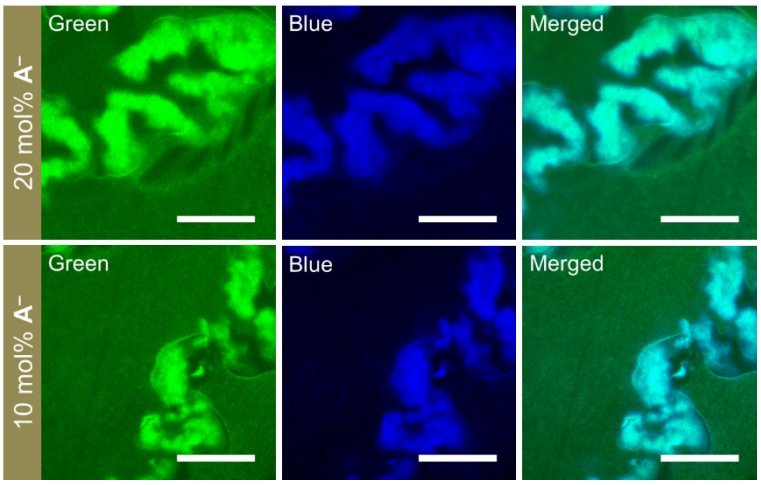

Figure S4.9. CLSM images of the homogeneous gel networks after three weeks incubation. Samples are prepared by 20 mM aged **H**, 120 mM (**A** + **A**$^{-}$) (different mol% **A**$^{-}$), 30 µM **A-FL** (green) and 20 µM **Hoechst 33342** (blue). Scale bars = 20 µm.

References

1. Boekhoven, J.; Poolman, J. M.; Maity, C.; Li, F.; van der Mee, L.; Minkenberg, C. B.; Mendes, E.; van Esch, J. H.; Eelkema, R., Catalytic control over supramolecular gel formation. *Nat. Chem.* **2013,** *5*, 433-7.
2. Poolman, J. M.; Boekhoven, J.; Besselink, A.; Olive, A. G.; van Esch, J. H.; Eelkema, R., Variable gelation time and stiffness of low-molecular-weight hydrogels through catalytic control over self-assembly. *Nat. Protoc.* **2014,** *9*, 977-88.
3. Wang, Y.; Lovrak, M.; Liu, Q.; Maity, C.; le Sage, V. A. A.; Eelkema, R.; van Esch, J. H., Hierarchically compartmentalized supramolecular gels through multilevel self-sorting. *Submitted for publication*.

Chapter 5

Controlled fabrication of micropatterned supramolecular gels by directed self-assembly of small molecular gelators

Abstract: Herein, the micropatterning of supramolecular gels with oriented growth direction and controllable spatial dimensions by directing the self-assembly of small molecular gelators is reported. This process is associated with an acid-catalyzed formation of gelators from two soluble precursor molecules. To control the localized formation and self-assembly of gelators, micropatterned poly(acrylic acid) (PAA) brushes were employed to create a local and controllable acidic environment. The results showed that the gel formation can be well confined in the catalytic surface plane with dimensions ranging from micro- to centimeter. Furthermore, the gels showed a preferential growth towards the normal direction of the catalytic surface, and the thickness of the resultant gel patterns can be easily controlled by tuning the grafting density of PAA brushes. This work shows an effective "bottom-up" strategy towards control over the spatial organization of materials and is expect to find promising applications in, e.g., microelectronics, tissue engineering, and biomedicine.

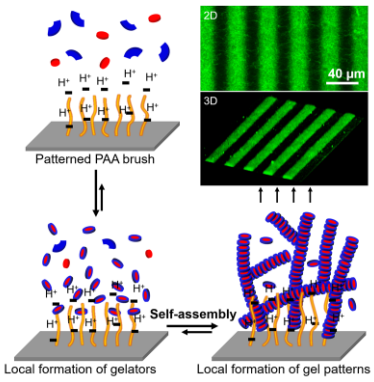

The content of this chapter is based on:
Yiming Wang, Sander Oldenhof, Frank Versluis, Maulik Shah, Kai Zhang, Volkert van Steijn, Xuhong Guo*, Rienk Eelkema*, and Jan H. van Esch*, Controlled fabrication of micropatterned supramolecular gels by directed self-assembly of small molecular gelators. *Small*, **2019**, *15*, 1804154.

5.1 Introduction

Directed molecular self-assembly (DMSA) has emerged as a promising approach to achieve the spatial organization of materials from molecular to macroscopic length scale, showing enticing applications in e.g. molecular robots,[1-3] microelectronics,[4] and energy materials.[5, 6] In recent years, some strategies toward DMSA have been developed. For instance, the employment of self-assembly systems that are sensitive to external stimuli such as light,[7-10] enzymatic action,[11-15] pH,[16-18] and nucleation seeds,[19-21] has led to DMSA by controlling the spatial distribution of these stimuli. Another example of DMSA is achieved by reaction-diffusion,[22, 23] i.e. molecular reactants are separately distributed in space and allowed to react after meeting by diffusion, leading to local self-assembly at a certain pre-programmed location. Despite the recent progress, a major challenge for further advance lies in control of the spatial parameters of the self-assembled structures.[24]

We have recently proposed a catalysis-responsive supramolecular self-assembly system that involves an *in situ* formation of hydrazone-based gelator (**HA_3**) from water-soluble tris-hydrazide (**H**) and aldehyde (**A**) (Figure 5.1). The rate of **HA_3** formation can be remarkably increased by acid catalysis, thereby providing a handle to control subsequent gelation.[25, 26] Using this gelator system, we previously achieved the surface confined formation of gels using surfaces modified with a monolayer of sulfonic acid that act as a catalyst for gelator formation.[27] That system has, however, several limitations which hamper further progress. First, the spatial resolution of gel formation along the surface plane is limited, presumably by the low interfacial catalytic activity. And second, the growth of the gels along the surface normal to form three dimensional (3D) objects is hampered by adhesion of gel fibers to the surface, which blocks the influx of reagents to the catalytic surface. With these problems in mind, in this work, we aim to develop interfacial catalytic patterns that enable control over the growth of gels in all three dimensions, and additionally, to obtain a better understanding of the local reaction-diffusion coupled self-assembly process that is required for the rational design of DMSA systems.

To reach this goal, we hypothesized that the catalytic activity of the patterned catalyst needs to be increased and become tunable, while simultaneously the adhesion of the gel fibers onto the catalytic surface needs to be prevented to allow for continuous growth of the gel patterns. As a possible solution, we focused on surfaces patterned with catalytic polymer brushes. Polymer brushes composed of a surface densely grafted with polymer chains show considerable potential to effectively increase the catalytic activity by using acidic polymers,[28] which would be benificial for reinforcing the spatial controllability. Importantly, compared to self-assembled

monolayers (SAMs), the fabrication of polymer brushes can be precisely controlled by using controlled "living" radical polymerization techniques,[29, 30] offering a handle to control the local catalytic activity and hence the gel growth. Moreover, it has been demonstrated that polymer brushes show anti-fouling behavior by preventing the adsorbance of foreign objects, such as nanoparticles and macromolecules, through the steric repulsions of polymer chains,[31-34] which may provide a solution to the problem of adhesion of gel fibers.

Here we investigate if patterned poly(acrylic acid) (PAA) brushes can be used to spatially control the formation of gels through local catalytic formation and self-assembly of **HA$_3$** (Figure 5.1). We find that gel formation can be precisely controlled in the surface plane with spatial dimensions varying from micro- to centimeter. Importantly, the gels show a preferential growth along the surface normal direction, which can be controlled by tuning the local catalytic activity *via* simply changing the grafting density of the PAA brushes.

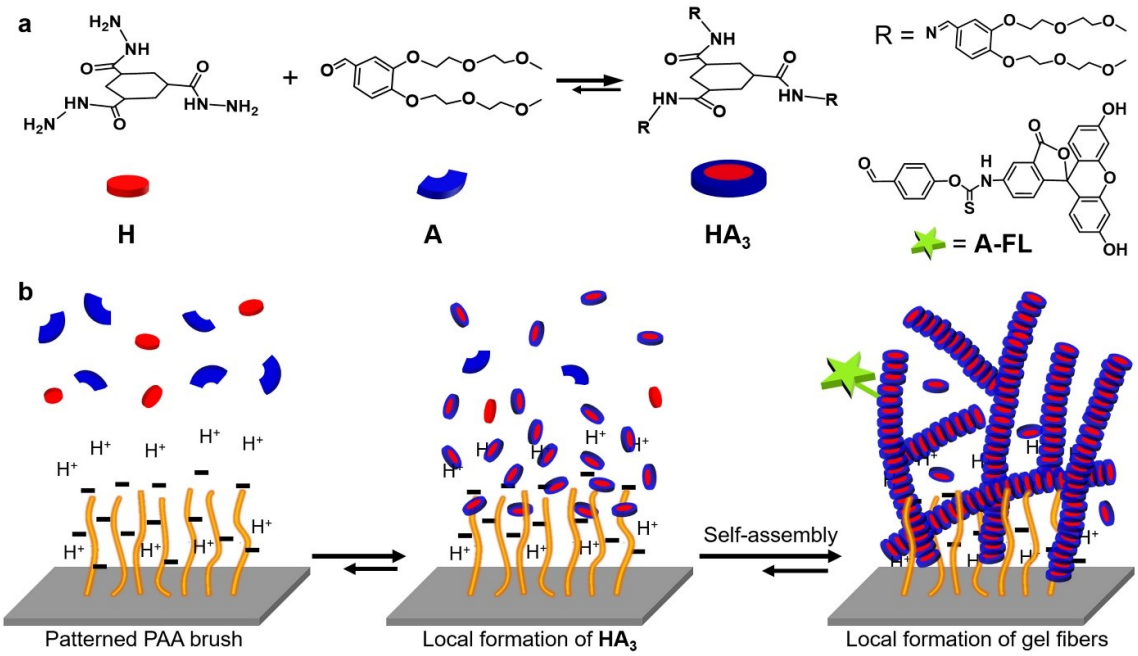

Figure 5.1. Illustration of localized hydrazone gel formation at the surface of micropatterned PAA brush through the local catalysis formation and self-assembly of **HA$_3$**.

5.2 Results and discussion

Patterned PAA brushes were prepared by surface-initiated atom-transfer radical polymerization (SI-ATRP) (supporting information).[35, 36] To this end, microcontact printing (μCP) was employed to prepare micropatterns of (3-aminopropyl)triethoxysilane (APTES) on the glass surface,[37] which were then converted to ATRP initiators by coupling of the amino moieties with α-bromoisobutyryl bromide. These patterns were subsequently used to grow PAA

brushes from the monomers of sodium acrylate (Figure S5.1). Characterization of the functionalized glass slides by atomic force microscopy (AFM) showed that the patterns of the stamps, including the shape and dimensions, were precisely transferred to the resultant PAA brushes (Figure S5.2). Furthermore, using different concentrations of APTES ink, increasing from 0.5 to 3.0 wt%, during μCP resulted in brushes with different thickness, increasing from 10 to 55 nm, correspondingly (Figure S5.2). This clearly shows that the grafting density can be easily controlled by varying the concentration of APTES ink during μCP.

Since pH is a key parameter for catalyzing the formation of **HA_3**, we first estimated the electrostatic potential and pH distribution near the brush surface using a simple simulation based on Grahame and Poisson-Boltzmann equations (Supporting Information). The calculations show that a drop in pH from 5.5 in bulk solution to ~3.7 at the brush surface can be obtained (Figure S5.3), suggesting a large enough pH difference to catalyze gelator formation preferentially near the brush surface. In addition, we found that the addition of salt dramatically reduced the pH difference between bulk solution and brush surface due to screening of interfacial charges (Figure S5.3). Thus, milli-Q water was used for the gel formation in this study with the aim to obtain a high efficiency of interfacial catalysis.

To examine the local catalysis formation and self-assembly of **HA_3** near the brush surface, a glass surface with grafted PAA brushes was brought into contact with a freshly prepared gelator precursor solution composed of 10 mM **H** and 60 mM **A** (a six-fold excess of **A** was used to ensure full conversion of **H** to **HA_3**) in milli-Q water under the protection of a homemade poly(dimethylsiloxane) (PDMS) chamber (Figure S5.4). To visualize the growth of gel fibers using confocal laser scanning microscopy (CLSM), 30 μM aldehyde modified fluorescein (**A-FL**) was added to covalently label the gel fibers.[25] After an overnight incubation, we found that gel patterns with designed shapes, including squares, lines, rings, and letters, were indeed formed at the brush areas and reproduce with excellent fit of the shapes and dimensions of the parent PAA brushes (Figure 5.2a and b). Importantly, the pattern dimensions in the interfacial plane can be varied over a broad length scale ranging from micro- to centimeters (Figure 5.2 and S5.5). These experiments indicate that **HA_3** are formed and have rapidly self-assembled into gel fibers before diffusing away into the bulk solution. This fast time scale for reaction compared to diffusion results from the excellent local catalysis of the PAA brushes. Nucleation by templates has also been exploited for local growth of supramolecular structures,[19-21] however, in our case a separated catalyst-free self-assembly of **HA_3** confirms that the PAA brushes did not show nucleation effect on the self-assembly of **HA3** (Figure S5.6).

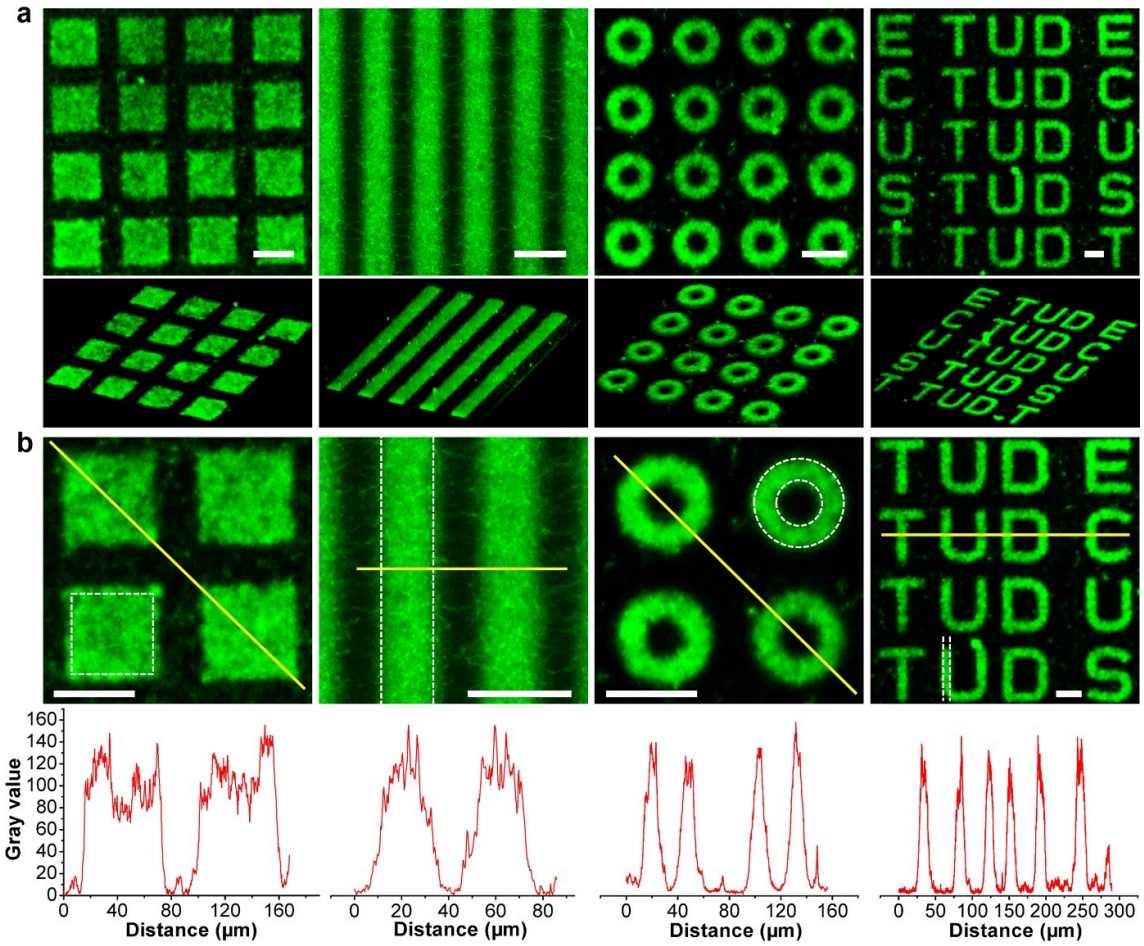

Figure 5.2. a) Confocal images of gel patterns in different shapes (top: 2D images, bottom: the corresponding 3D images), from left to right are squares, lines, rings, and letters; b) magnified confocal images of the gel patterns and gray intensity profiles corresponding to the yellow lines on the confocal images, the white dashed lines on the confocal images indicate the corresponding brush areas. Scale bars = 40 μm.

To further investigate the catalytic effect of the brush patterns on local gel formation, we investigated how the growth rate and thickness of the gel patterns can be controlled by the brushes. For this purpose, brush patterns with various grafting densities, denoted as B1 < B2 < B3 < B4, were prepared by performing μCP with 0.5, 1.0, 2.0, and 3.0 wt% APTES inks, respectively. We monitored the growth of gel patterns from these brushes over time by CLSM (Figure 5.3a). Snapshots of the time series of gels grown from these brushes and time traces of the gel thickness are shown in Figure 5.3a and b, respectively. It can be seen clearly that increasing the grafting density of PAA brush led to a decrease in the critical growth time of the gel fibers (defined as the time at which the thickness of the gel fibers start to increase) from ~9.0 min for B1 to ~1.5 min for B4 (Figure 5.3b and c), which can be attributed to the decrease in local pH upon the increase in grafting density of PAA chains. After that, an oriented growth of gel fibers along the surface normal direction was

observed (Figure 5.3a), leading to the formation of 3D gel patterns. However, the gels did not grow infinitely, for instance, in B4, the growth of gel fibers at the brush surface slowed down after ~13 min and effectively halted after ~20 min (Figure 5.3b and c). Similar growth profiles, though with different time scales, were observed in the samples of B1 to B3 (Figure 5.3c). The final thickness of the gels was also found to depend on the grafting density of PAA brushes, increasing from ~16 μm for B1 to ~29 μm for B4 (Figure 5.3a and d). The increase of the gel thickness with the grafting density can be attributed to increased acidity of the polymer brushes at higher grafting densities, leading to formation of more $\mathbf{HA_3}$, thereby resulting in thicker gel layers.

To account for the halted growth and finite gel thickness, we initially hypothesized that this is due to the depletion of the precursor molecules near the catalytic brushes after a certain time of reaction. To test this hypothesis, we performed a gelation experiment in a flow cell to provide a continuous supply of precursor solutions to the brush surface (Figure S5.7). However, instead of a continuous gel growth, a similar growth profile with the previous batch experiment was found, indicating that the growth of the gel patterns is not limited by depletion of the precursor molecules. Interestingly, during these flow experiments we noticed that the gel patterns were strongly attached to the PAA brushes, even upon washing vigorously with water (Figure S5.8), suggesting the presence of strong interactions between the gel fibers and the brush surfaces. These results are in line with a previous finding, which showed that in acidic condition the hydrazone fibers are protonated and hence slightly positively charged.[28] Therefore, most likely the electrostatic interactions between positively charged fibers and negatively charged PAA brushes are responsible for the adhesion of gel fibers. Given these results, it is reasonable that the physically attached gel fibers make the catalytic brush surface inaccessible for **H** and **A**, thus resulting in the limited growth of gel fibers.

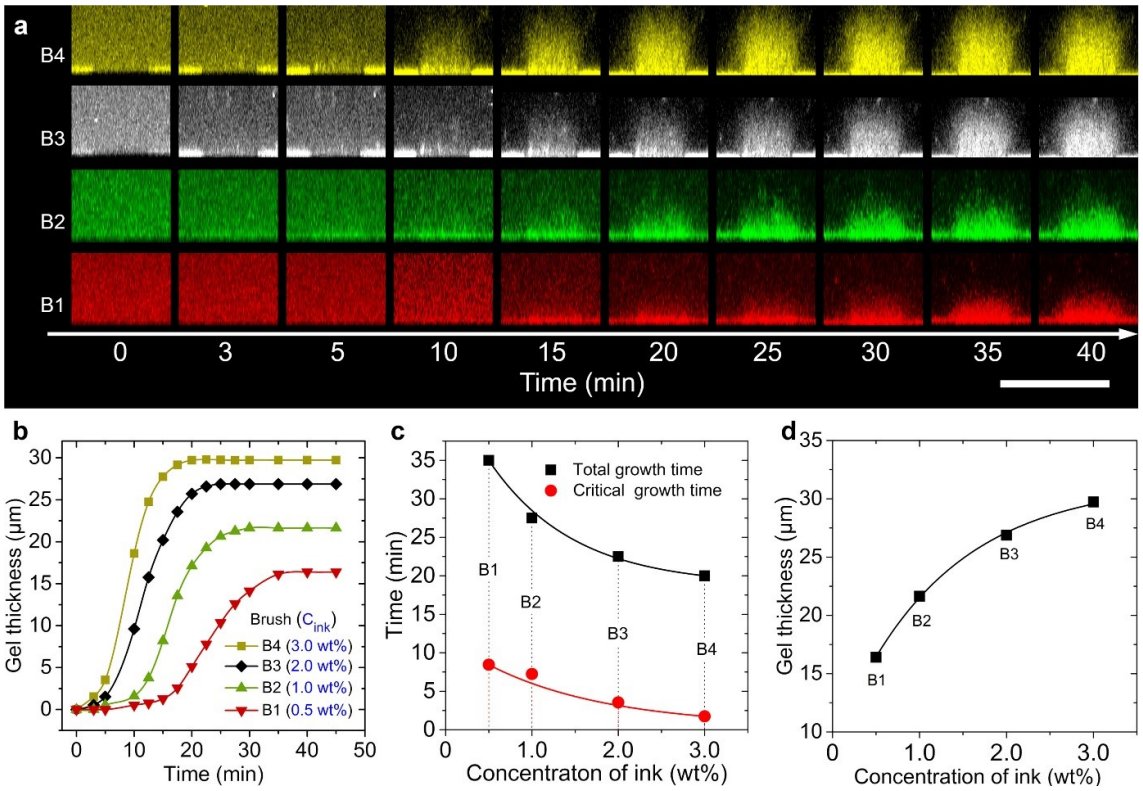

Figure 5.3. a) Confocal images of the growth of gels in the normal direction of the brush surface, scale bar = 40 μm; b) variation of gel thickness as a function of grafting density of the PAA brushes; c) the critical growth time (the time that the first fiber was observed) and the total growth time (the time that the gel thickness reached at a plateu) as a function of the brush density; d) the effects of brush density on the final thickness of the gel patterns.

The preceding results suggest that our brushes do not present obvious anti-fouling against the gel fibers due to the presence of electrostatic interactions, which lead us to investigate the mechanism by which gel fibers can be promoted to grow along the normal direction of the brush surface. From the experiments discussed so far, we know that the gelators are always formed preferentially at the brush areas due to the local catalysis. To drive the growth of gels along the normal direction of the brush surface, three kinds of growth mechanisms can be expected (Figure 5.4a): I) the newly formed gelators diffuse to the top area and add to the upper end of the already formed gel fibers, leading to the growth of new gel fibers from the top area of the old ones, as a result, the fluorescence profile of the gel fibers along the normal direction should extend upward (case I in Figure 5.4a); II) the new gelators add to the bottom of the already formed gel fibers, thereby pushing the gel fibers upward, in this case, the fluorescence profiles should shift toward the normal direction (case II in Figure 5.4a); and III) the newly formed gelators diffuse from the catalytic surface into the already formed gel matrix, and nucleate at the old gel fibers, leading to occurrences of branching, bundling, and/or elongation of fibers, which would not

only lead to the increase of fluorescence intensity at each location, but also lead to a shift of the fluorescence profile upward (case III in Figure 5.4a).

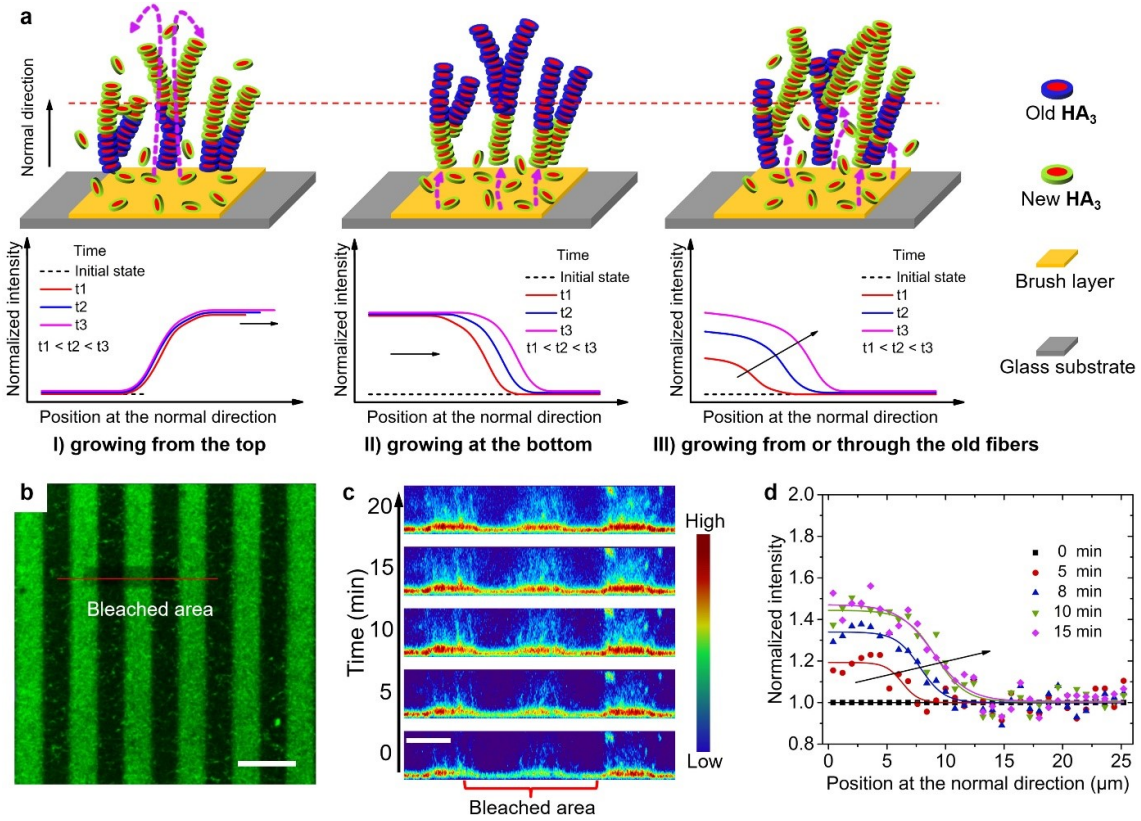

Figure 5.4. a) Scheme of the possible mechanisms of gel growth (top) and the corresponding evolution of fluorescence intensity over time along the surface normal direction (bottom); b) confocal images with bleached area acquired from the surface plane, scale bar = 40 μm; c) growth of the gel patterns in the surface normal direction after bleaching, scale bar on the left image is 20 μm and the right colour gradient indicates the fluorescence intensity of the gel fibers; d) spatiotemporal fluorescence intensity curves normalized by the one after bleaching. B2 was used in b-d).

To confirm the mechanism of gel growth, we performed a bleaching treatment on the growing gel fibers (Figure 5.4b). We found that the bleached gel fibers further grown from ~15 to ~20 μm in thickness and the fluorescence intensity was increased over time after bleaching, suggesting the addition of new gelators into the previously formed gel fibers. Importantly, upon monitoring the evolution of the fluorescence intensity profile of the gel pattern over time along the surface normal direction, we found the fluorescence intensity was increased from the bottom to the top area (Figure 5.4d), in addtion, the intensity profiles showed a shift along the normal direction, which is in good agreement with case III illustrated in Figure 5.4a. These results clearly show that the newly formed gelators diffuse from the brush surface into the previously formed fibers, leading to the increase of fluorescence intensity from the bottom area. The new glators in turn nucleate at the old fibers and results in

branching, bunlding and/or elongation of fibers, thereby leading to the increase in the gel thickness as well as the fiber density. The intensity reached at an equilibrium state within 15 min, however, the fluorescence intensity of the bleached area is still lower than the unbleached pattern (Figure 5.4c). It thus indicates that the old gel fibers stay at their original position which subsequently block the influx of new **H** and **A** and limit the further growth of gel fibers.

5.3 Conclusions

In conclusion, we have shown the micropatterning of supramolecular gels with controllable spatial dimensions and oriented growth direction through directing the self-assembly of low molecular weight gelators. The efficient local catalysis of micropatterned PAA brushes leading to local formation of gelators enables us to precisely control localized gel formation in different spatial shapes and at broad length scales varying from micro- to centimeter. Importantly, the gel patterns present preferential growth along the normal direction of the brush surface, and their thickness can be easily controlled by simply tunning the grafting density of PAA brushes. We believe this reported "bottom-up" approach for precise control of spatial organization of materials would be of great potential for high-tech applications, for instance, microelectronics, biotherapy, and sensors.

5.4 References

1. Hess, H.; Ross, J. L., Non-equilibrium assembly of microtubules: from molecules to autonomous chemical robots. *Chem. Soc. Rev.* **2017,** *46*, 5570-5587.
2. Thubagere, A. J.; Li, W.; Johnson, R. F.; Chen, Z. B.; Doroudi, S.; Lee, Y. L.; Izatt, G.; Wittman, S.; Srinivas, N.; Woods, D.; Winfree, E.; Qian, L. L., A cargo-sorting DNA robot. *Science* **2017,** *357*.
3. Cera, L.; Schalley, C. A., Under Diffusion Control: from Structuring Matter to Directional Motion. *Adv. Mater.* **2018**, 1707029.
4. Galland, R.; Leduc, P.; Guerin, C.; Peyrade, D.; Blanchoin, L.; Thery, M., Fabrication of three-dimensional electrical connections by means of directed actin self-organization. *Nat. Mater.* **2013,** *12*, 416-421.
5. Li, W. Z.; Fan, J. D.; Li, J. W.; Mai, Y. H.; Wang, L. D., Controllable Grain Morphology of Perovskite Absorber Film by Molecular Self-Assembly toward Efficient Solar Cell Exceeding 17%. *J. Am. Chem. Soc.* **2015,** *137*, 10399-10405.
6. Han, L. L.; Jiang, H. X.; Ouyang, D.; Chen, W. C.; Hu, T.; Wang, J. Y.; Wen, S. G.; Sun, M. L.; Yang, R. Q., Cyclic alkyl chains promote the polymer self-assembly and packing orders for solar cells. *Nano Energy* **2017,** *36*, 110-117.

7. Kundu, P. K.; Samanta, D.; Leizrowice, R.; Margulis, B.; Zhao, H.; Borner, M.; Udayabhaskararao, T.; Manna, D.; Klajn, R., Light-controlled self-assembly of non-photoresponsive nanoparticles. *Nat. Chem.* **2015,** *7*, 646-52.
8. Cornwell, D. J.; Daubney, O. J.; Smith, D. K., Photopatterned Multidomain Gels: Multi-Component Self-Assembled Hydrogels Based on Partially Self-Sorting 1,3:2,4-Dibenzylidene-D-sorbitol Derivatives. *J. Am. Chem. Soc.* **2015,** *137*, 15486-92.
9. He, X.; Fan, J.; Zou, J.; Wooley, K. L., Reversible photo-patterning of soft conductive materials via spatially-defined supramolecular assembly. *Chem. Commun.* **2016,** *52*, 8455-8.
10. Groombridge, A. S.; Palma, A.; Parker, R. M.; Abell, C.; Scherman, O. A., Aqueous interfacial gels assembled from small molecule supramolecular polymers. *Chem. Sci.* **2017,** *8*, 1350-1355.
11. Williams, R. J.; Smith, A. M.; Collins, R.; Hodson, N.; Das, A. K.; Ulijn, R. V., Enzyme-assisted self-assembly under thermodynamic control. *Nat. Nanotechnol.* **2009,** *4*, 19-24.
12. Pires, R. A.; Abul-Haija, Y. M.; Costa, D. S.; Novoa-Carballal, R.; Reis, R. L.; Ulijn, R. V.; Pashkuleva, I., Controlling Cancer Cell Fate Using Localized Biocatalytic Self-Assembly of an Aromatic Carbohydrate Amphiphile. *J. Am. Chem. Soc.* **2015,** *137*, 576-579.
13. Zhou, J.; Du, X. W.; Yamagata, N.; Xu, B., Enzyme-Instructed Self-Assembly of Small D-Peptides as a Multiple-Step Process for Selectively Killing Cancer Cells. *J. Am. Chem. Soc.* **2016,** *138*, 3813-3823.
14. Zhou, J.; Du, X.; Xu, B., Regulating the Rate of Molecular Self-Assembly for Targeting Cancer Cells. *Angew. Chem. Int. Edit.* **2016,** *55*, 5770-5.
15. Rodon Fores, J.; Martinez Mendez, M. L.; Mao, X.; Wagner, D.; Schmutz, M.; Rabineau, M.; Lavalle, P.; Schaaf, P.; Boulmedais, F.; Jierry, L., Localized Supramolecular Peptide Self-Assembly Directed by Enzyme-Induced Proton Gradients. *Angew. Chem. Int. Edit.* **2017,** *56*, 15984-15988.
16. Ziemecka, I.; Koper, G. J. M.; Olive, A. G. L.; van Esch, J. H., Chemical-gradient directed self-assembly of hydrogel fibers. *Soft Matter* **2013,** *9*, 1556-1561.
17. Spitzer, D.; Marichez, V.; Formon, G.; Besenius, P.; Hermans, T., Surface‐assisted self‐assembly of a hydrogel by proton diffusion. *Angew. Chem. Int. Edit.* **2018**.
18. Chang, Y. C.; Huang, Z. H.; Jiao, Y.; Xu, J. F.; Zhang, X., pH-Induced Charge-Reversal Amphiphile with Cancer Cell-Selective Membrane-Disrupting Activity. *Acs Applied Materials & Interfaces* **2018,** *10*, 21191-21197.
19. Tiller, J. C., Increasing the local concentration of drugs by hydrogel formation. *Angew. Chem. Int. Edit.* **2003,** *42*, 3072-5.
20. Bieser, A. M.; Tiller, J. C., Surface-induced hydrogelation. *Chem. Commun.* **2005**, 3942-4.
21. Angelerou, M. G. F.; Sabri, A.; Creasey, R.; Angelerou, P.; Marlow, M.; Zelzer, M., Surface-directed modulation of supramolecular gel properties. *Chem. Commun.* **2016,** *52*, 4298-4300.
22. Lovrak, M.; Hendriksen, W. E. J.; Maity, C.; Mytnyk, S.; van Steijn, V.; Eelkema, R.; van Esch, J. H., Free-standing supramolecular hydrogel objects by reaction-diffusion. *Nat. Commun.* **2017,** *8*, 15317.

23. Lovrak, M.; Picken, S.; Eelkema, R.; van Esch, J., Supramolecular gluing of polymeric hydrogels. *ChemNanoMat* **2018**.
24. Vigier-Carrière, C.; Boulmedais, F.; Schaaf, P.; Jierry, L., Surface ‐ assisted self ‐ assembly strategies leading to supramolecular hydrogels. *Angew. Chem. Int. Edit.* **2017,** *57*, 1448-1456.
25. Boekhoven, J.; Poolman, J. M.; Maity, C.; Li, F.; van der Mee, L.; Minkenberg, C. B.; Mendes, E.; van Esch, J. H.; Eelkema, R., Catalytic control over supramolecular gel formation. *Nat. Chem.* **2013,** *5*, 433-7.
26. Poolman, J. M.; Boekhoven, J.; Besselink, A.; Olive, A. G.; van Esch, J. H.; Eelkema, R., Variable gelation time and stiffness of low-molecular-weight hydrogels through catalytic control over self-assembly. *Nat. Protoc.* **2014,** *9*, 977-88.
27. Olive, A. G.; Abdullah, N. H.; Ziemecka, I.; Mendes, E.; Eelkema, R.; van Esch, J. H., Spatial and directional control over self-assembly using catalytic micropatterned surfaces. *Angew. Chem. Int. Edit.* **2014,** *53*, 4132-6.
28. Wang, Y.; Versluis, F.; Oldenhof, S.; Lakshminarayanan, V.; Zhang, K.; Wang, Y.; Wang, J.; Eelkema, R.; Guo, X.; van Esch, J. H., Directed Nanoscale Self-Assembly of Low Molecular Weight Hydrogelators Using Catalytic Nanoparticles. *Adv. Mater.* **2018,** *30*, 1707408.
29. Pyun, J.; Kowalewski, T.; Matyjaszewski, K., Synthesis of polymer brushes using atom transfer radical polymerization. *Macromol. Rapid Commun.* **2003,** *24*, 1043-1059.
30. Edmondson, S.; Osborne, V. L.; Huck, W. T., Polymer brushes via surface-initiated polymerizations. *Chem. Soc. Rev.* **2004,** *33*, 14-22.
31. McPherson, T.; Kidane, A.; Szleifer, I.; Park, K., Prevention of protein adsorption by tethered poly(ethylene oxide) layers: Experiments and single-chain mean-field analysis. *Langmuir* **1998,** *14*, 176-186.
32. Halperin, A., Polymer brushes that resist adsorption of model proteins: Design parameters. *Langmuir* **1999,** *15*, 2525-2533.
33. Szleifer, I.; Carignano, M. A., Tethered polymer layers: phase transitions and reduction of protein adsorption. *Macromol. Rapid Commun.* **2000,** *21*, 423-448.
34. Drobek, T.; Spencer, N. D.; Heuberger, M., Compressing PEG brushes. *Macromolecules* **2005,** *38*, 5254-5259.
35. Chen, T.; Chang, D. P.; Zauscher, S., Fabrication of Patterned Polymer Brushes on Chemically Active Surfaces by in situ Hydrogen-Bond-Mediated Attachment of an Initiator. *Small* **2010,** *6*, 1504-1508.
36. Wang, W. Q.; Ren, G. H.; Cai, W. J., 3D-gold superstructures grown on a poly(acrylic acid) brush. *Rsc Adv.* **2015,** *5*, 60857-60860.
37. Li, H.; Zhang, J.; Zhou, X.; Lu, G.; Yin, Z.; Li, G.; Wu, T.; Boey, F.; Venkatraman, S. S.; Zhang, H., Aminosilane micropatterns on hydroxyl-terminated substrates: fabrication and applications. *Langmuir* **2010,** *26*, 5603-9.

5.5 Supplementary information

Materials

All commercial chemicals were purchased from Sigma Aldrich. Molecule **H**, **A**, and **A-FL** were synthesized based on the method which has been reported in previous work.[1, 2]

Experimental

Preparation of PDMS stamp

To prepare the PDMS stamp with different patterns, the base of Sylgard® 184 silicone elastomer was first mixed with curing agent in a weight ratio of 10:1. After stirring for 3 min, the mixture was fully degassed and then poured onto a silicon master in a petri dish. After a further degassing treatment, the dish was placed in an oven and incubated at 68 ^{o}C for 7 h. After curing, the generated PDMS stamp was carefully peeled from the wafer and cut into certain size for the subsequent use.

Preparation of (3-Aminopropyl)triethoxysilane (APTES) patterns on glass by microcontact printing with PDMS stamps

We first printed APTES onto a glass surface to immobilize the functional groups on the surface with different patterns and different grafting density according to a literature procedure (Figure S5.1).[3] Basically, an appropriate amount of APTES aqueous solution was dropped onto the surface of PDMS stamp and removed after incubating for 2 min. The inked stamp was first dried under an N_2 flow and then pressed onto the surface of a glass slide that was treated by an oxygen-plasma for 15 s. After peeling off the stamp, the glass slide was then placed in a 100 ^{o}C oven for 2 h to achieve a complete bonding between APTES and the glass surface. Different concentrations of APTES ink solution were used as a way to control the grafting density of the brushes.

Immobilization of ATRP initiators

The APTES functionalized glass slides were immersed in 15 mL anhydrous THF containing 0.9 mL anhydrous triethylamine. After bubbling with N_2 for 30 min, 0.8 mL α-Bromoisobutyryl bromide (BiBB) was added dropwise into the above solution under ice cooling within 10 min. After reacting under ice cooling for 1 h, the temperature was allowed to increase to room temperature and the solution was left to react for another 2 h. The experiment was carried out in N_2 atmosphere. After the reaction, the glass slides were taken out from the solution, rinsed with excess ethanol

to clean the surface, and dried under N_2 flow to give the glass substrate grafted with patterned ATRP initiators.

Polymerization of sodium acrylate

Polymerization of sodium acrylate was carried out as the literature described (Figure S5.1).[4] Basically, a monomer solution of sodium acrylate (1.88 g, 20.00 mmol) in water (8 mL) was bubbled with argon for at least 30 min to remove the dissolved oxygen. Simultaneously, a catalyst solution for the subsequent ATRP polymerization was prepared by dissolving CuBr (5.74 mg, 0.04 mmol) and 2,2'-dipyridine (13.74 mg, 0.088 mmol) into 1 mL deoxygenated methanol. The monomer solution was then mixed with the catalyst solution and transferred into a Schlenck flask containing the previously prepared glass slides, the whole process was performed under the protection of argon. After evacuating and back-filling with argon for three times, the polymerization was carried out at room temperature for 3 h. At the end of the polymerization, the glass slide was taken out, rinsed with excess milliQ water to remove the unreacted traces and to protonate the polymer chains, and then dried over a N_2 flow.

XPS characterization

The XPS measurement was carried out on a Thermo scientific instrument (K-alpha surfaces analysis) using a 400 μm beam spot. Obvious carbon and oxygen signals were observed in the survey spectrum, which demonstrated the composition of PAA chains (Figure S5.2a). However, no sodium signal was observed from the survey spectrum, demonstrating the complete protonation of the PAA brush after rinsing with excess water (Figure S5.2a). The fitting results showed that the C1s peak was formed by 3 sub-peaks with binding energy of 285.10, 285.65, and 288.80 eV (Figure S5.2b), the corresponding area ratio was 42.2%, 28.8%, and 28.9%, respectively. This result is in good agreement with the reported data.[5]

Atomic force microscopy (AFM) characterization

The AFM characterization of patterned PAA brushes was performed using a Ntegra P8 from NT-MDT equipped with a NSG01 series tip (Resonant Frequency 140 KHz, force constant 3.5 N/m) received from NT-MDT. The images were acquired in a semi-contact mode (Figure S5.2c and d).

Estimation of the electrostatic potential and pH distribution near the surface of PAA brush in miliQ water

Grahame (Eq. 1) and Poisson-Boltzmann (Eq. 2 and 3) equations were employed to estimate the distribution of electrostatic potential ($\psi(x)$) and pH ($C_{H^+}(x)$) near the surface of PAA brush (Figure S5.3a and b).

$$\psi(0)=\frac{2k_BT}{e}\sinh^{-1}\left(\frac{\sigma}{\sqrt{8\varepsilon\varepsilon_o k_B T C^b_{salt} N_A}}\right) \quad (1)$$

$$\psi(x)=\frac{2k_BT}{e}\ln\left(\frac{1+\varphi\cdot\exp(-\kappa x)}{1-\varphi\cdot\exp(-\kappa x)}\right) \quad (2)$$

$$C_{H^+}(x)=C^b_{H^+}\left(\frac{1+\varphi\cdot\exp(-\kappa x)}{1-\varphi\cdot\exp(-\kappa x)}\right)^{-2} \quad (3)$$

where k_B is Boltzman constant, e electron charge, σ the surface charge density, ε permittivity constant of the medium, ε_o permittivity of vacuum, T the temperature, C_{salt} the concentration of salt, N_A Avogadro constant, κ the inverse Debye length (κ = $(2C_{salt}e^2/\varepsilon\varepsilon_o\, k_BT)^{1/2}$), x the distance from the surface; $\varphi = \tanh(e\cdot\psi(0)/4k_BT)$.[6]

Confocal laser scanning microscope (CLSM) measurement

The confocal experiment was carried out on a Zeiss LSM 710 equipped with a Zeiss Axio Observer inverted microscope and 40× PlanFluor oil immersion objective lens (NA 1.3) using an incident laser with a wavelength of 488 nm to excite the fluorescein probe. To make the fibers visible, a fluorescein derivative dye was added to the samples at a concentration of 30. The pinhole was set to 1.0 airy unit; a slice size of 0.53 µm was used for the z-stacks scanning. An interval time of 0.5 min was set for the time series scanning. The images and movie were processed using ZEN 2011 software.

Gel fiber growth on the surface

A PDMS chamber (10 × 10 × 3 mm) was used in the confocal experiments. This chamber was completely filled with a gelator precursor solution prepared by mixing the stock solutions of **H** and **A**. A glass slide with grafted PAA brushes was placed on top of the chamber with the brush side facing to the solution to seal it, and then put upside down on the confocal microscope to observe the growth of gel fibers (Figure S5.4).

Nucleation effects

The nucleation effect of negatively charged PAA brush on the gelation process was investigated by performing the self-assembly of pre-synthesized catalyst-free gelator **HA$_3$** at the brush surface. Basically, 300 µL gelator precursor solution (10 mM **H** and

60 mM **A** in miliQ-water) was first prepared by mixing the stock solutions of **H** and **A**. This precursor solution was allowed to stay overnight for a full conversion of **H** into **HA$_3$**. The obtained gel sample was dissolved by adding 100 µL THF to give a homogeneous gelator solution. 200 µL of this gelator solution was then transferred to contact with the glass surface grafted with PAA brush and placed in a vacuum condition (100 mbar) at room temperature. After evaporating THF from the solution (~30 min), gelator **HA$_3$** can self-assemble into gel fibers. This gel sample was collected and characterized by LCSM to observe the gel fibers formation near the brush surface.

Bleaching experiment

The bleaching experiment was carried out during the gel fiber growth. Briefly, after 15 min of growth, the growing gel fibers was bleached using a 405 nm laser. After the bleaching treatment, a *z*-stacks plus time series scan was performed to monitor the fluorescence variation of the bleached area.

Flow cell test

In the flow cell experiment, a PDMS chamber with inlet and outlet tubes was used. Two syringes containing **H** (20 mM) and **A** (120 mM) solutions were fixed on a syringe pump to deliver the gelator precursor solutions into the chamber continuously (Figure S5.7). The velocity of the flow at the inlet area was set to be 20 µL/min to give a residence time of 15 min. The fiber growth was monitored by CLSM.

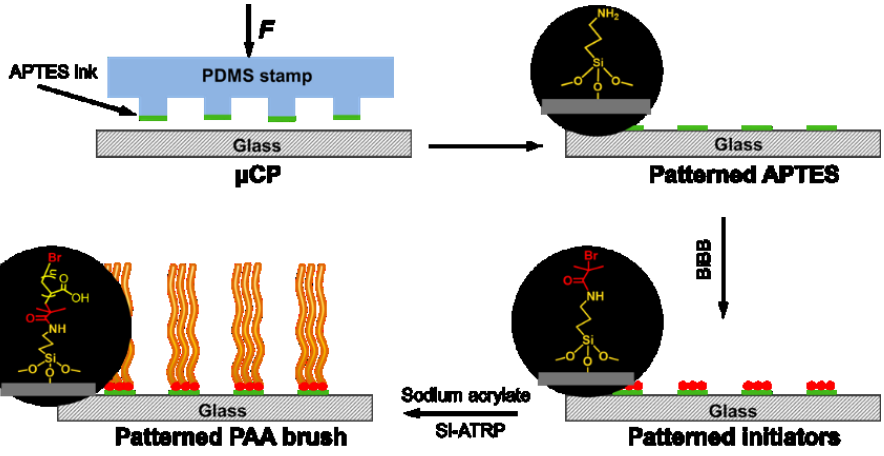

Figure S5.1. Scheme of the preparation of patterned PAA brush via SI-ATRP of sodium acrylate.

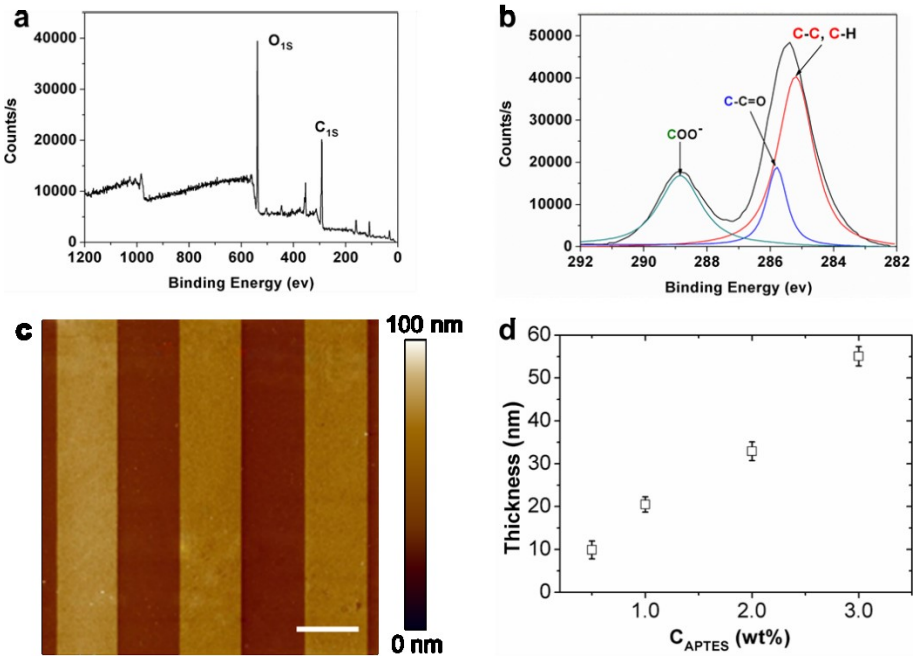

Figure S5.2. Characterization of the patterned PAA brush. a) XPS survey spectrum; b) high resolution C_{1s} spectrum of surface grafted PAA brush; c) topographical AFM image of strip-shaped PAA brushes, 20 µm width with 20 µm spacing, prepared using 2.0 wt% APTES ink for µCP, scale bar = 20 µm; and d) dependence of brush thickness on the concentration of APTES ink for µCP, these brushes were prepared under the same experimental conditions.

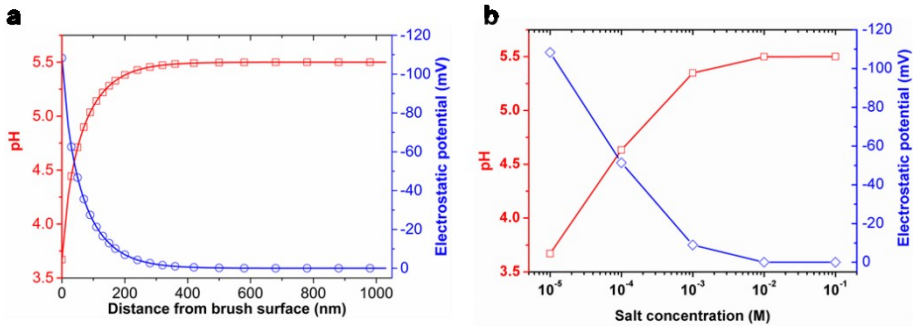

Figure S5.3. Estimation of a) pH and electrostatic potential as a function of the distance from the surface of the PAA brush; and b) salt effect on the local pH and electrostatic potential.

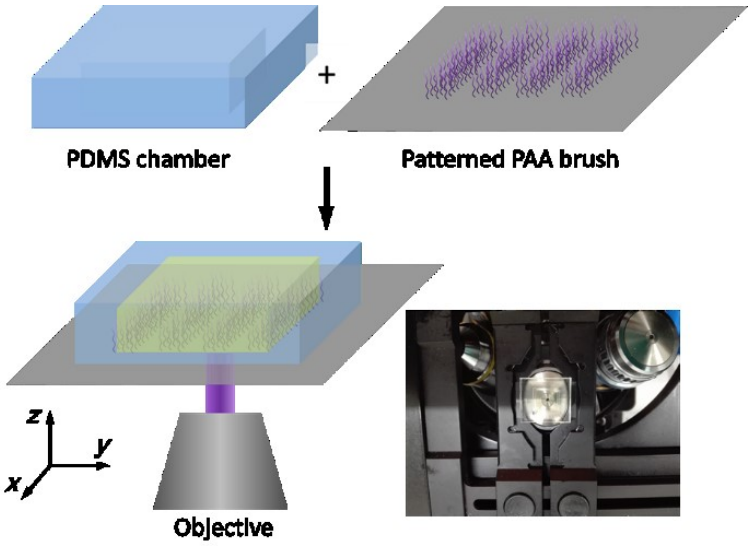

Figure S5.4. Illustration of confocal measurement setup for the observation of the growth of gel fibers.

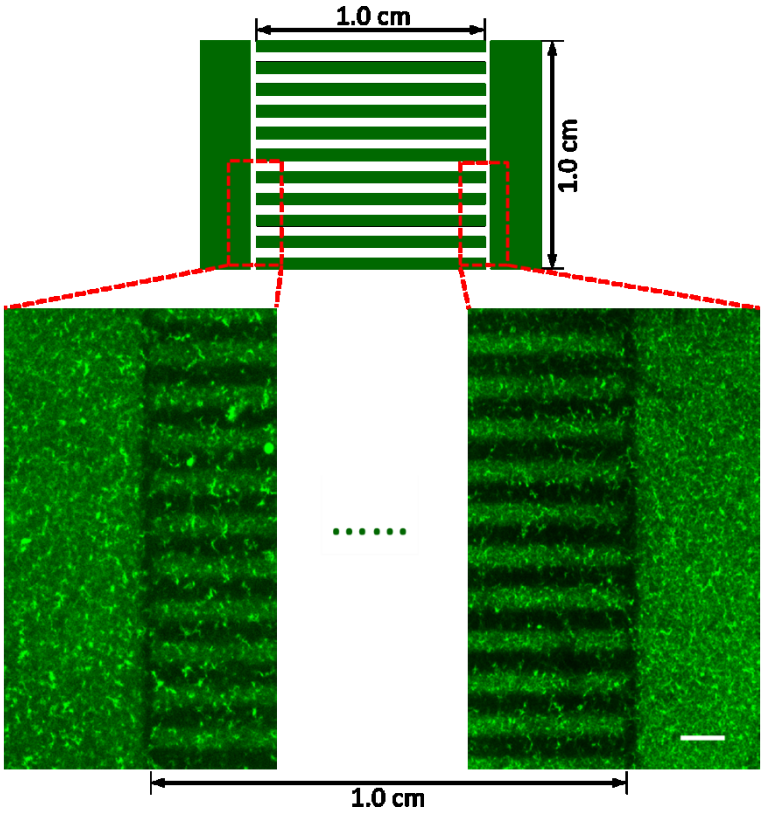

Figure S5.5. Confocal image of strip gel patterns with 1.0 cm length and 10 µm width. [**H**] = 10 mM, [**A**] = 60 mM, [**A-FL**] = 30 µM, strip B3 was used, scale bar = 20 µm.

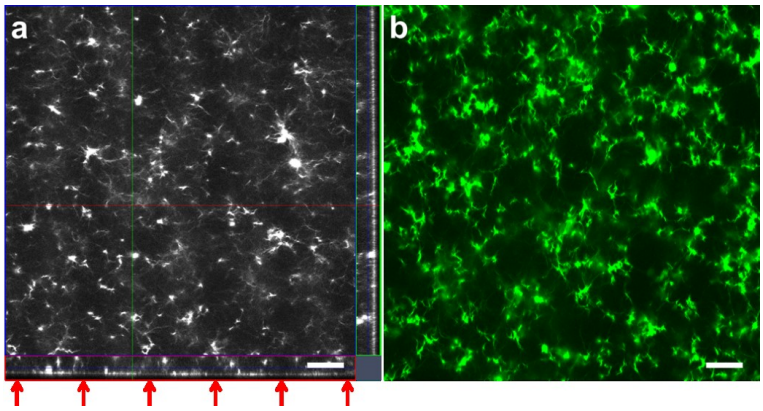

Figure S5.6. CLSM images of hydrazone gel formed by self-assembly of catalyst-free gelators: a) Orthogonal images from a *z*-stack scanning; and b) gel network in the bulk area. Sample before evaporation of THF: 10 mM **HA_3**, 30 mM **A** in 200 µL THF/H_2O (v/v = 1:3) co-solvent, scale bar = 20 µm.

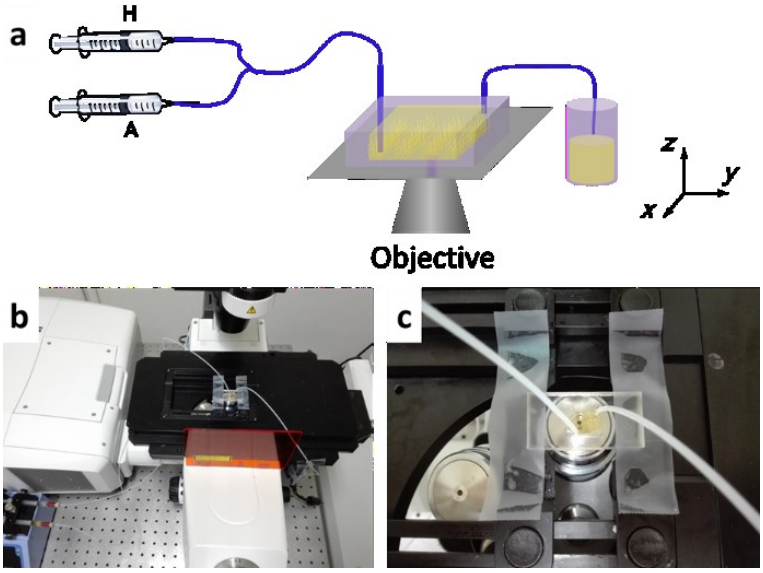

Figure S5.7. a) Illustration of the flow cell experiment; b and c) photos of the experimental setup.

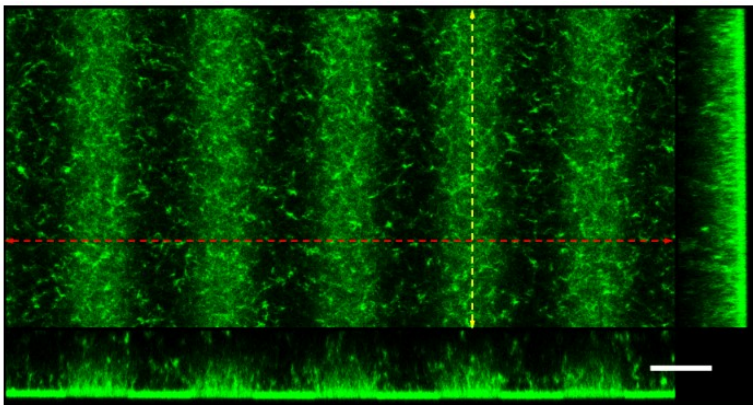

Figure S5.8. Confocal images of the gel fibers on the brush surfaces after washing with water, the lateral images indicating the gel patterns in *z*-direction corresponding to the lined areas on the 2D images. Scale bar = 20 μm.

Reference

1. Boekhoven, J.; Poolman, J. M.; Maity, C.; Li, F.; van der Mee, L.; Minkenberg, C. B.; Mendes, E.; van Esch, J. H.; Eelkema, R., Catalytic control over supramolecular gel formation. *Nat. Chem.* **2013,** *5*, 433-7.
2. Poolman, J. M.; Boekhoven, J.; Besselink, A.; Olive, A. G.; van Esch, J. H.; Eelkema, R., Variable gelation time and stiffness of low-molecular-weight hydrogels through catalytic control over self-assembly. *Nat. Protoc.* **2014,** *9*, 977-88.
3. Li, H.; Zhang, J.; Zhou, X.; Lu, G.; Yin, Z.; Li, G.; Wu, T.; Boey, F.; Venkatraman, S. S.; Zhang, H., Aminosilane micropatterns on hydroxyl-terminated substrates: fabrication and applications. *Langmuir* **2010,** *26*, 5603-9.
4. Chen, T.; Chang, D. P.; Zauscher, S., Fabrication of Patterned Polymer Brushes on Chemically Active Surfaces by in situ Hydrogen-Bond-Mediated Attachment of an Initiator. *Small* **2010,** *6*, 1504-1508.
5. Dong, R.; Krishnan, S.; Baird, B. A.; Lindau, M.; Ober, C. K., Patterned biofunctional poly(acrylic acid) brushes on silicon surfaces. *Biomacromolecules* **2007,** *8*, 3082-92.
6. Collier, G.; Vellore, N. A.; Latour, R. A.; Stuart, S. J., Development of molecular simulation methods to accurately represent protein-surface interactions: Method assessment for the calculation of electrostatic effects. *Biointerphases* **2009,** *4*, 57-64.

Chapter 6

Directed nanoscale self-assembly of low molecular weight hydrogelators using catalytic nanoparticles

Abstract: Herein we demonstrate that the growth of supramolecular hydrogel fibers can be spatially directed at the nanoscale by catalytic negatively charged nanoparticles (NCNPs). The NCNPs with surfaces grafted with negatively charged polymer chains create a local proton gradient that facilitates an acid-catalyzed formation of hydrogelators in the vicinity of NCNPs, ultimately leading to the selective formation of gel fibers around NCNPs. The presence of NCNPs has a dominant effect on the properties of the resulting gels, including gelation time, mechanical properties, and network morphology. Interestingly, local fiber formation can selectively entrap and precipitate out NCNPs from a mixture of different nanoparticles. These findings show a new possibility to use directed molecular self-assembly to selectively trap target nano-objects, which may find applications in therapy, such as virus infection prevention, or engineering applications, like water treatment and nanoparticle separation.

The content of this chapter is based on:

Yiming Wang, Frank Versluis, Sander Oldenhof, Vasudevan Lakshminarayanan, Kai Zhang, Yunwei Wang, Jie Wang, Rienk Eelkema*, Xuhong Guo*, and Jan H. van Esch*, Directed nanoscale self-assembly of low molecular weight hydrogelators using catalytic nanoparticles. *Adv. Mater.* **2018**, *30*, 1707408.

6.1 Introduction

In this work, we show how the self-assembly of low molecular weight gelators can be spatially controlled at the nanoscale. In recent years, directed molecular self-assembly (DMSA) has attracted wide-spread interests arising from the tremendous potential applications in e.g. microelectronics,[1-2] formulation technology,[3-6] and targeted therapy.[7-8] Current approaches to DMSA focus on triggering self-assembly by a variety of stimuli,[9-11] such as light,[12-14] enzymes,[15-18] and chemicals or even chemical reactions.[19-22] Along these lines, microscale DMSA has been achieved by, for example, Maruyama's group, who reported the self-assembly of small molecule hydrogelators at the surface of oil microdroplets through *in situ* formation of hydrogelators at the oil/water interface.[23] The groups of Xu, Ulijn, and others have demonstrated directed molecular self-assembly at the surface of living cells.[24-29] So far, however, DMSA is still limited to the micrometer length scale, and the realization of DMSA at the nanoscale remains a challenge because of the comparable time scale of diffusion and self-assembly of small molecules. To overcome this hurdle, a key issue is to develop a self-assembly system that can be triggered to self-assemble into nanostructures before the assembling molecules diffuse away from the nanoscale region of interest.

In recent years, we have developed a catalyst controlled supramolecular gel system,[30-31] which allows spatiotemporally directing self-assembly by controlling the distribution and content of the catalysts in space.[32-34] In this gelation system, the formation rate of gelator molecules can be dramatically accelerated by acidic catalysis, leading to faster gel formation and enhanced hydrogel properties. In the present work, we employ nanoparticles grafted with negatively charged polymers as nano-sized model catalytic triggers to explore the limits of directed self-assembly of the gelators at the nanoscale. We anticipated that the increased proton concentration, due to the high negative interfacial potential near the grafting surface of negatively charged nanoparticles (NCNPs), [35] will accelerate the local formation and self-assembly of gelators (Figure 6.1). Achieving of this goal will not only pave the way toward lower length scale DMSA, but also afford further advances in materials science for finding more potential applications, such as designing propulsion systems,[36-37] fabricating nano-devices,[38-39] and targeting repair of organs or tissues.[8]

We find that the use of these catalytic NCNPs has a significant impact on gel formation and the resultant properties, including the critical gelation concentration (CGC), mechanical performance, gelation rate, and network morphology. Importantly, the gel fibers are found to be selectively formed around the NCNPs

resulting from catalysis by the local proton gradient (Figure 6.1), demonstrating access to nanoscale DMSA. Moreover, when the gelator concentration was kept below the CGC, the NCNPs in a mixture of different nanoparticles can be selectively trapped and precipitated out from other non-catalytic nanoparticles.

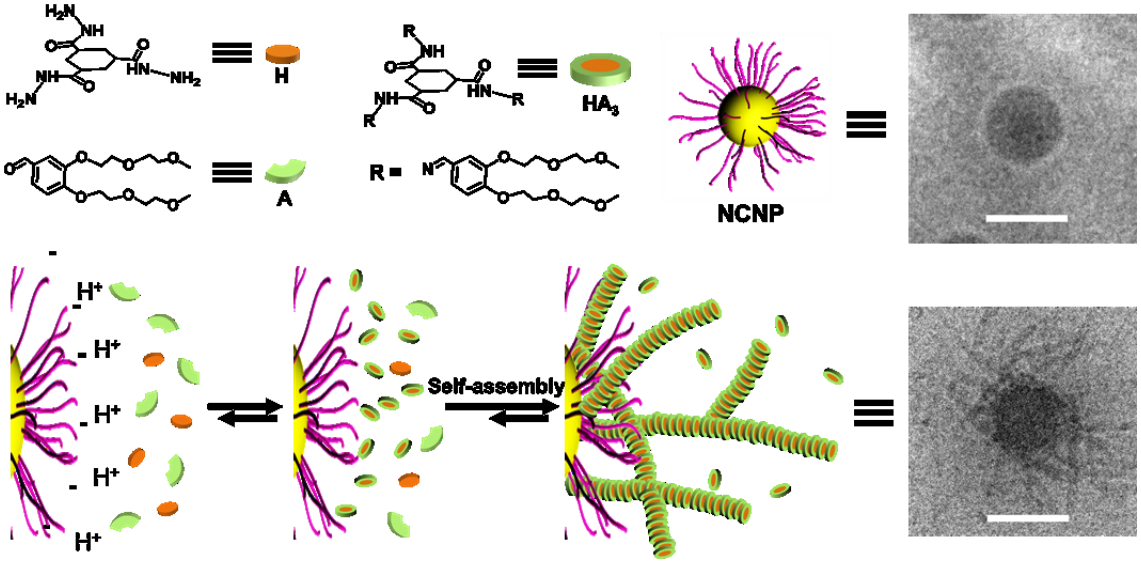

Figure 6.1. NCNPs directed hydrazone-based gel fibers formation. The formation of hydrazone gelator **HA$_3$** is catalyzed by protons near the surface of the NCNPs, ultimately leading to self-assembly of **HA$_3$** into fibers in the vicinity of the NCNPs. Scale bars in the cryo-TEM images are 100 nm.

6.2 Results and discussion

In our gel system, a low molecular weight gelator (**HA$_3$** in Figure 6.1) is formed through the formation of hydrazone bonds between two non-assembling building blocks (**H** and **A** in Figure 6.1).[30-31] In the presence of catalysts, such as protons, the rate of formation of **HA$_3$** is strongly enhanced, giving a handle to spatiotemporally control the self-assembly of **HA$_3$** into fibers. Model NCNPs were prepared by grafting poly (acrylic acid) (PAA) onto the surface of polystyrene nanoparticles (PSNPs) *via* surface-initiated photo-emulsion polymerization (Figure S6.1),[40] the grafting density of PAA chains was determined to be 0.042 nm^{-2} (see supporting information). As a control study, neutral nanoparticles (NNPs) were prepared by grafting neutral poly(*N*-hydroxyethylacrylamide) (PHEAA) onto the surface of PSNPs (Figure S6.1).[41] The diameters of the prepared PSNPs, NCNPs, and NNPs were determined to be 102 ± 11, 348 ± 7, and 254 ± 4 nm, respectively by dynamic light scattering (DLS) measurements (Figure S6.2). Zeta potential measurements revealed that the prepared NCNPs show a negative charge surface with a potential of -30.7 mV yet both PSNPs and NNPs present a nearly neutral surface (Figure S6.2). All the prepared particles showed typical spherical morphologies (Figure S6.3).

For the gelation experiments, stock solutions of **H** and **A** in 0.1 M phosphate buffer at pH 7.0 were used and mixed in a molar ratio of 1:6 to maintain pseudo first-order reaction kinetics and achieve near-complete conversion of **H** to gelator **HA_3**. We first explored the influence of NCNPs on the critical gelation concentration (CGC, the details of CGC measurement can be found in supporting information). We found that gelator **HA_3**, without the addition of any particles, displayed a CGC of ~20 mM (Figure 6.2a), which is consistent with previous results.[30] Upon the addition of NCNPs, the CGC was dramatically reduced, typically, lowering to 5 mM in the presence of 7.0 mg/mL NCNPs. In sharp contrast, both PSNPs and NNPs showed only very minor effects on the CGC (Figure 6.2a). These CGC experiments indicate that NCNPs can significantly promote the gelation process, resulting in a lower CGC.

Previous studies on reactive gel formation by hydrazone gelators showed that a lower CGC originates from an accelerated formation of **HA_3**.[30] To gain further insights, the influence of NCNPs on the rate of gel formation and the mechanical properties of the resulting gels was studied by oscillatory rheology. The rheology experiments were performed at [**H**] = 20 mM to ensure gel formation in all cases. All the resulted samples showed higher elastic modulus, *G'*, than their viscous modulus, *G''*, over the measured frequency range and presented a stable solid property over the strain below 1.0% (Figure S6.4), indicating the formation of typical hydrogels. We found that the gelation time (the time for *G'* to reach the plateau) decreased from 200 to 15 min by increasing the concentrations of NCNPs, (Figure 6.2b). Moreover, the corresponding mechanical stiffness was elevated from a storage modulus *G'* ~2.0 kPa for the sample without any particles to ~60 kPa with 7.0 mg/mL NCNPs (Figure 6.2c). Analogous to the CGC experiment, shorter gelation time and much stiffer gels demonstrate that NCNPs can effectively accelerate hydrazone gel formation.

On the basis of CGC and rheology data, it is likely that NCNPs act as catalysts for the formation of hydrazone **HA_3**, presumably due to an increase of the proton concentration in the vicinity of the negatively charged particles. To verify the catalytic effect of NCNPs on the formation of hydrazones, we investigated the formation kinetics of a non-assembling hydrazone product by performing a model reaction between **A** and hydrazide derivative **H'** (Figure S6.5). By monitoring the absorbance of the hydrazone products at 480 nm, we found that even when the NCNPs were diluted to a concentration as low as 0.05 mg/mL, they still showed a significant catalytic effect on the formation of hydrazone bonds with a reaction rate that was 1.4 times higher than the catalyst-free control sample (Figure S6.5). This result explains the aforementioned effects of NCNPs on CGC, gelation time, and mechanical strength of the resulting gels.

Previous work has demonstrated that faster formation of gelator molecules can lead to the formation of a denser gel network, affording gels with higher mechanical stiffness.[30-31] Along this line, we investigated the origin of the effect of NCNPs on the gel stiffness by observing the morphology of the resultant gel network, using confocal laser scanning microscopy (CLSM). The gels were prepared in the presence of fluorescein aldehyde derivative **A-FL** (the molecular structure of **A-FL** is shown in Figure S6.6) which results in fluorescently labeled gels. We found that the samples incubated with PSNPs and NNPs as well as the sample without any particles resulted in dispersions of large clustered aggregates (Figure 6.2d-f) without obvious network connections. In contrast, the addition of NCNPs led to the formation of a densely crosslinked gel network (Figure 6.2g). These observations corroborate the catalytic effect of NCNPs on the CGC, the rate of gelation, and stiffness of the gels.

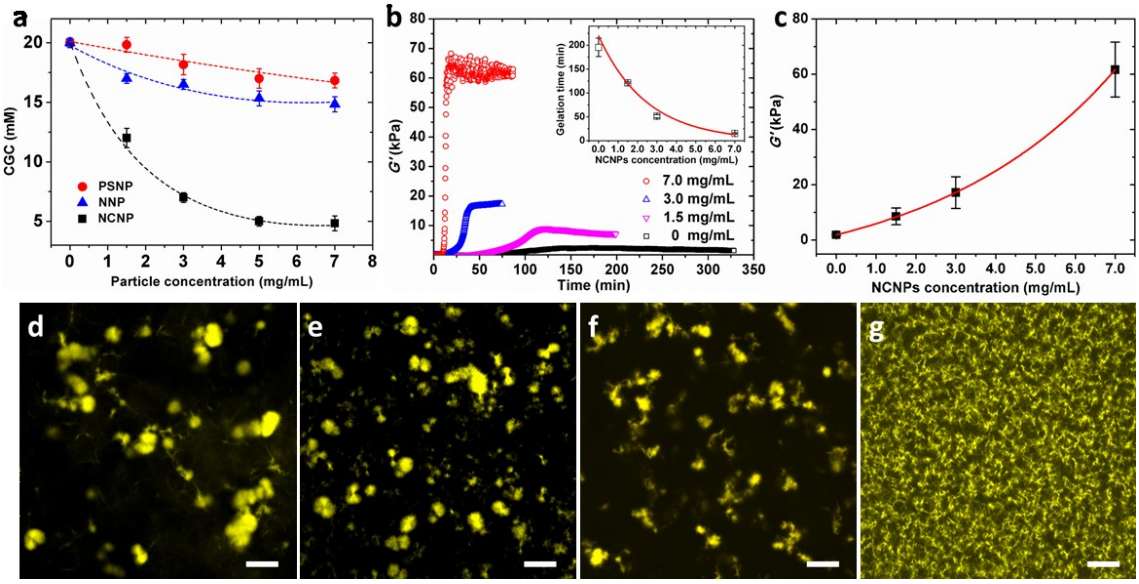

Figure 6.2. Effects of nanoparticles on hydrazone gel formation. a) Dependence of the CGC on the nanoparticle concentration; b) rheological evaluation of the gel formation as a function of the concentration of NCNPs, inset graph shows the dependence of gelation time on the concentration of NCNPs; c) plateau value of storage modulus (*G'*) of the gels formed with different concentration of NCNPs, [**H**] = 20 mM, [**H**]:[**A**] = 1:6; d-g) CLSM images of the gel samples prepared in the presence of d) no particles, e) PSNPs, f) NNPs, and g) NCNPs, [**H**] = 10 mM, [**H**]:[**A**] = 1:6, [**A-FL**] = 30 μM, particle concentration in e-g) is 3.0 mg/mL, scale bars are 40 μm. All samples were prepared in 0.1 M phosphate buffer at pH 7.0 and measured at room temperature. The lines in a-c) are added to guide the eyes, and error bars are the standard deviation calculated from three parallel measurements.

The experiments discussed so far indicate that NCNPs can facilitate hydrazone gel formation relying on their catalytic effect on the formation of gelator **HA$_3$**. To investigate whether this catalytic effect can direct the formation of gel fibers within the nano-space around the NCNPs, we performed cryo-transmission electron

microscopy (cryo-TEM) to observe the relative spatial distribution of fibers and NCNPs. For the cryo-TEM measurements, samples including 1.5 mg/mL particles, 5 mM **H** (lower than the CGC at the given particle concentration to avoid gelation), and 30 mM **A** were prepared and incubated overnight. In the cryo-TEM images (Figure 6.3a-c), all the self-assembled fibers showed a typical diameter of ~6 nm which is in agreement with previous results.[30] By comparing the TEM images, we found that for the suspension of NCNPs and gel fibers, most of the fibers were selectively formed around NCNPs (Figure 6.3a). In stark contrast, for the samples incubated with non-catalytic nanoparticles (PSNPs and NNPs), fiber bundles were formed and distributed randomly related to the positions of the nanoparticles (Figure 6.3b and c). This qualitative interpretation of the fiber and particle distribution in the TEM micrographs was corroborated by statistical analysis. In the sample of NCNPs, all the NCNPs were in close vicinity to fibers and each NCNP was on average surrounded by 21 fibers (Figure S6.7). However, in the case of non-catalytic nanoparticles, more than 80% of PSNPs as well as NNPs was not close to any fibers, and very few fibers can be found around the remaining few particles, which may originate from the random distribution of fibers and particles (Figure S6.7). These cryo-TEM results indicate that NCNPs can direct the self-assembly of gelators at the sub-micrometer length scale.

To obtain insights into this nanoscale DMSA, we further investigated the self-assembly mechanism. One can reason that there are two possible mechanisms. In one, the local catalytic formation of $\mathbf{HA_3}$ by NCNPs leads to supersaturation of $\mathbf{HA_3}$ in the vicinity of NCNPs, in turn leading to self-assembly into gel fibers before the monomers can diffuse away from the surface area. This catalytic effect has been demonstrated by the aforementioned experiments. In the other mechanism, NCNPs may act as a nucleation center to initiate the self-assembly of gelator molecules. Next, we investigated whether the NCNPs could nucleate the self-assembly of pre-synthesized catalyst-free gelators.

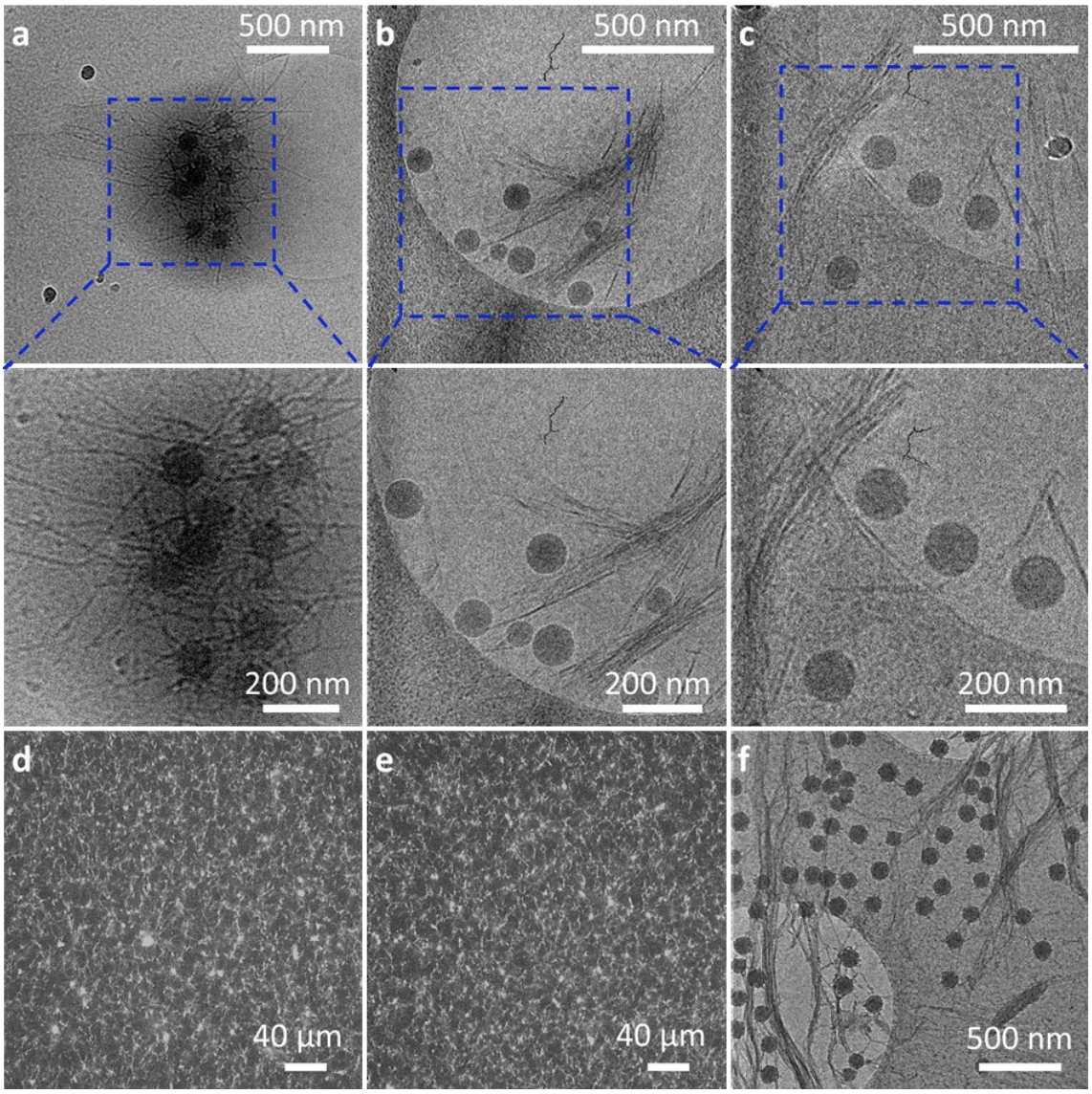

Figure 6.3. Cryo-TEM images of hydrazone gel fibers formed in the presence of a) NCNPs, b) PSNPs, and c) NNPs. Each samples: particle concentration is 1.5 mg/mL, [**H**] = 5 mM, [**H**]:[**A**] = 1:6 in 0.1 M phosphate buffer at pH 7.0. Gel fibers formation from the self-assembly of catalyst-free gelators (d-f). CLSM images of gel samples obtained from a THF/phosphate buffer (v/v = 1/3) solution of **HA$_3$**: d) without NCNPs, e) with NCNPs; f) cryo-TEM images of the gel sample formed from the self-assembly of pre-formed gelators in the presence of NCNPs. Samples after evaporating THF: 5 mM **HA$_3$**, 15 mM **A,** and 30 µM **A-FL** in d); 5 mM **HA$_3$**, 15 mM **A,** 30 µM **A-FL**, and 1.5 mg/mL NCNPs in e) and f).

To avoid initial self-assembly, we used tetrahydrofuran (THF) as co-solvent to completely dissolve **HA$_3$** (THF/phosphate buffer (0.1 M at pH 7.0) in 1/3 volume ratio). It should be mentioned that the addition of THF at this volume ratio presented no obvious effects on the size and surface charge of NCNPs (Figure S6.8). After mixing this gelator solution with a prescribed amount of NCNPs, self-assembly of **HA$_3$** was induced by slow evaporation of THF under a slight vacuum (see

supporting information for details). The evaporation of THF is able to induce an identical self-assembly of **HA$_3$** as we have proposed in previous study.[30] From the CLSM images, we found that well-connected gel networks were formed in both samples, with and without NCNPs (Figure 6.3d and e). The similar morphologies suggest that the presence of NCNPs has no significant effect on the gelation process beyond the formation of **HA$_3$**. Moreover, from the cryo-TEM images, no co-localization of gel fibers and NCNPs can be observed (Figure 6.3f), instead, it shows a similar result with the non-catalytic samples (Figure 6.3b and c). The statistical analysis displayed that most of the fibers have no interactions with the NCNPs (Figure S6.7). These results clearly show that NCNPs do not act as nuclei for the self-assembly of **HA$_3$**. We can therefore confirm that the local catalysis of gelator **HA$_3$** formation by NCNPs leads to the selective formation of gel fibers at the nanoscale.

To examine the selectivity of self-assembly around NCNPs, we performed fiber formation experiments in a mixture of NCNPs and non-catalytic nanoparticles. Based on the aforementioned results, we anticipated that the dispersion behavior of NCNPs in aqueous solution would be selectively changed owing to the local formation of gel fibers around the NCNPs (Figure 6.4a). To visualize the nanoparticles in suspensions, NCNPs and the non-catalytic nanoparticles were labeled by 1,1′-Dioctadecyl-3,3,3′,3′-tetramethylindocarbocyanine perchlorate (DIL, 30 μM, red channel) and 3,3′-Dioctadecyloxacarbocyanine perchlorate (DIO, 30 μM, green channel), respectively.

We first performed fiber formation in a mixture of NCNPs and PSNPs in 0.1 M phosphate buffer at pH 7.0. A sample solution containing 3 mg/mL for each particle species, 5 mM **H**, and 30 mM **A** was prepared by the addition of the stock solutions of **H** and **A** into a pre-mixed suspension of NCNPs and PSNPs. The concentration of **H** is controlled to be lower than the CGC in the presence of 3 mg/mL NCNPs (~8 mM, Figure 6.2a) to avoid bulk gel formation. This solution was then transferred to a microscopy cell to monitor the distribution of these two particles in the sample using CLSM. Initially, both NCNPs and PSNPs were found to disperse uniformly throughout the entire sample (Figure 6.4b, left, and Figure 6.4d, the imaging procedure and calculation method of particle ratio can be found in supporting information). After incubating overnight, we found that most of the NCNPs were deposited from the bulk solution to the bottom area of the cell (Figure 6.4b, right). Correspondingly, the relative ratio of NCNPs in the bulk solution was decreased to less than 10% (Figure 6.4d), leading to a stark increase at the bottom to more than 80%. In contrast, non-catalytic PSNPs were still uniformly dispersed in the solution (Figure 6.4b, right), and the relative ratio in the bulk was elevated to above 90% due to the decrease of NCNPs (Figure 6.4d), but the ratio at the bottom was decreased to

less than 20%, because the bottom area was occupied by the deposited NCNPs and gel fibers. Repeating this experiment using a mixture of NCNPs and NNPs gave similar results, with again the NCNPs preferentially depositing (Figure S6.9).

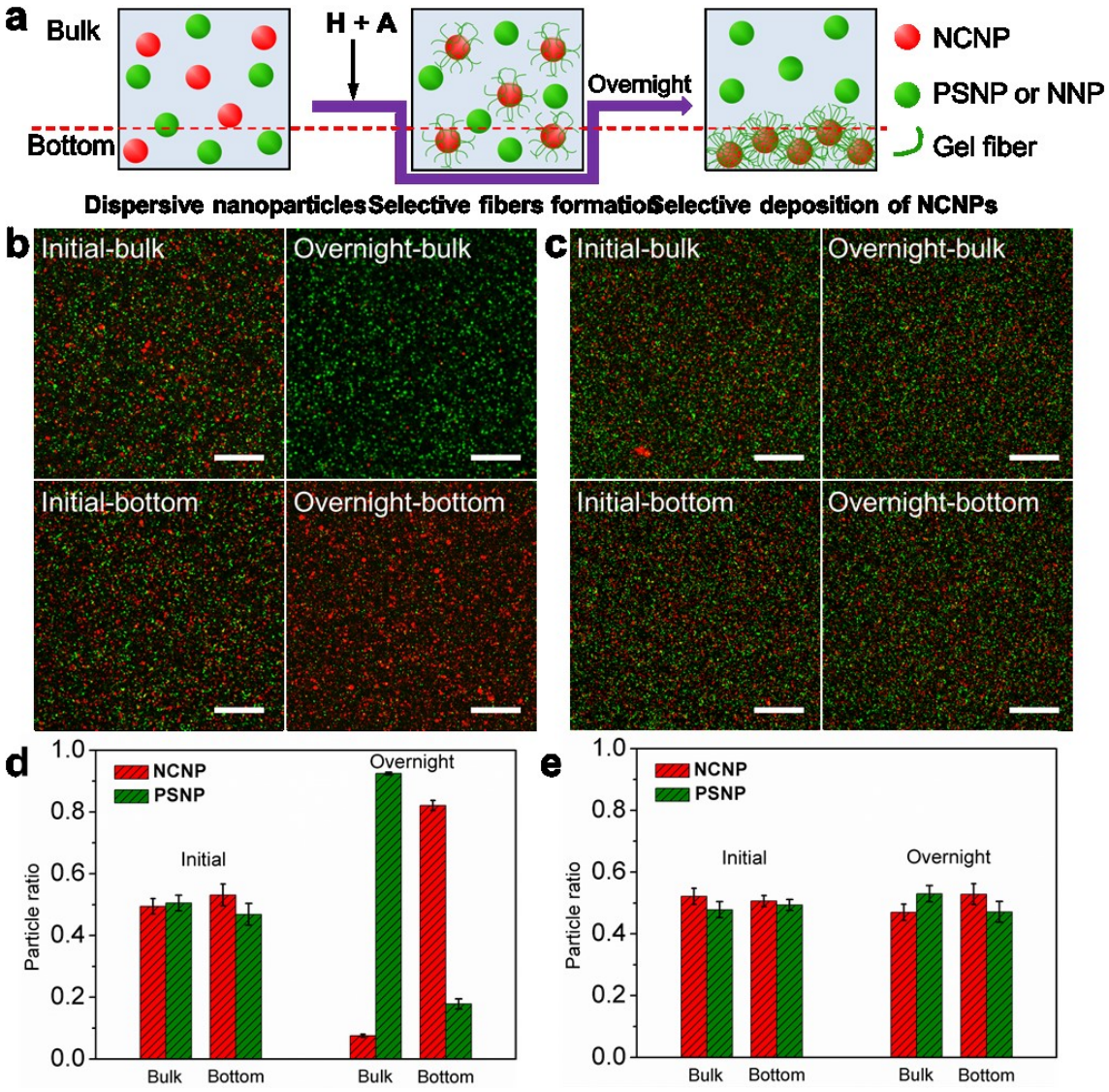

Figure 6.4. Selective trapping of NCNPs from the mixture suspensions with non-catalytic nanoparticles. a) illustration of local formation of fibers around NCNPs for selective trapping of NCNPs from the nanoparticles mixture; b, c) CLSM images of the suspension of NCNPs and PSNPs with addition of gelator precursors **H** and **A**, and pre-formed hydrazone fibers, respectively; d, e) relative ratio of each particle in the bulk and at the bottom of the suspension corresponding to the sample in b) and c), respectively. All samples: the concentration of each particle specie is 3 mg/mL, NCNPs and PSNPs are labeled by DIL (30 μM) and DIO (30 μM), respectively, [**H**] = 5 mM and [**A**] = 30 mM in b), [$\mathbf{HA_3}$] = 5 mM and [**A**] = 15 mM in c). Scale bars in b) and c) are 40 μm, error bars in d) and e) are the standard deviation of three images.

As a comparison, mixtures of NCNPs and non-catalytic nanoparticles lacking of gelator precursors (**H** and **A**), the dispersion and the relative ratio of the particles in the bulk or at the bottom did not show any differences after overnight incubating

(Figure S6.10), demonstrating the importance of fiber formation on the selective deposition of NCNPs.

It should be noted that the hydrazone moiety has a p*K*a of ~8.0.[42] Because of this basic property, the hydrazone fibers may be endowed with positive charges through protonation even at near neutral pH, and hence, the selective trapping of NCNPs by hydrazone fibers may be caused by electrostatic interactions. To clearly understand the trapping process, we measured the surface potential of hydrazone fibers in aqueous solution as a function of pH. We found that the hydrazone fibers present slight positive charge only when the pH was lower than 5.0 (Figure S6.11), suggesting that no electrostatic interaction can be formed between fibers and NCNPs under our experimental conditions (pH 7.0). Furthermore, by incubating pre-formed hydrazone fibers with the mixture of nanoparticles (NCNPs and PSNPs, pH 7.0) overnight, the distribution of NCNPs and NCNPs in the solution did not show any variations compared with the initial state (Figure 6.4c and e). The case of NCNPs and NNPs shows similar results (Figure S6.9). Thus the selective deposition of NCNPs is controlled by the local formation of fibers around the NCNPs without effect of electrostatic interactions.

6.3 Conclusions

In conclusion, we have shown here that the formation of supramolecular gel fibers can be spatially directed at the nanoscale by using catalytic NCNPs to control the local formation of low molecular weight gelators. NCNPs initiate supramolecular fiber formation near their surface resulting from local acid catalysis of hydrogelator formation. Due to the catalytic effect of NCNPs, the addition of NCNPs presents significant effects on the CGC, gelation time, stiffness as well as the network morphology of the created gels. Importantly, we have found that the local formation of gel fibers around NCNPs can selectively trap NCNPs and restrain their dispersion in aqueous solution, a potential way for trapping negatively charged nano-sized bioparticles such as virusses [43-45], for water treatment,[46-48] or for nanoparticles separation.[49-51] We believe these findings can serve as a first step toward nanoscale DMSA, which can be a new strategy to create more advanced functional objects for a variety of applications.

6.4 References

1. Reymann, A. C.; Martiel, J. L.; Cambier, T.; Blanchoin, L.; Boujemaa-Paterski, R.; Thery, M., Nucleation geometry governs ordered actin networks structures. *Nat. Mater.* **2010,** *9*, 827-32.

2. Galland, R.; Leduc, P.; Guerin, C.; Peyrade, D.; Blanchoin, L.; Thery, M., Fabrication of three-dimensional electrical connections by means of directed actin self-organization. *Nat. Mater.* **2013,** *12*, 416-421.
3. Bai, S.; Pappas, C.; Debnath, S.; Frederix, P. W.; Leckie, J.; Fleming, S.; Ulijn, R. V., Stable emulsions formed by self-assembly of interfacial networks of dipeptide derivatives. *Acs Nano* **2014,** *8*, 7005-13.
4. Scott, G. G.; McKnight, P. J.; Tuttle, T.; Ulijn, R. V., Tripeptide Emulsifiers. *Adv. Mater.* **2016,** *28*, 1381-6.
5. Moreira, I. P.; Sasselli, I. R.; Cannon, D. A.; Hughes, M.; Lamprou, D. A.; Tuttle, T.; Ulijn, R. V., Enzymatically activated emulsions stabilised by interfacial nanofibre networks. *Soft Matter* **2016,** *12*, 2623-2631.
6. Moreira, I. P.; Piskorz, T. K.; van Esch, J. H.; Tuttle, T.; Ulijn, R. V., Biocatalytic Self-Assembly of Tripeptide Gels and Emulsions. *Langmuir* **2017,** *33*, 4986-4995.
7. Furst, E. M., Directed self-assembly. *Soft Matter* **2013,** *9*, 9039-9045.
8. Stupp, S. I., Self-assembly and biomaterials. *Nano Lett* **2010,** *10*, 4783-6.
9. Vigier-Carrière, C.; Boulmedais, F.; Schaaf, P.; Jierry, L., Surface‐assisted self‐assembly strategies leading to supramolecular hydrogels. *Angew. Chem. Int. Edit.* **2017,** *57*, 1448-1456.
10. Tiller, J. C., Increasing the local concentration of drugs by hydrogel formation. *Angew. Chem. Int. Edit.* **2003,** *42*, 3072-5.
11. Bieser, A. M.; Tiller, J. C., Surface-induced hydrogelation. *Chem. Commun.* **2005**, 3942-4.
12. Kundu, P. K.; Samanta, D.; Leizrowice, R.; Margulis, B.; Zhao, H.; Borner, M.; Udayabhaskararao, T.; Manna, D.; Klajn, R., Light-controlled self-assembly of non-photoresponsive nanoparticles. *Nat. Chem.* **2015,** *7*, 646-52.
13. Cornwell, D. J.; Daubney, O. J.; Smith, D. K., Photopatterned Multidomain Gels: Multi-Component Self-Assembled Hydrogels Based on Partially Self-Sorting 1,3:2,4-Dibenzylidene-D-sorbitol Derivatives. *J. Am. Chem. Soc.* **2015,** *137*, 15486-92.
14. He, X.; Fan, J.; Zou, J.; Wooley, K. L., Reversible photo-patterning of soft conductive materials via spatially-defined supramolecular assembly. *Chem. Commun.* **2016,** *52*, 8455-8.
15. Williams, R. J.; Smith, A. M.; Collins, R.; Hodson, N.; Das, A. K.; Ulijn, R. V., Enzyme-assisted self-assembly under thermodynamic control. *Nat. Nanotechnol.* **2009,** *4*, 19-24.
16. Vigier-Carriere, C.; Wagner, D.; Chaumont, A.; Durr, B.; Lupattelli, P.; Lambour, C.; Schmutz, M.; Hemmerle, J.; Senger, B.; Schaaf, P.; Boulmedais, F.; Jierry, L., Control of Surface-Localized, Enzyme-Assisted Self-Assembly of Peptides through Catalyzed Oligomerization. *Langmuir* **2017,** *33*, 8267-8276.
17. Rodon Fores, J.; Martinez Mendez, M. L.; Mao, X.; Wagner, D.; Schmutz, M.; Rabineau, M.; Lavalle, P.; Schaaf, P.; Boulmedais, F.; JIERRY, L., Localized Supramolecular Peptide Self‐Assembly Directed by Enzyme‐Induced Proton‐Gradients. *Angew. Chem. Int. Edit.* **2017**.
18. Conte, M. P.; Sahoo, J. K. K.; Abul-Haija, Y. M.; Lau, K. H. A.; Ulijn, R. V., Biocatalytic Self-Assembly on Magnetic Nanoparticles. *ACS applied materials & interfaces* **2018**, 3069.

19. Ziemecka, I.; Koper, G. J. M.; Olive, A. G. L.; van Esch, J. H., Chemical-gradient directed self-assembly of hydrogel fibers. *Soft Matter* **2013,** *9*, 1556-1561.
20. Trausel, F.; Versluis, F.; Maity, C.; Poolman, J. M.; Lovrak, M.; van Esch, J. H.; Eelkema, R., Catalysis of Supramolecular Hydrogelation. *Accounts Chem. Res.* **2016,** *49*, 1440-7.
21. Wang, J.; Chao, J.; Liu, H.; Su, S.; Wang, L.; Huang, W.; Willner, I.; Fan, C., Clamped Hybridization Chain Reactions for the Self-Assembly of Patterned DNA Hydrogels. *Angew. Chem. Int. Edit.* **2017,** *56*, 2171-2175.
22. Epstein, I. R.; Xu, B., Reaction-diffusion processes at the nano- and microscales. *Nat. Nanotechnol.* **2016,** *11*, 312-319.
23. Nishida, Y.; Tanaka, A.; Yamamoto, S.; Tominaga, Y.; Kunikata, N.; Mizuhata, M.; Maruyama, T., In Situ Synthesis of a Supramolecular Hydrogelator at an Oil/Water Interface for Stabilization and Stimuli-Induced Fusion of Microdroplets. *Angew. Chem. Int. Edit.* **2017,** *56*, 9410-9414.
24. Tanaka, A.; Fukuoka, Y.; Morimoto, Y.; Honjo, T.; Koda, D.; Goto, M.; Maruyama, T., Cancer cell death induced by the intracellular self-assembly of an enzyme-responsive supramolecular gelator. *J. Am. Chem. Soc.* **2015,** *137*, 770-5.
25. Pires, R. A.; Abul-Haija, Y. M.; Costa, D. S.; Novoa-Carballal, R.; Reis, R. L.; Ulijn, R. V.; Pashkuleva, I., Controlling Cancer Cell Fate Using Localized Biocatalytic Self-Assembly of an Aromatic Carbohydrate Amphiphile. *J. Am. Chem. Soc.* **2015,** *137*, 576-579.
26. Zhou, J.; Du, X. W.; Yamagata, N.; Xu, B., Enzyme-Instructed Self-Assembly of Small D-Peptides as a Multiple-Step Process for Selectively Killing Cancer Cells. *J. Am. Chem. Soc.* **2016,** *138*, 3813-3823.
27. Zhou, J.; Du, X.; Xu, B., Regulating the Rate of Molecular Self-Assembly for Targeting Cancer Cells. *Angew. Chem. Int. Edit.* **2016,** *55*, 5770-5.
28. Kalafatovic, D.; Nobis, M.; Son, J.; Anderson, K. I.; Ulijn, R. V., MMP-9 triggered self-assembly of doxorubicin nanofiber depots halts tumor growth. *Biomaterials* **2016,** *98*, 192-202.
29. Wang, H.; Feng, Z.; Xu, B., Bioinspired assembly of small molecules in cell milieu. *Chem. Soc. Rev.* **2017,** *46*, 2421-2436.
30. Boekhoven, J.; Poolman, J. M.; Maity, C.; Li, F.; van der Mee, L.; Minkenberg, C. B.; Mendes, E.; van Esch, J. H.; Eelkema, R., Catalytic control over supramolecular gel formation. *Nat. Chem.* **2013,** *5*, 433-7.
31. Poolman, J. M.; Boekhoven, J.; Besselink, A.; Olive, A. G.; van Esch, J. H.; Eelkema, R., Variable gelation time and stiffness of low-molecular-weight hydrogels through catalytic control over self-assembly. *Nat. Protoc.* **2014,** *9*, 977-88.
32. Olive, A. G.; Abdullah, N. H.; Ziemecka, I.; Mendes, E.; Eelkema, R.; van Esch, J. H., Spatial and directional control over self-assembly using catalytic micropatterned surfaces. *Angew. Chem. Int. Edit.* **2014,** *53*, 4132-6.
33. Maity, C.; Hendriksen, W. E.; van Esch, J. H.; Eelkema, R., Spatial structuring of a supramolecular hydrogel by using a visible-light triggered catalyst. *Angew. Chem. Int. Edit.* **2015,** *54*, 998-1001.

34. Versluis, F.; van Elsland, D. M.; Mytnyk, S.; Perrier, D. L.; Trausel, F.; Poolman, J. M.; Maity, C.; le Sage, V. A. A.; van Kasteren, S. I.; van Esch, J. H.; Eelkema, R., Negatively Charged Lipid Membranes Catalyze Supramolecular Hydrogel Formation. *Journal of the American Chemical Society* **2016,** *138*, 8670-8673.
35. Gong, P.; Wu, T.; Genzer, J.; Szleifer, I., Behavior of surface-anchored poly(acrylic acid) brushes with grafting density gradients on solid substrates: 2. Theory. *Macromolecules* **2007,** *40*, 8765-8773.
36. Gao, W.; Pei, A.; Feng, X.; Hennessy, C.; Wang, J., Organized self-assembly of Janus micromotors with hydrophobic hemispheres. *J. Am. Chem. Soc.* **2013,** *135*, 998-1001.
37. Torelli, E.; Marini, M.; Palmano, S.; Piantanida, L.; Polano, C.; Scarpellini, A.; Lazzarino, M.; Firrao, G., A DNA Origami Nanorobot Controlled by Nucleic Acid Hybridization. *Small* **2014,** *10*, 2918-2926.
38. Carlson, A.; Bowen, A. M.; Huang, Y.; Nuzzo, R. G.; Rogers, J. A., Transfer printing techniques for materials assembly and micro/nanodevice fabrication. *Adv. Mater.* **2012,** *24*, 5284-318.
39. Hu, L.; Chen, M.; Fang, X.; Wu, L., Oil-water interfacial self-assembly: a novel strategy for nanofilm and nanodevice fabrication. *Chem. Soc. Rev.* **2012,** *41*, 1350-62.
40. Guo, X.; Weiss, A.; Ballauff, M., Synthesis of spherical polyelectrolyte brushes by photoemulsion polymerization. *Macromolecules* **1999,** *32*, 6043-6046.
41. Qin, X.; Chen, K.; Cao, L.; Zhang, Y.; Li, L.; Guo, X., Antifouling performance of nano-sized spherical poly(N-hydroxyethyl acrylamide) brush. *Colloids Surf B Biointerfaces* **2017,** *155*, 408-414.
42. Kalia, J.; Raines, R. T., Hydrolytic stability of hydrazones and oximes. *Angew. Chem. Int. Edit.* **2008,** *47*, 7523-6.
43. Lai, S. K.; Hida, K.; Shukair, S.; Wang, Y.-Y.; Figueiredo, A.; Cone, R.; Hope, T. J.; Hanes, J., Human immunodeficiency virus type 1 is trapped by acidic but not by neutralized human cervicovaginal mucus. *Journal of virology* **2009,** *83*, 11196-11200.
44. Martin, N.; Welsch, S.; Jolly, C.; Briggs, J. A.; Vaux, D.; Sattentau, Q. J., Virological synapse-mediated spread of human immunodeficiency virus type 1 between T cells is sensitive to entry inhibition. *J Virol* **2010,** *84*, 3516-27.
45. Waites, K. B.; Talkington, D. F., Mycoplasma pneumoniae and its role as a human pathogen. *Clin Microbiol Rev* **2004,** *17*, 697-728, table of contents.
46. Li, H.; Gui, X.; Zhang, L.; Wang, S.; Ji, C.; Wei, J.; Wang, K.; Zhu, H.; Wu, D.; Cao, A., Carbon nanotube sponge filters for trapping nanoparticles and dye molecules from water. *Chem. Commun.* **2010,** *46*, 7966-8.
47. Mahanta, N.; Valiyaveettil, S., Surface modified electrospun poly(vinyl alcohol) membranes for extracting nanoparticles from water. *Nanoscale* **2011,** *3*, 4625-31.
48. Mahanta, N.; Leong, W. Y.; Valiyaveettil, S., Isolation and characterization of cellulose-based nanofibers for nanoparticle extraction from an aqueous environment. *J. Mater. Chem.* **2012,** *22*, 1985-1993.

49. Hanauer, M.; Pierrat, S.; Zins, I.; Lotz, A.; Sonnichsen, C., Separation of nanoparticles by gel electrophoresis according to size and shape. *Nano Lett* **2007,** *7*, 2881-5.
50. Liang, H. W.; Wang, L.; Chen, P. Y.; Lin, H. T.; Chen, L. F.; He, D.; Yu, S. H., Carbonaceous nanofiber membranes for selective filtration and separation of nanoparticles. *Adv. Mater.* **2010,** *22*, 4691-5.
51. Krieg, E.; Weissman, H.; Shirman, E.; Shimoni, E.; Rybtchinski, B., A recyclable supramolecular membrane for size-selective separation of nanoparticles. *Nat. Nanotechnol.* **2011,** *6*, 141-6.

6.5 Supplymentary information

Materials

All commercial chemicals were purchased from Sigma Aldrich. Compound **H**, **A** and fluorescein aldehyde derivative **H'** were synthesized according to our previous work,[1-2] compound **A-FL** was synthesized as previously described.[3] 1,1'-Dioctadecyl-3,3,3',3'-tetramethylindocarbocyanine perchlorate (DIL) and 3,3'-Dioctadecyloxacarbocyanine perchlorate (DIO) were purchased from Thermo Fisher Scientific.

Experimental

Preparation of nanoparticles

Nanoparticles, including polystyrene particles (PSNPs), negatively charged particles (NCNPs) and neutral particles (NNPs) were prepared as described in our previous work.[4-5] PSNPs were obtained using an emulsion polymerization method. To prepare NCNPs and NNPs, negatively charged polymers (poly (acrylic acid), PAA) and neutral polymers (poly(N-hydroxyethylacrylamide), PHEAA) were grafted from the PSNPs surface. To this end, a thin layer of photoinitiator was introduced onto the surface of the PSNPs *via* copolymerization with the remaining styrene monomers in the PSNPs. The NCNPs and NNPs were made by initiating the polymerization of monomers of AA and HEAA respectively at the surface of PSNPs under the irradiation of UV light (Fig. S1). All the prepared particles were dialyzed against deionized water for one week for the subsequent experiments.

Determination of particle concentration of the prepared particle solutions

To determine the solid content of prepared nanoparticle solutions, 2 mL of each particle solution were added into a flask and evaporated under vacuum to remove the solvent using a rotary evaporator at room temperature until the total weight of the flask showed no change. The solid content of these particles can be calculated based on the mass balance.

Measurement of the grafting density of PAA chains on the PSNPs

The grafting density was measured according to method we previously proposed.[6] The NCNPs were incubated in 2.0 M sodium hydroxide solution for 12 days to cleave the PAA chains from the PSNP surface. The PAA chains were separated from the solution through nanofiltration. The molecular weight of PAA, *Mn*, was determined by gel permeation chromatography (GPC). The grafting density (*GD*) of the PAA

chains then can be calculated by the following equition: GD = $(m/Mn)/(4\pi R^2)$. where m is the total amount of obtained PAA, R is the radius of PSNPs. The grafting density of the NCNPs we used in this study was determined to be 0.042 nm^{-2}.

Size distribution and zeta potential measurements of nanoparticles

The size distribution and zeta potential of these particles were determined by using a Malvern Nano ZS 3600 Zetasizer. For the measurements, the concentrations of these particles were adjusted to be 0.05 mg/mL diluted by 100 mM, pH 7.0 phosphate buffer. The laser wavelength was 633 nm with a scattering angle of 173°. All the samples were allowed to equilibrate for 2 min and measured at 25 °C. The results were shown in Fig. S2.

Determination of the critical gelation concentration (CGC)

A series of samples including controlled concentration of particles and different concentration of gelator precursors were prepared by mixing the stock solutions of the gelator precursors (**H**: 40 mM, **A**: 240 mM) and particles in a vial. These prepared samples were left overnight at room temperature to ensure complete conversion to gelator $\mathbf{HA_3}$ and subsequent self-assembly. Gel formation was determined by vial inversion test, testing if an inverted sample would resist flow for at least 30 seconds. The lowest concentration of **H** or the generated hydrogelator $\mathbf{HA_3}$ at which the sample can form a gel was defined as the corresponding CGC.

Rheological test

The Oscillatory rheology experiments were performed on a AR G2 TA rheometer equipped with a parallel-plate made of stainless steel with a diameter of 40 mm and a solvent trap to prevent the evaporation of solvent from the samples. The measurements were performed in a strain controlled mode at 25 °C, the strain is 0.05% and the frequency is 1.0 Hz. All the samples were prepared using 100 mM, pH 7.0 phosphate buffer. As an example, stock solutions of **H**, **A** and particles were added into a sample vial and diluted with phosphate buffer to yield a final concentration of 20 mM **H** and 120 mM **A**. After mixing, the sample solution was transferred immediately onto the rheometer plate for the measurement.

Confocal laser scanning microscopy (CLSM)

Confocal images of the samples were obtained with a Zeiss LSM 710 confocal laser scanning microscope equipped with a Zeiss Axio Observer inverted microscope and 40x PlanFluor oil immersion objective lens (NA 1.3) using an incident laser with a

wavelength of 488 nm to excite the fluorescein probe. The pinhole was set to 1.0 airy unit and the data were processed using ZEN 2009 software. Each Sample was prepared in an imaging chamber (CoverWell PCI-0.5) and incubated at room temperature overnight before measurement.

UV-vis measurements

The catalysis effect of particles on the hydrazone bond formation was monitored using an Analytik Jena Specord 250 spectrophotometer. The samples containing quartz cuvettes were placed in a 6-sample holder and the data points were recorded at an interval time of 5 min at 480 nm with a slit of 1 nm. The relative reaction rates were calculated from the slope of each curve and normalized based on a blank specimen which did not contain particles, as shown in Fig. S3.

Cryo-TEM

The morphologies of the particles and the formed fibers were observed in a Gatan model 626 cryo-stage in a JEOL JEM 1400 Plus electron microscope, the operating voltage was 120 kV. All the samples were prepared by mixing the stock solutions of particles and the gelator precursors to get a final solution with 1.5 mg/mL particles, 5 mM **H** (below CGC), and 30 mM **A**, and left overnight to form sol solutions. For the measurements, all the samples were diluted 2 times and 5 µL of the diluted sol solutions were carefully deposited on a Quantifoil R 1.2/1.3 100 Holey carbon films coated Cu 200 mesh grid. After blotting, the grid was rapidly inserted into liquid ethane. The frozen-hydrated sample was always stored in liquid nitrogen before the observation. The cryo-TEM images were recorded under low-dose conditions on a slow scan CCD camera (Gatan, model 830).

Nucleation effects on the directed self-assembly

The effect of negatively charged particles on the gelation process was investigated by observing the connections between fibers and particles using cryo-TEM. To eliminate the catalysis effects, in this experiment, pre-prepared gelator **HA$_3$** was used directly to self-assemble in water in the presence of negatively charged particles. By using cryo-TEM to check the connections between self-assembled fibers and particles, the roles of the particles played (only as a catalyst, or a nucleation center, or both) in the gelation process will be clearly enclosed. To make gelator **HA$_3$** dissolve in phosphate buffer at the beginning, THF was used as a co-solvent. The evaporation of THF allowed the fibers formation in buffer solution. Briefly, 200 µL solutions with **H** (7.5 mM) and **A** (45 mM) was prepared using 0.1 M phosphate buffer at pH 7.0 and left

for overnight at room temperature to ensure the conversion of gelator **HA_3** was finished completely. 100 µL THF was added into the obtained sol solution, leading to the formation of a homogeneous gelator solution (without any self-assembled structures). After mixing with 100 µL NCNP stock solutions (5 mg/mL), the homogeneous solutions were stored in a vacuum environment (100 mbar) at room temperature to evaporate the THF, leading to the self-assembly of dissolved gelators. It needs to be noted that the addition of this few THF showed no obvious effect on the structure and properties of particles (see Fig. S7). THF was removed completely within 1 hour, and gel was formed at the end (the final concentration of NCNP, **A** and **HA_3** are 1.5 mg/mL, 15 mM, and 5 mM, respectively). This gel sample was collected and characterized by cryo-TEM to observe the connections between particles and fibers.

Calculation of relative particle ratio in the suspension

Particle ratio was calculated by analyzing the area ratio of the two fluorescence channels in the confocal microscopy images using Fiji software.[7] The confocal images were first split into two channels and respectively smoothed by filtering the high frequency noise using Gaussian blur filter, after which, setting the background of the images to red in threshold. The area of each fluorescence channel in the image, A_{red} and A_{green}, can be calculated by using the tool of "measure". After extracting the area value of each channel, the ratio of each particle can be expressed by the area ratio as $A_{red}/(A_{red} + A_{green})$ and $A_{green}/(A_{red} + A_{green})$, respectively.

Measurement of zeta potential of hydrazone fibers

The zeta potential was measured on a Malvern Nano ZS 3600 zetasizer. The laser wavelength was 633 nm and the scattering angle was 173°. The phosphate buffer solution of gelator precursors was prepared by mixing **H** and **A** in a ratio of 1:6 at a concentration of [**H**] = 5 mM, and left to react overnight. The fibers suspension was homogenized and diluted 100 times for zeta potential measurement. The zeta potential of the fibers at different pH was recorded (Fig. S10).

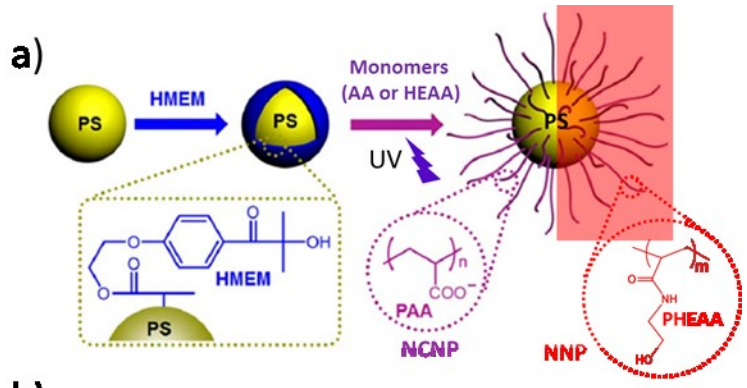

Particles	PSNP	NNP	NCNP
Concentration (mg/mL)	71.5	12.7	10.6

Figure S6.1. a) Preparation of PSNP, NCNP, and NNP and b) the concentrations of the prepared nanoparticles.

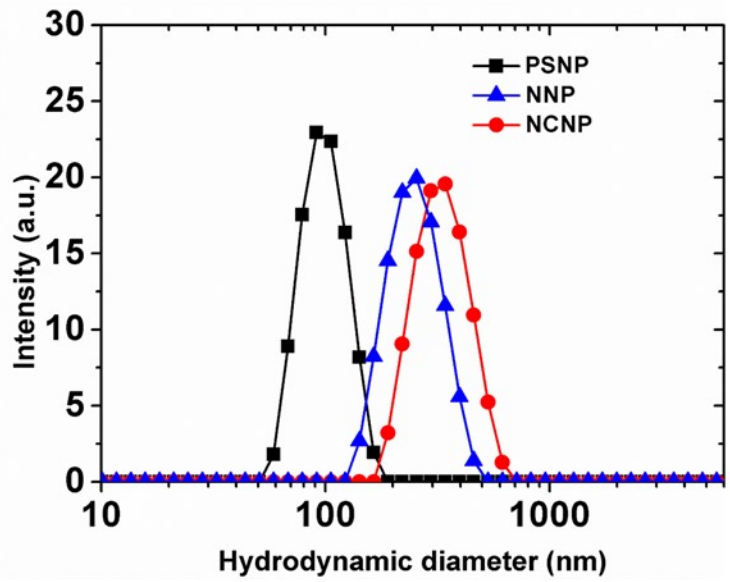

Particles	Diameter (nm)	PDI	Zeta potential (mV)
PSNP	102	0.030	-0.010
NNP	254	0.071	-0.206
NCNP	348	0.097	-30.70

Figure S6.2. Size distribution and zeta potential of the prepared particles in 0.1 M phosphate buffer at pH 7.0.

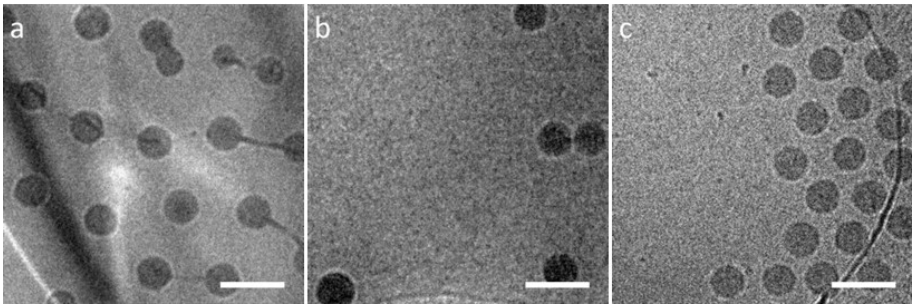

Figure S6.3. Cryo-TEM images of a) NCNPs, b) PSNPs, and c) NNPs. Scale bars are 200 nm.

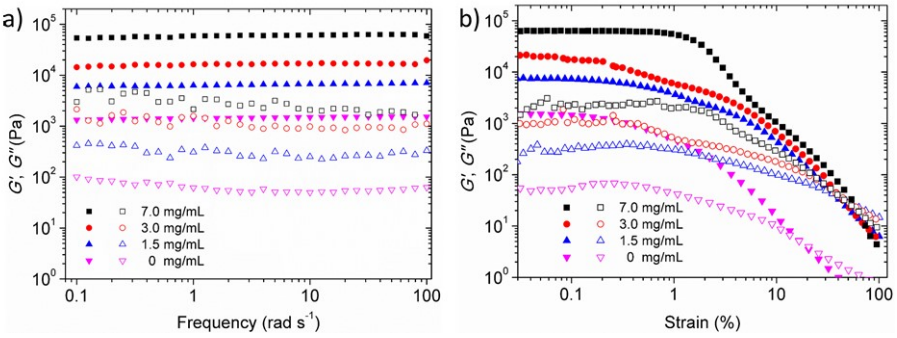

Figure S6.4. a) Frequency and b) strain sweep measurements on the NCNPs catalyzed gels. Samples: [**H**] = 20 mM, [**H**]:[**A**] = 1:6, with different concentration of NCNPs in 0.1 M phosphate buffer at pH 7.0.

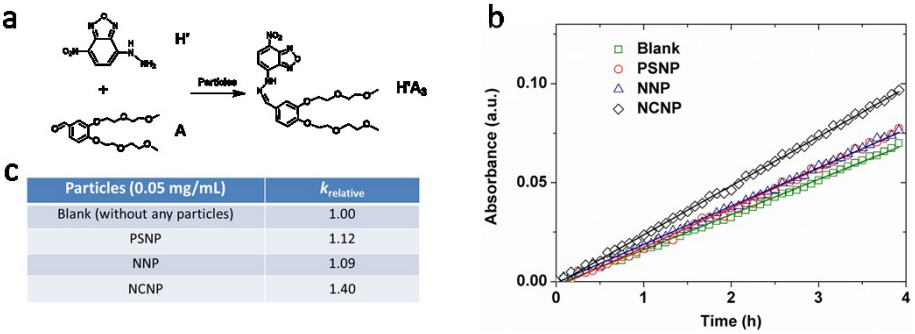

c

Particles (0.05 mg/mL)	$k_{relative}$
Blank (without any particles)	1.00
PSNP	1.12
NNP	1.09
NCNP	1.40

Figure S6.5. Catalysis effects of the particles on the hydrazone bond formation. a) a reaction for characterizing the catalysis of particles on hydrazone bond formation; b) UV absorbance of product **H'A**$_3$ (at 480 nm) over time; and c) the relative reaction rates of hydrazone formation in the presence of different particles. All samples: [**H'**] = 0.045 mM, [**A**] = 2.5 mM in 0.1 M phosphate buffer at pH 7.0, all the measurements were performed at 25 °C.

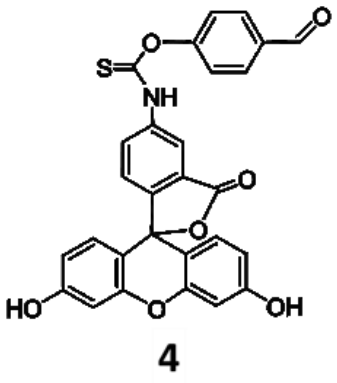

Figure S6.6. The molecular structure of aldehyde fluorescein **A-FL**.

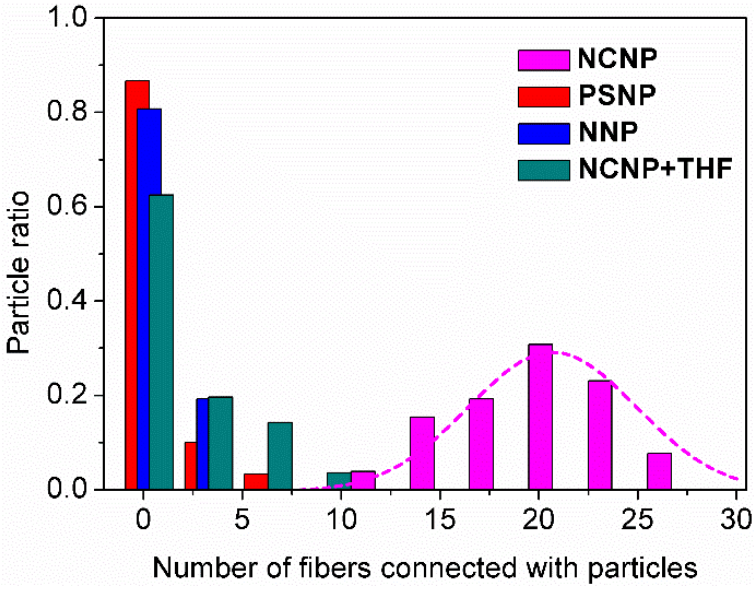

Figure S6.7. Histogram of the number of fibers connected with particles and the corresponding particle ratios. The number of fibers and particles are counted from at least four cryo-TEM images.

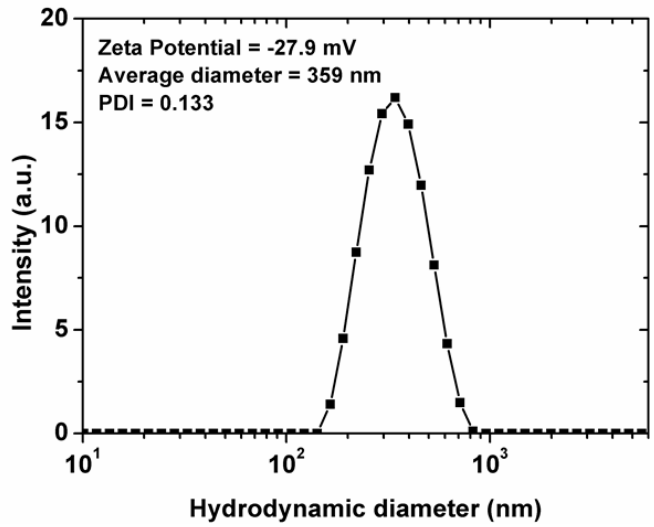

Figure S6.8. Size distribution and zeta potential of NCNPs after incubating with THF (300 µL 1.5 mg/mL NCNPs in 0.1 M phosphate buffer at pH 7.0 with 100 µL THF).

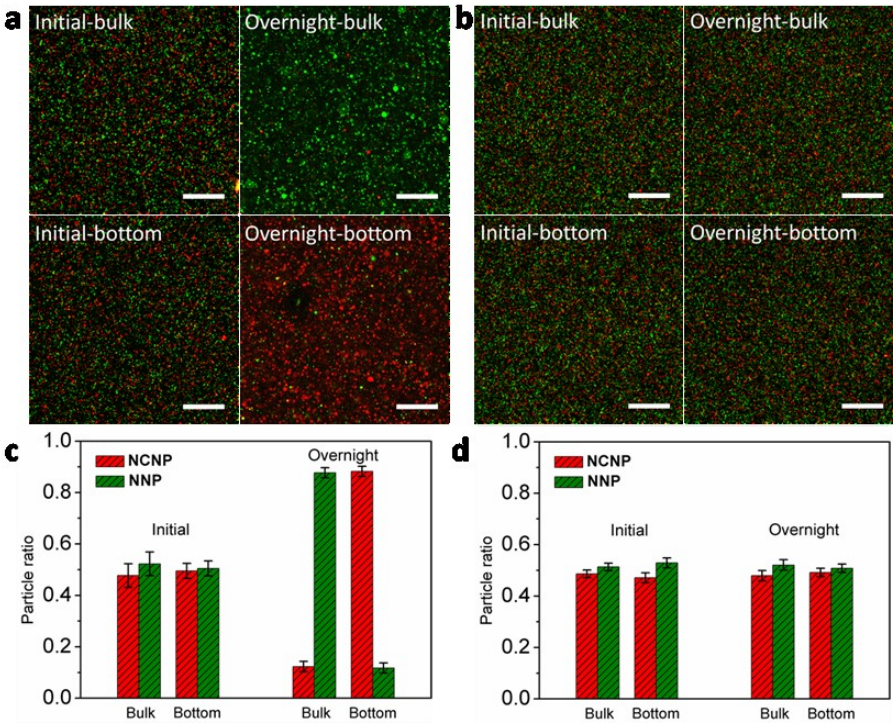

Figure S6.9. a, b) CLSM images of the suspension of NCNPs and NNPs with addition of gelator precursors **H** and **A**, and preformed hydrazone fibers, respectively; c, d) relative ratio of each particle in the bulk and at the bottom of the suspension corresponding to the sample in a) and b), respectively. All samples: the concentration of each particle specie is 3 mg/mL. NCNPs and NNPs are labeled by DIL (30 µM) and DIO (30 µM), respectively, [**H**] = 5 mM and [**A**] = 30 mM in a), [$\mathbf{HA_3}$] = 5 mM and [**A**] = 15 mM in b). Scale bars in a) and b) are 40 µm, error bars in c) and d) are the standard deviation of three images.

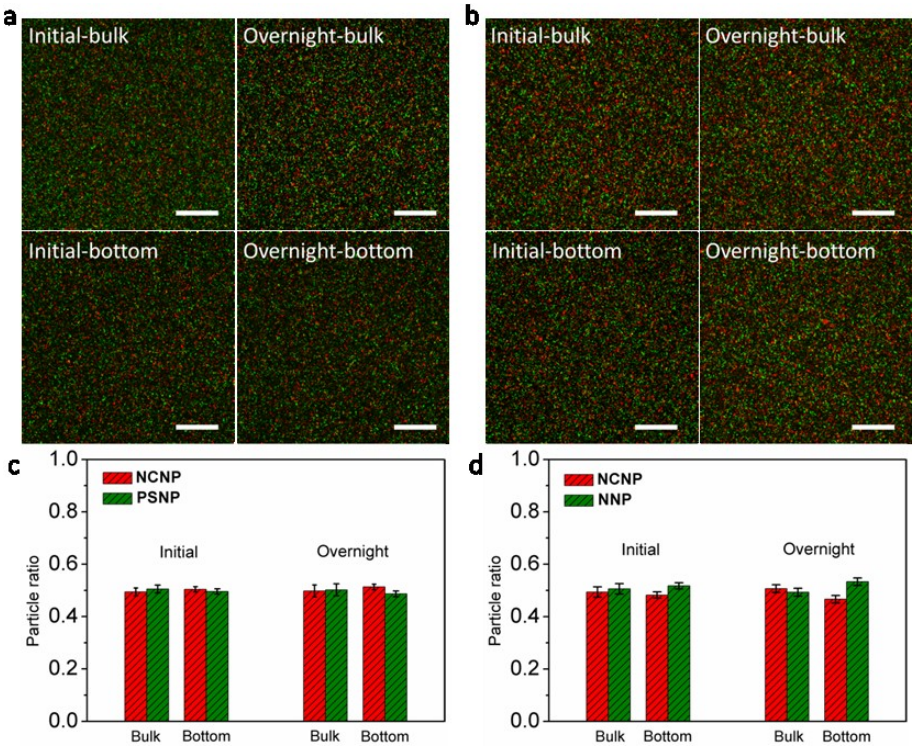

Figure S6.10. CLSM images scanned from the bulk and the bottom areas of the suspension of a) NCNPs and PSNPs, and b) NCNPs and NNPs without addition of **H** and **A**; c, d) relative ratio of each particle in the bulk and at the bottom of the suspension corresponding to the samples in a) and b). All samples: the concentration of each particle specie is 3 mg/mL, NCNPs and non-catalytic nanoparticles are labeled by DIL (30 μM) and DIO (30 μM), respectively. Scale bars in a) and b) are 40 μm, error bars in c) and d) are the standard deviation of three image samples.

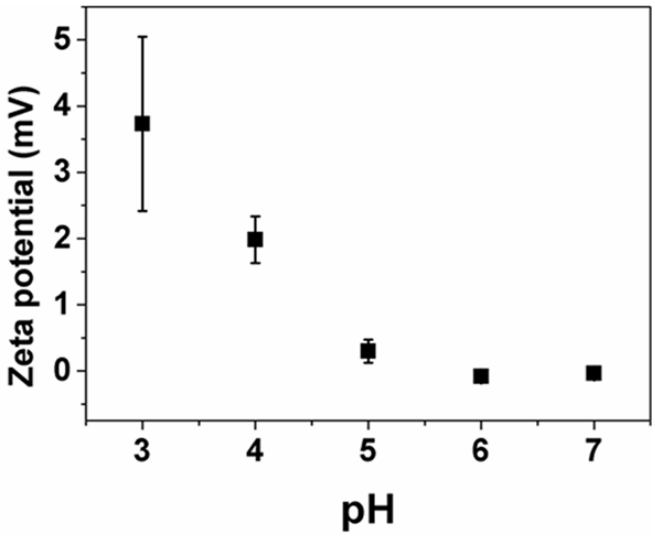

Figure S6.11. Zeta potential of hydrazone fibers in aqueous solution as a function of pH. The measurement medium is 0.1 M phosphate buffer.

References

1. Boekhoven, J.; Poolman, J. M.; Maity, C.; Li, F.; van der Mee, L.; Minkenberg, C. B.; Mendes, E.; van Esch, J. H.; Eelkema, R., Catalytic control over supramolecular gel formation. *Nat. Chem.* **2013,** *5*, 433-7.
2. Poolman, J. M.; Boekhoven, J.; Besselink, A.; Olive, A. G.; van Esch, J. H.; Eelkema, R., Variable gelation time and stiffness of low-molecular-weight hydrogels through catalytic control over self-assembly. *Nat. Protoc.* **2014,** *9*, 977-88.
3. Crisalli, P.; Kool, E. T., Water-soluble organocatalysts for hydrazone and oxime formation. *J. Org. Chem.* **2013,** *78*, 1184-9.
4. Guo, X.; Weiss, A.; Ballauff, M., Synthesis of spherical polyelectrolyte brushes by photoemulsion polymerization. *Macromolecules* **1999,** *32*, 6043-6046.
5. Qin, X.; Chen, K.; Cao, L.; Zhang, Y.; Li, L.; Guo, X., Antifouling performance of nano-sized spherical poly(N-hydroxyethyl acrylamide) brush. *Colloid Surface B* **2017,** *155*, 408-414.
6. Guo X., Synthesis and study of the colloidal polyelectrolyte brushes prepared by photo-emulsion polymerization, Logos Verlag Berlin **2001**.
7. Schindelin, J.; Arganda-Carreras, I.; Frise, E.; Kaynig, V.; Longair, M.; Pietzsch, T.; Preibisch, S.; Rueden, C.; Saalfeld, S.; Schmid, B.; Tinevez, J. Y.; White, D. J.; Hartenstein, V.; Eliceiri, K.; Tomancak, P.; Cardona, A., Fiji: an open-source platform for biological-image analysis. *Nat. Methods* **2012,** *9*, 676-682.

Summary

Self-sorting and directed molecular self-assembly (DMSA) are ubiquitous in nature, leading to complex supramolecular objects with sophisticated functions. The implementation of such molecular organization approaches in artificial systems has emerged as a powerful approach towards new generation of functional materials. The work described in this thesis shows our efforts to develop new synthetic self-sorting and DMSA systems. A multilevel self-sorting at different length scales, which can only be observed in biological system before, has been achieved. Furthermore, a series of new synthetic DMSA systems under well control have been developed.

In Chapter 1 after introducing the concept of supramolecular self-assembly, a literature overview of the development of multicomponent self-assembly and DMSA in artificial systems has been presented. Chapter 2 describes how hierarchically compartmentalized supramolecular gels can be spontaneously formed by a multilevel self-sorting at both the molecular level and the macroscopic level. We have shown that the different component molecular gelators undergo a molecular level self-sorting resulting in distinct gel fibers; this mixture of fibers in turn undergo a higher-level self-sorting resulting in hierarchically compartmentalized supramolecular gels consisting of separated microdomains. Such a spontaneously multilevel self-sorting system provides a "bottom-up" approach towards hierarchically structured functional materials, and adds to our understanding of the biological counterpart.

In Chapter 3 seeding-driven metastable supramolecular gels have been described. The addition of seeds can interfere with the nucleation of the molecular gelators, by which the self-assembly of gelators is forced to proceed along a kinetically controlled pathway. As a consequence, kinetically favored metastable gels are formed. Interestingly, these gel networks are capable of transforming into the thermodynamically more stable gel state over time. This work shows a simple seeding-drive out-of-equilibrium self-assembly and would benefit to the development of pathway-dependent supramolecular materials.

Chapter 4 describes metastable supramolecular gels that are formed by an aging-induced out-of-equilibrium self-assembly. We have found that one of the gelator precursor molecules studied in thesis is capable of self-assemble into tiny aggregates upon an aging treatment on their aqueous solution. These generated tiny aggregates can serve as seeds to force the self-assembly of the gelators along a kinetically controlled pathway analogous to the work described in Chapter 3, leading to

kinetically favored gels. These gels can convert into the thermodynamic state over time as well.

In Chapter 5 micropatterned supramolecular gels with controllable spatial dimensions and oriented growth direction have been achieved by using catalysis-tunable catalytic templates. Due to the catalysis-responsiveness of the involved gelators, gels are preferentially formed at the catalytic sites. The geometrical shapes and the dimensions of the resulting gel patterns can be precisely controlled by controlling the distribution or the density of the catalysts in the templates. This work shows an effective "bottom-up" approach towards control over the spatial organization of materials, which may find promising applications in, e.g., microelectronics, tissue engineering, and biomedicine.

Chapter 6 shows our access to spatially control the self-assembly of the gelators used in Chapter 5 at the nanoscale. By using nano-sized catalytic templates, we have found that the gel fibers are locally formed around the catalytic nanoparticles due to the local catalysis of the nanoparticles. Interestingly, such a local fibers formation limits the dispersion of the catalytic nanoparticles in aqueous solution, which has been used to selectively trap the catalytic nanoparticles. This work shows the potential of using DMSA strategy to selectively trap nano-objects.

Overall, the work performed in this thesis presents a series of new examples of synthetic self-sorting and DMSA systems. These bio-inspired artificial supramolecular systems are expected to open the routes towards new generation of functional soft materials for high-tech applications, such as artificial life, catalysis, biomedicine, and some fundamental scientific researches.

Samenvatting

Zelf-sorterende en gestuurde moleculaire zelf-assemblage (GMZA) zijn veelvoorkomend in de natuur in de vorm van complexe supramoleculaire structuren met geavanceerde functies. Het toepassen van moleculaire organisatie in kunstmatige systemen is een krachtige methode voor de ontwikkeling van nieuwe functionele materialen. Het werk beschreven in dit proefschrift toont onze inspanningen voor de ontwikkeling van nieuwe synthetische zelf-sorterende en GMZA systemen. Een multilevel zelf-sorterend systeem van verschillende lengtes, systemen welke voorheen alleen geobserveerd zijn in biologische systemen, is ontwikkeld. Verder is een serie van nieuwe synthetische controleerbare GMZA systemen ontwikkeld.

In Hoofdstuk 1 wordt, na de introductie van het concept van supramoleculaire zelf-assemblage, een overzicht van de literatuur over de ontwikkelingen van multicomponent zelf-assemblage en GMZA in kunstmatige systemen gegeven. In Hoofdstuk 2 wordt beschreven hoe hiërarchische gecompartimentaliseerde supramoleculaire gels spontaan vormen via multilevel zelf-sortering op zowel het moleculaire niveau als het macroscopische niveau. We laten zien dat verschillende component gelatoren op moleculair niveau zelf-sorteren tot aparte gel fibers; dit mengsel aan fibers ondergaat vervolgens zelf-sortering op een hoger niveau wat resulteert in hiërarchisch gecompartimentaliseerde supramoleculaire gels opgebouwd uit verschillende micro-domeinen. Dergelijke spontane multilevel zelf-sorterende systemen bieden een “bottom-up” benadering tot hiërarchisch gestructureerde functionele materialen en leren ons iets over hun biologische equivalenten.

In hoofdstuk 3 worden seeding-gestuurde metastabiele supramoleculaire gels beschreven. Het toevoegen van seeds kan interfereren met de nucleatie van de moleculaire gelatoren, waardoor de zelf-assemblage via een kinetisch gecontroleerde route verloopt. Met als consequentie dat kinetisch metastabiele gels gevormd worden. Deze gel netwerken transformeren in de tijd tot een thermodynamisch stabielere gel. Dit onderzoek laat simpele seeding-gedreven uit-evenwicht zelf-assemblatie zien en draagt bij aan de ontwikkelingen van route-afhankelijk supramoleculaire materialen.

In Hoofdstuk 4 worden metastabiele supramoleculaire gels, welke gevormd worden via aging-geinduceerd uit-evenwicht zelf-assemblage, beschreven. We laten zien dat één van de grondstoffen van de gelator, onderzocht in dit proefschrift, in staat is te zelf-assembleren in kleine aggregaten na een aging-behandeling van hun waterige oplossing. Deze geproduceerde kleine aggregaten kunnen functioneren als seeds voor de zelf-assemblage via een kinetisch gecontroleerde route, vergelijkbaar

met het werk beschreven in Hoofdstuk 3, wat kinetische gels produceert. Ook deze gels kunnen met de tijd omzetten tot hun thermodynamisch stabielere vorm.

Hoofdstuk 5 beschrijft de ontwikkeling van micropatterned supramoleculaire gels met controleerbare ruimtelijke dimensies en groei richting via een katalytische sjablonen. Vanwege de responsiviteit van de gelatoren aan de katalysator, worden de gels bij voorkeur gevormd bij katalytische plekken. De geometrische vormen en dimensies van de resulterende gel patronen kunnen nauwkeurig gecontroleerd worden door de distributie en de dichtheid van de katalysator in het sjabloon te controleren. Dit onderzoek laat een effectieve "bottom-up" benadering zien voor de ruimtelijke ordening van materialen welke mogelijk veelbelovende toepassingen vinden in bijvoorbeeld micro-elektronica, weefsel engineering en bio-medicijnen.

Hoofdstuk 6 omschrijft de toepassing van onze gecontroleerde ruimtelijk geordende zelf-assemblage van de gelatoren toegepast in Hoofdstuk 5 op de nanoschaal. Door gebruik te maken van katalytische sjablonen op nanoschaal hebben we ontdekt dat gel fibers lokaal vormen om katalytische Nanodeeltjes heen door middel van lokale katalyse van deze Nanodeeltjes. Deze lokale fiber vorming limiteert de dispersie van de katalytische Nanodeeltjes in een waterige oplossing wat vervolgens gebruikt is om selectief de katalytische Nanodeeltjes te scheiden. Deze bevindingen laten de potentie van GMZA zien om selectief Nano objecten te scheiden.

Het werk in dit proefschrift omschrijft nieuwe voorbeelden van synthetische zelf-sorterende en GMZA systemen. Naar verwachting openen deze bio-geïnspireerde kunstmatige supramoleculaire systemen routes naar nieuwe functionele zachte materialen voor high-tech toepassingen zoals kunstmatig leven, katalyse, bio-medicijnen en in fundamenteel onderzoek.

Acknowledgements

PhD is a challenge work that cannot be entirely accomplished by an individual effort. But it is achievable if there is a group of nice people around you to give you help and courage. I am very lucky that I can arrive at the final stage of this challenge journey, of course, this is not only contributed by my own effort, but also contributed by those nice people that I would like to thank here.

First of all, I would like thank my promoter, Jan van Esch. I thank you very much for giving me this opportunity and the courage to pursue a second PhD at TU Delft. Within the past three and half years, you inspired me how to think scientifically and how to express the researches in a scientific way. You can always give me some very useful suggestions on a challenge issue in my project. I appreciate that you can always take some time from your tight agenda to have a discussion with me or have a look on my manuscript. Without your contribution, I cannot imagine that I can now sit here to write the last part of my thesis.

Rienk, thank you for being my promoter. High-efficiency can be the keyword of you in my mind. You can quickly raise key questions followed by smart suggestions on the experiment results; whenever I send you the manuscript, you can always response them with careful check within a very short period. Your contributions make my PhD go faster. Thank you.

I would like to thank the committee members, Xuhong Guo, Job Boekhoven, Burak Eral, Nico Sommerdjik, Stephen Picken, and Ernst Sudhölter. Thank you for reviewing my thesis and accepting to present in my defense ceremony.

Eduardo, we have some nice discussions on my work, thanks for your time and patience; Stephen, thank you for the discussion on my crystal-like structures and for lending me the nice book associated with crystals; Ger, because of your warmly organization, I have very good communications with Pierre Schaaf, and Martien Cohen Stuart Martin, thank you.

I also appreciate the efforts made by our support staffs. Mieke, thank you for your warm help when I just joined ASM, I adapted the new life in ASM quickly with your help; Veby, although you are a new secretary of ASM, I already got a lot of help from you, thanks for your highly efficient work; Lars, your presence makes our lab functions normally, without your efforts, our work cannot be proceeded; Marcel, you trained me how to use the AFM and how to perform safely in the lab, my first AFM image had been published, thanks, and I very enjoyed the Sinterklaas party in your place; Ben, rheology brings us together to know each other, we had many nice chatting in the rheometer room, thank you for your help in my experiments as well

as your suggestions and encouragements. Bart, XPS makes my manuscript more strong, thanks for your help with the measurements and the training.

In this challenge journey, I have met many nice colleagues who help me a lot during my PhD study, I am very grateful to them. Kai, the first Chinese student that I met in ASM, you shared your experiences of study at TU Delft and the life in Netherlands with me, which helped me a lot. We also had many deep discussions on research, which dramatically broadened my mind, thanks. Sander, I still remember the scene during my first day in ASM that we sit in Jan's office to discuss my future project, your careful explanation on my project at that moment gave me a good start in ASM. In the subsequent time, we discussed a lot on researches as well as life, thanks. Frank, I am impressed by your working efficiency and excellent writing skills, thank you so much for your kind help in my manuscript writing. I wish you a successful career in any kind of fields. Vincent, my previous roommate, I enjoyed the time with you in the previous office in the old ChemE building, I am impressed by that you can do many things (like analyzing data, watching game video and listening to music) at the same time. Karolis, also my previous roommate, you don't have too much words, but I know you are a very helpful guy. Chandan, you synthesized so many useful compounds, they helped me a lot, thanks. Jos, my roommate in the new building, I like your communication style, you like to make jokes, but are very serious on people's questions, thanks for your patience to answer my questions. Matija, my another new roommate, language is a big problem to me, but to my surprise, you can always understand what I am saying, we have many discussions on researches as well as other funny things, we usually have drinks together, I really enjoy them. Fanny, you always have the patience to answer my questions, and are generous to share your chemicals to me, thanks, and all the best in your new position. Susan, you are very helpful in the lab, I must have used the tissues that were replaced by you, glassware that were cleaned by you and so on. Thanks and all the best in your next stage. Tomasz, you are a very nice guy, we have many fun chatting together. How about your long paper, I believe you will tell a very nice and enjoyable story in your simulation world. Thanks for helping me to do the simulations; Serhii, we also have many discussions regarding to researches and PhD life, you are well skilled with rich knowledge and experiment experiences, I learned some useful tips from you in the past time, thanks. Vasu, I would like to thank you for measuring my samples and raising helpful suggestions on my work; Emma, thanks for the discussions in the coffee corner as well as in the lab, to be chemistry teacher in high school would be great; Qian, we discussed a lot together when we got success or failure in the experiments. Encouragements are always there. I wish you

can ultimately reach the goal that you expected in academia; Cancel, I clearly remembered we joined the ASM at almost the same time, you were a very sunny girl, and brought us a lot of fun; Angie, we usually talked during lunch time, good luck in your next step; Benjamin, we know each other during your master stage, you are a smart PhD and work very hard, I believe you can manage every goals during your PhD. Tobias, I am looking forward to hearing the news from your mechanically sensitive materials, that would be super cool, good luck; Bowen, we have discussed many times with broad topics. Thanks for telling me your research story, and I believe you can bring your plan to real. Michelle, what an excellent girl! I wish you more successes in your research; Peggy, you are a very responsible colleague in our group, your smile makes everything easy, so keep smile; Guotai, I like the discussions with you, I wish all the huge ideas in your mind come true one day; Fan, thanks for all the discussions in our office, good luck for your researches, and I wish you a successful career in the future; Jianwu, I appreciate your positive attitude towards PhD life, you will be able to manage it, let's keep contact; Zhenyu, we have known each other long time ago, many thanks for your help during my PhD study, enjoy your new journey in China; Hendrik, it is good to know that you are interested in Chinese words and our ancient story. I enjoyed the time with you as well as your nice dog in the office; Irene, Sahil, Elmira, and Yongjun, it is very nice to meet you guys at the final stage of my PhD, good luck. Robin, thanks for helping me to do the cryo-TEM measurements. Maulik, although we are from different groups, we spent much time on discussion, thanks a lot for your contribution to my calculation project.

Besides these people who helped me during my work, there is a group of nice Chinese friends who makes my life in Netherlands enjoyable, here I would like to thank Xinlei Liu, Zhen Liu, Ming Ma, Xuerui Wang, Meixia Shan, Kai Liu, Wuyuan Zhang, Liangyong Chu, Xiaohui Sun, Min Wang, Yujie Zhao, Anping Cao, Quan Pan, Riming Wang, Zilong Liu, Donglong Fu, and Shuqing Cao. I have always enjoyed the time together with you, I wish all of you good luck in your future career.

最后，我要感谢我的父母、兄弟姐妹，感谢你们对我在外求学的大力支持；感谢我的妻子，感谢你这些年无私的守候和支持！

About the Author

Yiming Wang was born on January 18th, 1990 in Anhui province, China. In 2012, He obtained his Bachelor degree in Chemical Engineering and Technology at Anhui University of Science and Technology. Afterwards, he started his first Ph.D. in Professor Xuhong Guo's group in the School of Chemical Engineering at East China University of Science and Technology. The project was associated with the development of polyelectrolyte-based carriers for drug delivery. He obtained his first Ph.D. degree in Chemical Technology in 2017. During his first Ph.D., he joined in Professor Jan van Esch's group to start his second Ph.D. cosupervised by Dr. Rienk Eelkema with the topic of molecular self-sorting and directed molecular self-assembly at Delft University of Technology funded by China Scholarship Council (CSC). Since September 2017, he started to work as a postdoctoral researcher in Professor Jan van Esch's group.

List of Publications

1. **Yiming Wang**, Matija Lovrak, Qian Liu, Chandan Maity, Vincent A. A. le Sage, Xuhong Guo, Rienk Eelkema, Jan H. van Esch. Hierarchically compartmentalized supramolecular gels through multilevel self-sorting. *J. Am. Chem. Soc.* **2019**, *141*, 2847. (Supplementary Cover)
2. **Yiming Wang**, Robin M. de Kruijff, Matija Lovrak, Xuhong Guo, Rienk Eelkema, Jan H. van Esch. Access to metastable gel states using seeded self-assembly of low molecular weight gelators. *Angew. Chem. Int. Ed.* **2019**, *58*, xx. DOI: 10.1002/anie.201812412.
3. **Yiming Wang**, Sander Oldenhof, Frank Versluis, Maulik Shah, Kai Zhang, Volkert van Steijn, Xuhong Guo, Rienk Eelkema, Jan H. van Esch. Controlled fabrication of micropatterned supramolecular gels by directed self-assembly of small molecular gelators. *Small* **2019**, *15*, 1804154.
4. **Yiming Wang**, Frank Versluis, Sander Oldenhof, Vasudevan. Lakshminarayanan, Kai Zhang, Yunwei Wang, Jie Wang, Rienk Eelkema, Xuhong Guo, Jan H. van Esch. Directed nanoscale self-assembly of low molecular weight hydrogelators using catalytic nanoparticles. *Adv. Mater.* **2018**, *30*, 1707408.
5. **Yiming Wang**, Matija Lovrak et al, Self-seeding self-assembly towards out-of-equilibrium supramolecular gels. *Under submission*.
6. **Yiming Wang**, Matija Lovrak et al, Strain-stiffening hydrogels through self-assembly of synthetic molecular gelators. *Under submission*.
7. **Yiming Wang**, Jie Wang, Zhenyu Yuan, Haoya Han, Tao Li, Li Li, Xuhong Guo. Chitosan cross-linked poly(acrylic acid) hydrogels: drug release control and mechanism. *Colloid Surf. B* **2017**, *152*, 252.

8. **Yiming Wang**, Jie Wang, Tongshuai Wang, Yisheng Xu, Lei Shi, Yongtao Wu, Li Li and Xuhong Guo. Pod-like supramicelles with multicompartment hydrophobic cores prepared by self-assembly of modified chitosan. *Nano-Micro Lett.* **2016**, *8*, 151.
9. **Yiming Wang**, Jie Wang, Haoya Han, Jianjia Liu, Hanqing Zhao, Muxian Shen, Yisheng Xu, Jun Xu, Li Li and Xuhong Guo. Self-assembled micelles of *N*-phthaloylchitosan-*g*-poly(*N*-vinylcaprolactam) for temperature-triggered non-steroidal anti-inflammatory drug delivery. *J. Mater. Sci.* **2016**, *51*, 1591.
10. Z. Yuan, J. Wang, **Y. Wang**, Y. Zhong et al, Redox-Controlled Voltage Responsive Micelles Assembled by Noncovalently Grafted Polymers for Controlled Drug Release. *Macromolecules* **2019**, *52*, 1400.
11. Q. Liu, M. Zhao, S. Mytnyk, B. Klemm, K. Zhang, **Y. Wang** et al, Self-orienting hydrogel micro-buckets as novel cell carriers. *Angew. Chem. Int. Ed.* **2018**, *58*, 547.
12. K. Zhang, A. Arranja, H. Chen, S. Mytnyk, **Y. Wang** et al, A nano-fibrous platform of copolymer patterned surfaces for controlled cell alignment. *RSC Adv*. **2018**, *8*, 21777.
13. H. Han, L. Li, Y. Tian, **Y. Wang**, Z. Ye, Q. Yang, Y. Wang et al, Spherical polyelectrolyte nanogels as templates to prepare hollow silica nanocarriers: observation by small angle X-ray scattering and TEM. *RSC Adv.* **2017**, *7*, 47877.
14. K. Zhang, P. J. Glazer, L. Jennings, S. Vedaraman, S. Oldenhof, **Y. Wang** et al, A facile approach for the fabrication of 2D supermicelle networks. *Chem. Commun.* **2016**, *52*, 12360.
15. J. Wang, Z. Qiu, **Y. Wang** et al, Supramolecular polymer assembly in aqueous solution arising from cyclodextrin host–guest complexation. *Beilstein J. Org. Chem.* **2016**, *12*, 50.
16. M. Wang, J. Wang, **Y. Wang** et al, Synergetic catalytic effect of α-cyclodextrin on silver nanoparticles loaded in thermosensitive hydrogel. *Colloid Polym. Sci.* **2016**, *294*, 1087.
17. J. Wang, Y. Xu, **Y. Wang** et al, Bridged-cyclodextrin supramolecular hydrogels: host–guest interaction between a cyclodextrin dimer and adamantyl substituted poly (acrylate)s. *RSC Adv.* **2015**, *5*, 46067.
18. J. Liu, J. Wang, **Y. Wang** et al, A thermosensitive hydrogel carrier for nickel nanoparticles. *Colloid Interfac. Sci. Commun.* **2015**, *4*, 1.